CRACK INITIATION AND GROWTH BEHAVIOR AT CORROSION PIT IN 7075-T6 UNDER BIAXIAL AND UNIAXIAL FATIGUE

THESIS

Zafer DOLU, Captain, Turkish Army

AFIT-ENY-T-14-J-33

DEPARTMENT OF THE AIR FORCE
AIR UNIVERSITY

AIR FORCE INSTITUTE OF TECHNOLOGY

Wright-Patterson Air Force Base, Ohio

The views expressed in this thesis are those of the author and do not reflect the official policy or position of the Turkish Army, Department of Defense, or the Turkish Government.

AFIT-ENY-T-14-J-33

CRACK INITIATION AND GROWTH BEHAVIOR AT CORROSION PIT IN 7075-T6 UNDER BIAXIAL AND UNIAXIAL FATIGUE

THESIS

Presented to the Faculty

Department of Aeronautics and Astronautics

Graduate School of Engineering and Management

Air Force Institute of Technology

Air University

Air Education and Training Command

In Partial Fulfillment of the Requirements for the

Degree of Master of Science in Aeronautical Engineering

Zafer DOLU, BS

Captain, Turkish Army

June 2014

AFIT-ENY-T-14-J-33

CRACK INITIATION AND GROWTH BEHAVIOR AT CORROSION PIT IN 7075-T6 UNDER BIAXIAL AND UNIAXIAL FATIGUE

Zafer DOLU, BS

Captain, Turkish Army

Approved:

//signed//	04 June 2014
Shankar Mall, PhD (Chairman)	Date
//signed//	04 June 2014
Lt Col Timothy C. Radsick, PhD (Member)	Date
//signed//	04 June 2014
Vinod K. Jain, PhD (Member)	Date

To my father who passed away in 1994, to my wife and my son for their love, support, patience, and for understanding of the long hours I spent studying and to my mother, brother, and sister for their encouragement and love – Thank you all.

Abstract

This thesis was investigated the effects of pre-existing corrosion on the fatigue crack initiation and fatigue crack growth behavior of the typical aircraft aluminum alloy 7075-T6, by using a fracture mechanics approach. Initiation and crack growth behavior was investigated under in-plane biaxial tension–tension fatigue with stress ratio of 0.1 and biaxiality stress ratio, λ =1. Cruciform specimens with a center hole, having a corrosion pit at 45° to the specimen's arms, were tested in a biaxial fatigue test machine in laboratory air and saltwater (3.5% NaCl) environments. Crack initiated and propagated coplanar with the pit in L–T orientation. For the sake of comparison, uniaxial fatigue tests with stress ratio of 0.1 in laboratory air and saltwater (3.5% NaCl) environments were also conducted. The number of cycles until initiation of the fatigue crack and the crack growth rate were observed and measured by optical and scanning electron microscopy. This research shows that corrosive environment of saltwater reduces the required number of cycles for crack initiation under uniaxial and biaxial loading conditions when compared to those in ambient laboratory air. In all tests corrosive environment shortens the fatigue life of the specimens under uniaxial and biaxial loading conditions. In ambient air, numbers of cycles for crack initiation under biaxial and uniaxial loading conditions are almost the same; on the other hand in saltwater environment crack occurs in lesser number of cycles in biaxial loading condition relative to uniaxial loading condition. The crack growth rate is faster in the saltwater environment than the corresponding value in ambient air environment at a given ΔK in both loading conditions. In ambient air environment biaxial and uniaxial crack growth rates are almost similar. But in saltwater environment biaxial fatigue have faster crack growth rate than uniaxial fatigue. For

uniaxial fatigue with the stress ratio of 0.1 crack initiates later than the one with R=0.5 for a given ΔK value because of the crack closure effect. Also the crack growth rate for R=0.5 is higher than the one with R=0.1.

Acknowledgments

I would like to express my sincere appreciation to my advisor, Dr. Shankar Mall, for his continuous support and guidance throughout my thesis. His vast knowledge and encouragement were essential to the successful completion of this research.

I would like to extend my gratitude to Dr. Volodymyr Sabelkin who has been extremely supportive during my study and reviewed my thesis as a reader. I would also like to thank Dr. Victor Perel for his help in developing the finite element models, and Dr. Heath Misak for showing me how to capture the SEM images of the fatigue specimens. This thesis would not have been possible without the help of these three gentlemen.

My special thank is for my friend Lt. Ibrahim Alqahtani for his fellowship during the whole thesis work.

I would also like to acknowledge the support of this work from the Technical Corrosion Collaboration (TCC), Office of Secretary of Defense (OSD), Washington D.C.

Zafer DOLU

Table of Contents

Page

List of Figures

Page

List of Tables

Page

List of Symbols

Symbol	Definition
α	Angle between the principal stresses and the crack
Δ	Change in a variable
λ	Biaxiality stress ratio
σ	Stress (MPa)
a	Crack length (mm)
C	Constant for Paris law
da/dN	Crack growth rate
E	Young's modulus
F	Applied load (N)
K	Stress intensity factor ($MPa*m^{0.5}$)
K_I	Mode I stress intensity factor ($MPa*m^{0.5}$)
ΔK_I	Mode I stress intensity factor range ($MPa*m^{0.5}$)
m	Exponent for Paris law
M	material
max	Maximum load values
min	Minimum load values
n	Number of moles (moles)
R	Stress ratio
r	Radius of hole (mm)
t	Thickness of specimen (mm)
w	Width of specimen (mm)

CRACK INITIATION AND GROWTH BEHAVIOR AT CORROSION PIT IN 7075-T6 UNDER BIAXIAL AND UNIAXIAL FATIGUE

1. Introduction

1.1 Corrosion and Fatigue Concerns

The Aloha Airlines Accident on April 28, 1988, was a warning to aircraft industry for the long-term need to improve design rules [8]. After the accident, it was reported that the corrosive operating environments might reduce the life of aircraft components significantly. Corrosion can directly affect on the structural integrity of aircraft components. The effect of occurrence of the preexisting corrosion and fatigue cracking simultaneously may be even worse [14, 26]. An attempt was started to examine the effects of corrosion on fatigue crack initiation and fatigue crack growth in test panels and specimens to get data for evaluation process [26].

Corrosion is a natural phenomenon frequently defined as the chemical degradation of materials, because of the reaction with their environment [25, 31]. Corrosion has the overall effect of reducing the strength of a structure, and if not detected, may result in catastrophic failure [21]. Corrosion is a hazardous force that attacks components from inside out. This is the reason for referring it as a hidden cost. The economic affect of corrosion is impossible to ignore. The annual cost of corrosion in the United States is estimated to be about $300 billion which is about 4% of the gross domestic product [32]. As shown in Figure 1.1, corrosion impacts almost every industry sector.

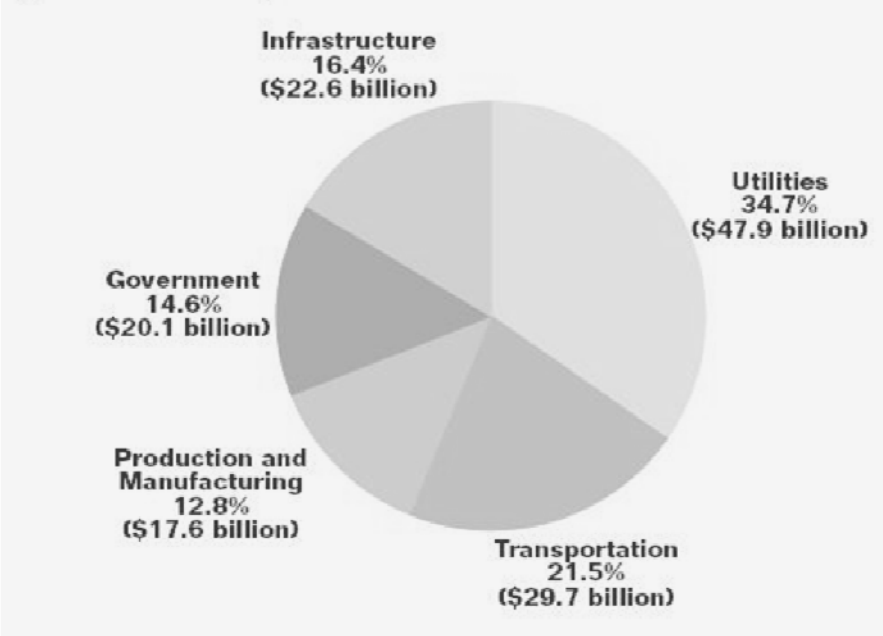

Figure 1.1: Cost of corrosion in industry categories [25].

Beside the cost, just like other natural hazards, corrosion can cause dangerous damage to everything from cars, home appliances, and drinking water systems to public buildings, and to environment [25].

One of the major concerns of the aircraft and airline industry is the aging of aircrafts beyond their original design life. Operators have been having more frequent inspections and maintenance for the safety of older aircrafts. Despite improvements in the corrosion design and manufacturing of new aircrafts, like using more corrosion resistant materials, for extending structure and components life, operators should have a good corrosion control program [25].

The major focus of structural design in the early development of aircraft was on strength, but now designers also deal with fail-safety, fatigue, corrosion, maintenance etc. So to guarantee safe operation of the aircraft, corrosion is not the only concern.

According to the damage tolerance approach, flaws exist in all structures and propagate with usage, e.g. due to fatigue [34]. Being dynamic structures, aircrafts always experience cycling loading, so fatigue is an important issue for aircraft industry.

Fatigue is the structural damage that occurs when a material is subjected to cyclic loading. When this load is above a certain threshold, crack will initiate and grow. The fatigue life of a component can be divided into two phases: the number of loading cycles required to initiate a crack (the fatigue crack initiation life) and the number of cycles it takes that crack to propagate to failure (the corrosion fatigue crack propagation life) [42,43]. Environmental factors have great influence on crack initiation and propagation under cyclic loading. The characteristic case is the corrosion fatigue when interaction of cycling loading and corrosion takes place [5]. The corrosion fatigue is usually referred as the acceleration of fatigue crack growth under a corrosive environment [35]. Majority of aircraft structures are made of aluminum alloys. The heterogeneous microstructures of aluminum alloys such as 2024 and 7075, which are widely used in aircraft structures, make them extremely susceptible to corrosion [45]. The main source of corrosion for aircraft structures is water or water vapor which contains salt. Aircrafts operating in a nautical environment or in certain geographical areas are particularly sensitive to this corrosive attack [35]. Corrosion can harmfully affect aircraft structural integrity since fatigue cracks can nucleate from corrosion pits and grow very fast in corrosive environment [45]. The interaction between the corrosion and the fatigue life of a structural component is very important concern and this interaction should be fully explored for each material.

1.2 Scope of Thesis

Since corrosion is a ubiquitous phenomenon and a threat everywhere from infrastructure and transportation to production and manufacturing, there are many aspects of corrosion. This study is focused on crack initiation and growth after corrosion has occurred.

1.3 Background

There have been many researches, experiments, efforts dedicated to understand the concept of corrosion and fatigue for many years. These experiments have been performed with many different materials under different loading conditions. In 1958 McEvily developed a wide range of cracks growth in aluminum alloys [4, 33]. Then Paris firstly used the stress intensity factor range, ΔK, versus the crack propagation rate, da/dN, as the primary parameters [4, 27]. After these steps in fracture mechanics, many experiments have been performed in different aspects of the issue.

There has been large number of studies dealing with fatigue crack growth behavior of metals in the salt water environments. Gangloff, highlighted modern laboratory methods for characterizing the corrosion fatigue behavior of metals [17]. He summarized the principles and mechanisms of corrosion fatigue, and discussed experimental methods, i.e. specimen design, loading, environment control, crack size measurement etc. Wei et al. conducted a 3-year research to develop a basic understanding of the material degradation processes of localized corrosion and corrosion fatigue crack nucleation and growth in aluminum alloys [50]. They tried to characterize beginning of localized corrosion damage, transition from pitting to fatigue crack growth, and corrosion

fatigue crack growth. Pitting was strongly dependent on temperature and solution pH. The crack nucleation size was found to depend on the cyclic-load frequency, and was larger at lower frequencies. The crack growth rates showed a strong influence of environment and were nearly 10 times faster than in air.

The effect of pitting and corrosion on fatigue life has also been investigated by many researchers. Wang et al. investigated the effect of pre-existing corrosion pits on the fatigue behavior of 7075-T6 aluminum alloy [49]. Their results indicated that the presence of corrosion pits notably reduces the fatigue life of the aluminum alloy by a factor of 10–100. Sankaran et al. found this factor as 6 to 8 [45]. In another study, Chlistovsky et al. reported that due to corrosion pit formation, the fatigue life is reduced in the corrosive environment [10]. Similarly, Kim et al. stated that fatigue life is reduced significantly by pre-corrosion [24].

The transition from pit to crack is another aspect of the area. Pao et al. performed studies of the effects of pre-existing pits on fatigue crack initiation [39]. After their tests and analyses they concluded that corrosion pits shorten the fatigue crack initiation life in ambient air by a factor of two to three and decrease the fatigue crack initiation threshold by about 50 percent. And they emphasized that for the specimens containing pre-existing corrosion pits, cracks always initiate from these corrosion pits. In their corrosion fatigue study, Nan et al. concluded that at the lower stress levels 70–80% of the corrosion fatigue life is the corrosion pit growth period [38]. They also stated that corrosion fatigue life is significantly decreased in comparison with the laboratory air. Another study concerning about transition from pit to crack was conducted by Ro et al. [40]. They investigated the mechanisms of corrosion fatigue in aluminum samples. Their results showed that the

fatigue crack growth rate is strongly affected by the stress intensity range and stress ratio, environment, and microstructure of the material. Xu-Dong et al. examined the effect of prior corrosion state on fatigue crack initiation and propagation behavior of aluminum alloy [51]. They observed that cracks always initiate at the corrosion pits. Lukas and Kunz studied the mechanisms of the crack nucleation from pit and transition to propagation in micro level [30]. They stated that the initiation and early propagation of fatigue cracks can occupy a major part of the fatigue life of materials. And they also concluded that the fatigue cracks always initiate from corrosion pits. Burns et al. also examined the effect of existing corrosion pits on the fatigue cracking [7]. Their experiments showed that the geometry near the pits edges effects the crack initiation rate considerably [7]. In a research conducted by the Air Force Institute of Technology, Hunt [20] investigated the fatigue crack initiation and growth behaviors from corrosion pits in 7075-T6 aluminum alloy under uniaxial loading, with stress ratio R=0.5. He studied both through and corner corrosion pits. He performed his experiments in both laboratory air and saltwater environments. And he concluded that corrosive environment decreases the required cycles for crack initiation in both types of corrosion pits, and corrosive environment reduces the fatigue life of specimens under cyclic uniaxial loading in comparison to ambient laboratory air for both of the corrosion pits.

In the light of the examples above, much is currently known about how a crack propagates and how different environments change the crack growth behavior under the uniaxial fatigue condition [2, 11]. Current research focuses on the characterization of the transition of crack initiation from corrosion pit to fatigue crack growth behavior of 7075-T6 aluminum alloy under biaxial loading in both ambient air and the salt water (3.5%)

environment, using a fracture mechanics approach. Thus, studies about biaxial loading conditions also need to be mentioned. In 1978, Liu and Dittmer introduced their study about the effect of multiaxial loading on the fatigue crack growth behavior [29]. They stated that the direction of the crack is oriented by the biaxial stress ratio, and the larger biaxial stress component controls the crack growth rate. Hopper and Miller studied the propagation of fatigue cracks in notched and un-notched plates under biaxial stresses [18]. Their results showed that the fatigue crack propagation rate is affected by stress biaxiality, and there is a retarding effect of tensile transverse stress on crack growth rate. In their study, Anderson and Garrett examined the influence of biaxial stress fields on the crack growth behavior [1]. They observed that biaxial stress field causes change in crack growth rate. Sunder and Ilchenko attempted to investigate fatigue crack growth under biaxial loading condition, particularly for pressurized transport aircraft fuselage panels under the combined action of strong wind loading and internal pressurization that causes a biaxial cyclic loading action [48]. After all tests and analyses they concluded that the rates of fatigue crack growth are obviously sensitive to load biaxiality under both constant amplitude and spectrum loading. Shanyavskiy also performed fatigue crack growth experiments and stated that in aluminum based alloys subjected to biaxial loading, fatigue cracks grow faster with the larger the applied stress ratios [46]. Lee and Taylor conducted a study to investigate the effect of biaxial stressing on the fatigue life, fatigue crack growth, and path [28]. They concluded that the fatigue life is reduced for a greater biaxiality ratio. Yuuki et al. examined the effect of biaxial loading on the fatigue crack growth [52]. They observed a considerable biaxial stress effect on crack growth when the stress level was high and the crack was short, but negligible effect at low stress

levels in comparison to uniaxial fatigue [52]. Some fatigue tests has also been conducted at the Air Force Institute of Technology. Misak et al. investigated effects of in-plane biaxiality fatigue on the crack growth behavior of aluminum alloy 7075-T6 in their two studies [35, 36]. They examined the biaxial and uniaxial fatigue crack growth under ambient laboratory air and salt water (3.5% NaCl) environments in one study [35], and only in air in the other [36]. Their results may be summarized as followings:

(1) Cracks grow parallel to the notch under uniaxial and biaxial fatigue for biaxiality ratio of $\lambda = 1$, while the path is not parallel to the notch for $\lambda = 1.5$ [35, 36].

(2) Biaxial fatigue increases the crack growth rate in region I in comparison to uniaxial fatigue under both environments. Biaxial fatigue increases the crack growth rate in region II relative to uniaxial fatigue under salt environment. Crack growth rates in region II are faster in salt water than air environment [35].

(3) Fatigue crack growth rates are affected by biaxial fatigue, and it increases with increase of biaxiality ratio [36].

As a result, there are limited numbers of studies under biaxial loading condition. These studies have shown that biaxial fatigue has an effect on the crack growth rate. However there is no study for the biaxial fatigue crack initiation. Therefore, there is a need to investigate both fatigue crack initiation and growth behaviors of materials under biaxial loading conditions using fracture mechanics approach, and to compare these results with the ones conducted under uniaxial conditions.

1.4 Problem Statement

The focus of this research is the fundamental understanding of the transition from a localized corrosion (i.e. corrosion pit) to a fatigue crack. There are a great number of studies about fatigue and corrosion pit formation, but further research is needed to understand the interaction between these two using the fracture mechanics principles. In the aircraft industry, the main sources of fatigue damage are fastener holes. A study of fatigue failures in aircraft structures showed that 70% of fatigue cracks are initiated from the rivet holes or bolted joints [8]. So particularly fatigue crack growth in specimens containing pits that exist around holes should be examined. Conventionally, material fatigue data are obtained from tests carried out under uniaxial stress, but the majority of aircraft structural components experience complex stress states. There are many possible non-uniaxial loading conditions [1, 34, 36]. One of these conditions is the in-plane biaxial tension–tension fatigue, which is the focus of this research. Only a few studies which involve the fatigue crack growth behavior under the biaxial loading are existing, and almost all of them are under ambient air. Also the previous studies which involve corrosion fatigue crack growth are under the uniaxial fatigue loading condition except ones, where in-plane biaxial fatigue crack growth of aluminum alloy 7075-T6 was described [34, 35, 36]. Thus, characterization of the behavior under biaxial loading, using a fracture mechanics approach, is highly desirable. In this research the fatigue crack initiation and growth behavior in 7075-T6 aluminum alloy, which is widely used material in aircraft structures [36], was examined in both ambient air and salt water (3.5% NaCl) environments under biaxial loading which is not studied by anybody until now, which makes this research unique in the field. And for comparison, fatigue crack initiation and

growth behavior in the same alloy under uniaxial fatigue in ambient air and salt water environments was also characterized. Lastly, fatigue damage mechanisms in all cases were analyzed [34]. For biaxial loading ($R = 0.1$, $\lambda = 1$) tests, cruciform specimens machined from a 3.18 mm thick sheet of 7075-T6 aluminum alloy were used. Length and width of each arm was 120 mm and 45 mm, and the radius of curvature at the junction of arms was 45 mm. First, a hole of 6 mm diameter was drilled at the center of the specimen, then through corrosion pit was electrochemically created at 45° to horizontal and vertical arms. For uniaxial loading ($R = 0.1$, $\lambda = 0$) tests, 50 mm wide and 3.18 mm thick rectangular 7075-T6 aluminum alloy specimens with 6 mm diameter circular holes at the center were used. On these specimens corrosion pits were electrochemically created at the edge of hole. A high magnification camera was used to determine the crack initiation and to measure the crack growth [20]. The scanning electron microscope was used to examine how cracks initiated and grew from the electrochemical corrosion pits. Finite element analyses of crack growth from a corrosion pit at a hole for both biaxial and uniaxial loading conditions were carried out to calculate the range of stress intensity factor, ΔK. Then ΔK was correlated with the number of cycles until crack initiation and crack growth rate. This research will provide a great deal of useful information for fatigue crack initiation and growth from a corrosion pit. It will make a useful data available to compare different loading conditions (biaxial and uniaxial loading) to better predict the lifetimes of an aging fleet of aircraft, and finally will help to fill the void that exists from the previous studies.

2. Background

2.1 Corrosion Basics

The initial force that causes metals to corrode is the natural result of their temporary existence in metallic form. To manufacture metals from natural minerals and ores, it is compulsory to give a certain quantity of energy. Therefore when these metals are exposed to their environments they may naturally go back to the original state in which they were found [41]. So, any metallic component will somehow corrode and the only thing that a user can do is fighting with corrosion with some precautions and changing the corroded part before a catastrophic failure occurs.

All corrosion processes require electrochemical reactions. An electrochemical reaction is defined as a chemical reaction involving the transfer of electrons. Every corrosion process consists of anodic reaction and cathodic reaction. The anodic process involves oxidation of a metal to its ion, as shown in Equation 2.1, where n is number of electrons produced. The value of n also equals the valence of the ion, which depends primarily on the nature of the metal. In general, oxidation refers to the material that loses electrons during a reaction, while reduction refers to the material that gets electrons during a reaction [2, 20, 41].

$$\text{General anodic reaction:} \quad M(s) \rightarrow M^{n+} + ne^{-} \tag{2.1}$$

$$\text{General cathodic reaction:} \quad M^{n+} + ne^{-} \rightarrow M(s) \tag{2.2}$$

In brief, for occurrence of corrosion there must be formation of ions and release of electrons at an anodic surface where oxidation of the metal occurs. And simultaneously there must be a reaction at the cathodic surface to consume the electrons

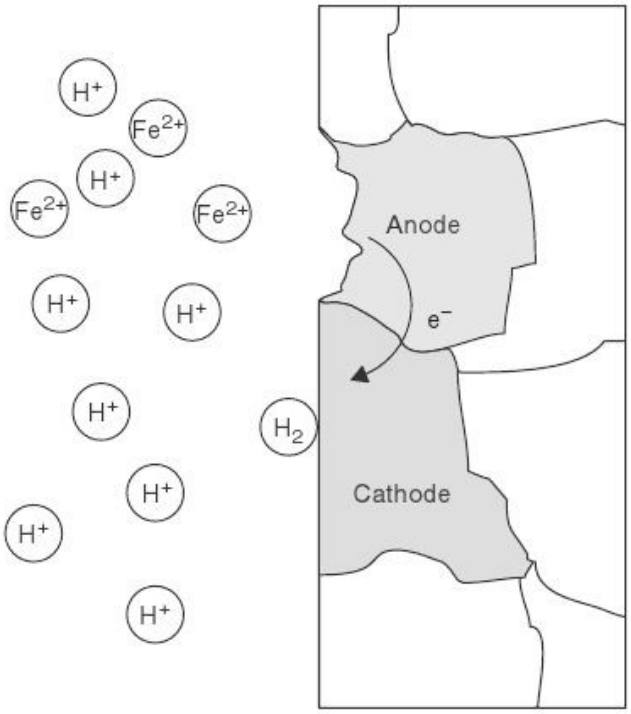

Figure 2.1: Formation of ions at an anodic area and release of hydrogen at a cathodic area on an iron surface [41].

created by the anode, as illustrated in Figure 2.1 for iron surface. The anodic and cathodic reactions must continue simultaneously and at equivalent rates [41].

2.2 Types of Corrosion

Corrosion is the continuing destruction of materials, by chemical reaction with their environment. There are many valid methods of classifying corrosion, and no universally accepted terminology is in use. But the degree of localization would be a good way to organize corrosion types according to the surface selectivity of attack. Corrosion can be classified into general corrosion and localized corrosion [23]. Uniform or generalized corrosion indicates the corrosion attack with a great weight loss, the whole

surface experiences a similar removal of material. Uniform corrosion is the most often occurring corrosion damage but also the less dangerous because it is predictable. Structures will usually turn out to be bad-looking and be a focus for maintenance before they become structurally affected [41]. In localized corrosion there is intense attack at localized sites on the structure while the rest of the structure is corroding at a lower rate, or remains uncorroded. Common forms of localized corrosion include pitting, corrosion in a creviced region, intergranular corrosion, galvanic corrosion, and exfoliation corrosion [16]. These localized corrosions often end up with stress corrosion cracking (SCC) or corrosion fatigue (CF) because they act as a flaw that increases the stress intensity factor in the material, which causes decrease in fatigue life [20]. Basic understanding and prediction of localized corrosion is a difficult problem. The event happens on a very small scale. Just after initiation, the rate of pit growth can be extremely high. As a result, it may not possible to guess exactly when and where failure will occur [16]. Corrosion in aircraft aluminum alloys occurs in several different forms. Corrosion pits are common in the 2000- and 7000-series aluminum alloys which are the principal materials of aircraft structures [21, 26]. This research will focus on the effect of localized corrosion (i.e. pitting) on the initiation and growth of fatigue cracks.

2.3 Pitting

Pitting corrosion is an important failure mechanism of industrial structures. It is the most common type of localized corrosion. Small volumes of metal are removed by corrosion from specific areas on the surface which creates craters or pits. These pits grow with time. The growth rate depends on both the environment and the metal itself. Failure

because of pitting corrosion is expected when the pit size exceeds the critical size at any location. Pitting is more dangerous than uniform corrosion damage because it is difficult to notice and predict. A small pit can cause the failure of an entire system [23, 41]. Some factors causative to initiation and propagation of pitting corrosion are the followings: localized damage of a protective oxide film, water chemistry factors that can cause collapse of a passive film like acidity, localized damage, and the presence of heterogeneous microstructures in the metal [41].

Shapes of pits might differ broadly, but are in general conical, hemispherical, and roughly saucer-shaped for steel and many alloys [41], as shown in Figure 2.2.

Pits usually nucleate at chemical or physical heterogeneity at the surface, such as inclusions, flaws, or mechanical damage. Particularly, the aluminum alloys have several constituent particles, which is main factor for corrosion pit formation. The presence of corrosion pits alters the local stress and may eventually reduce fatigue life and lower the threshold stress for crack nucleation and propagation [49]. Corrosion pits are potential fatigue crack nucleation sites in most structural materials like steel and aluminum, depending on their depth, local stresses and the fatigue crack growth properties of the material [9, 12, 21].

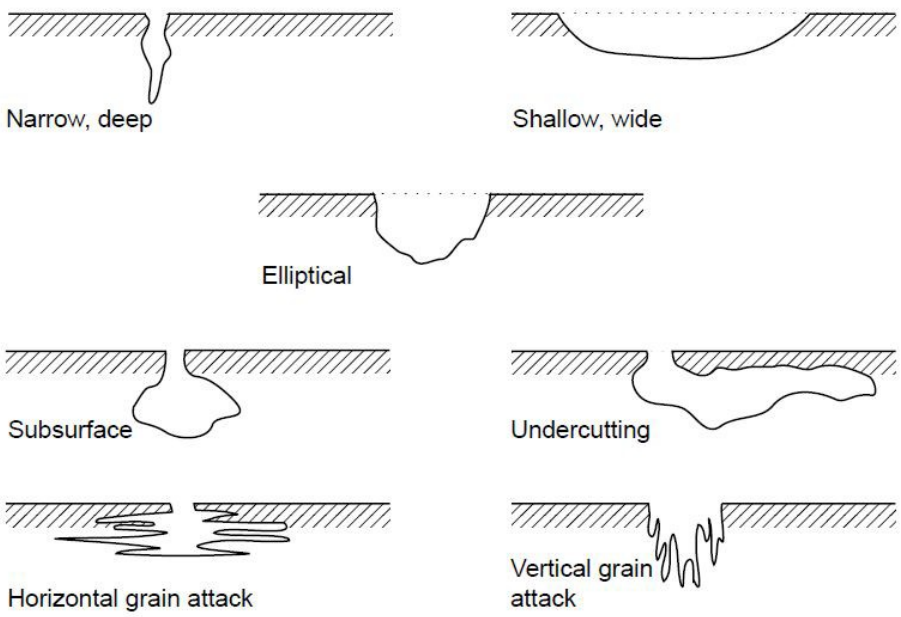

Figure 2.2: Shapes of corrosion pits [41].

Pitting is usually associated with other forms of corrosion. For example, intergranular corrosion and cracks may grow from the main pit hole. As an example shown in Figure 2.3, pitting at the edge of an aluminum alloy has advanced as intergranular corrosion at the root of the pits [41].

2.4 Corrosion Fatigue

Factors affecting the fatigue life of a material may be grouped as followings: microstructure of the material, processing, load spectrum, environment, and geometry of the component [15]. Of those we will focus on environmental factors, particularly on corrosive environment. When a structural component is subjected to both cyclic loading and corrosive environment, mixed phenomenon called corrosion fatigue takes place [5].

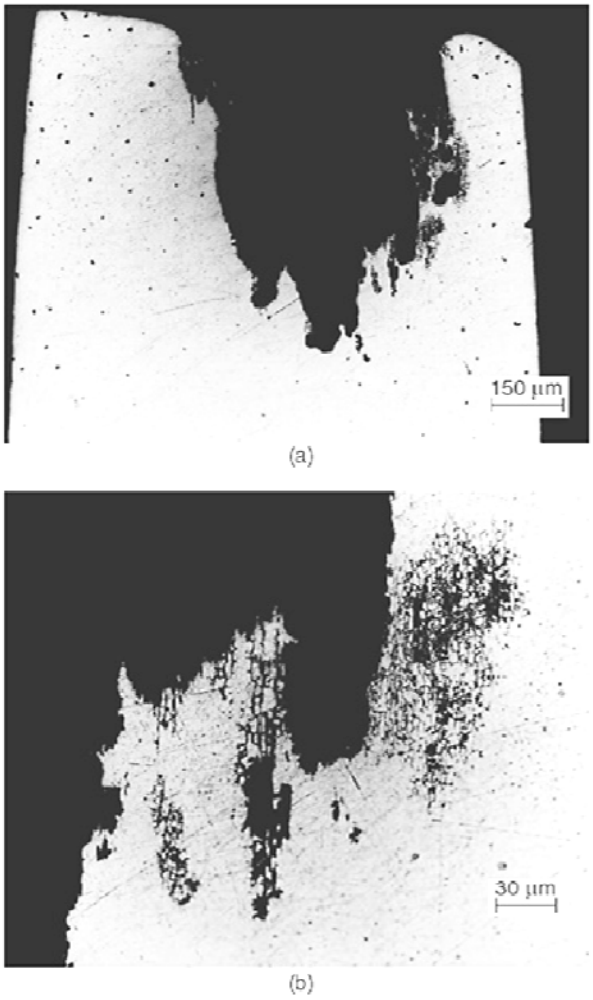

Figure 2.3: Photomicrograph of a section of 8090-T851 panel placed in seawater for four months; (a) at 64X and (b) at 320X [41].

The number of cycles required to cause fracture reduces when a metal is subjected to cyclic loading in a corrosive environment, comparing to required cycles in air, as shown in Figure 2.4. This acceleration of fatigue crack growth as a result of interaction with the environment is called corrosion fatigue. The solid line is corrosion fatigue curve, and it shows that metal life under this condition is lower than metal life in air [2, 41].

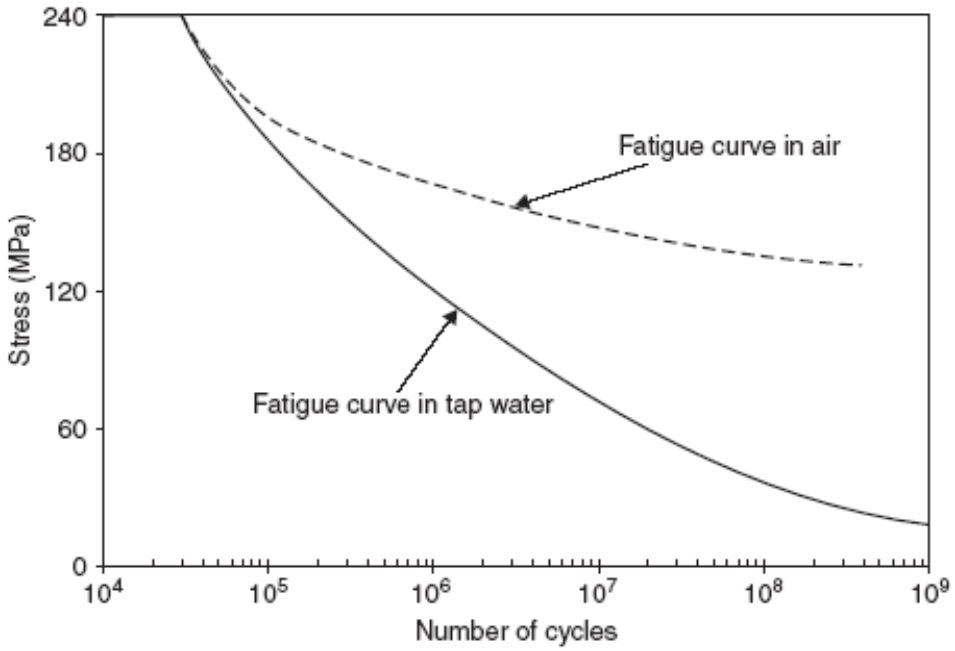

Figure 2.4: The effect of corrosion on fatigue curves [41].

DuQuesnay et al. [14] examined the material 7075-T6511 aluminum alloy in their study. They investigated the growth behavior of fatigue cracks initiated at corrosion pits. They performed fatigue tests on pre-corroded and uncorroded specimens under aircraft loading spectrum in laboratory air at room temperature. For all pre-corroded specimens fatigue cracks initiated from the corrosion damage and shortened the fatigue life. They observed that least corroded specimen had a life at least 3.5 times lower than the uncorroded specimens and the worst corroded specimen had a life at least 13 times lower. And this result was parallel to the one by Sankaran et al. [45] who found this factor about 6-8 times in their study. Jones and Hoeppner [21] also mentioned in their paper that the presence of pitting was associated with noteworthy fatigue life reductions, as a result of cracks originating from corrosion pits. In their experiment they used dog-bone specimens

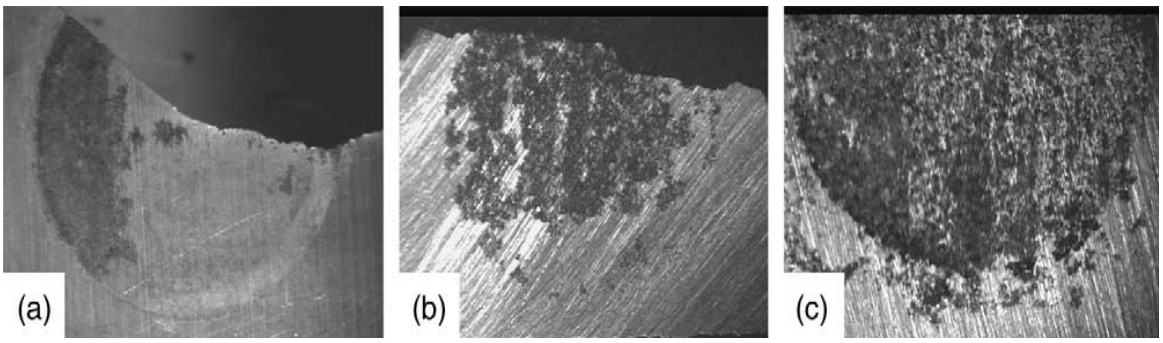

Figure 2.5: Examples of corrosion damage in fatigue coupons, (a) mild, (b) medium, (c) severe [14].

with center holes from 2024-T3 aluminum alloy sheets. The specimens were corroded with different pit depth up to 30 μm and they characterized the pitting corrosion using microscope. As a result they indicated that pit shape, pit surface area, pit depth are major factors in determining when and where a crack will form. And after initiation, corrosion has still effect on propagation of the crack.

2.5 Fracture Mechanics

Fracture mechanics is the field of mechanics, which deals with the study of the propagation of cracks in materials. The fracture mechanics approach has three important variables; flaw size, applied load, and fracture toughness. It uses solid mechanics to set relationship between these variables. There are three types of loading that can be applied to a crack, as illustrated in Figure 2.6. Mode I loading is known as opening mode because it tends to open the crack. In Mode I principal load is applied normal to the crack plane. Since Mode II tends to slide one crack face from the other, it is called sliding mode.

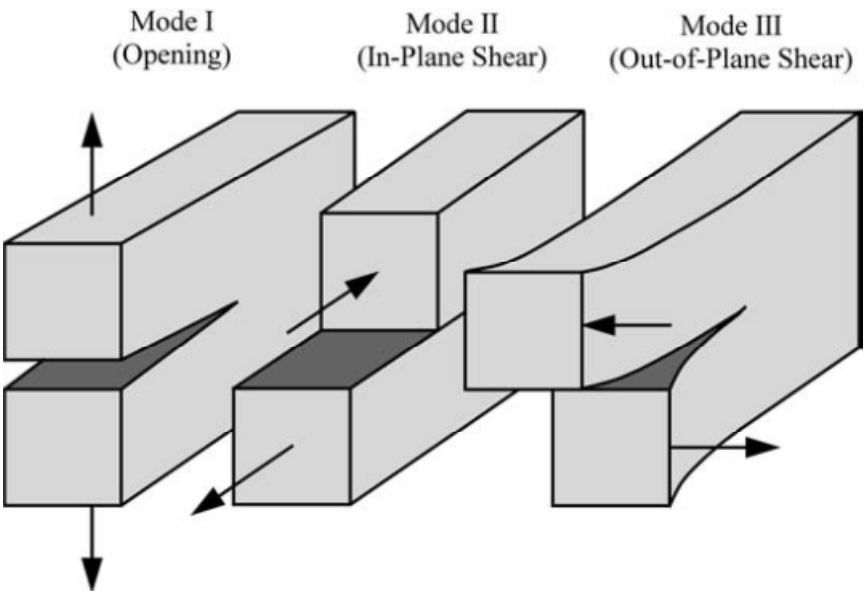

Figure 2.6: Types of loading in fracture mechanics [2].

Sliding mode corresponds to in-plane shear loading. And finally Mode III refers to out-of-plane shear, and also known as tearing mode. A crack can experience any of these modes, or a combination of two or three [2]. Since the focus of this research is the in-plane biaxial tension–tension fatigue, Mode I will be the only concern.

The stress intensity factor for Mode I is given in Equation 2.3, where σ is the applied stress, and a is the crack length [2, 19].

$$K_I = \sigma * (\pi * a)^{1/2} \qquad (2.3)$$

In the presence of cycling stresses, we have to modify the stress intensity factor with the range of the stress intensity factor, ΔK [2, 19].

$$\Delta K = K_{max} - K_{min} \qquad (2.4)$$

Figure 2.7 illustrates typical fatigue crack growth behavior in metals which is the log-log plot of da/dN vs. ΔK. The curve has three regions. At an initial region (I), da/dN approaches zero at a threshold ΔK. Below the threshold stress, the crack does not grow. In a linear region (II) curve is linear. And there is a final region (III) of acceleration to fracture. On this log–log plot, the slope of the linear region equals to m [2, 19].

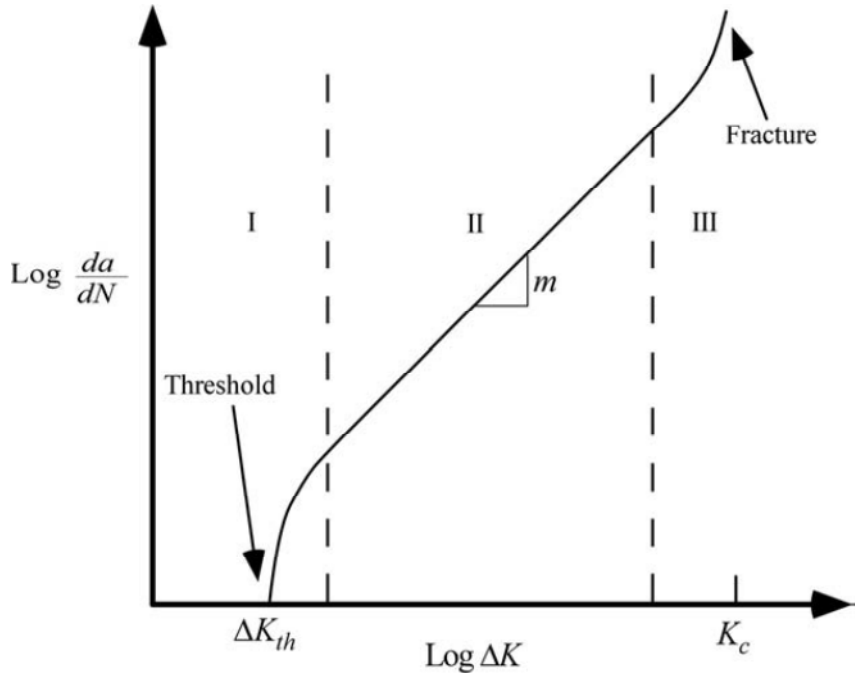

Figure 2.7: Typical fatigue crack growth behavior in metals [2].

The linear region of log-log plot in Figure 2.7 can be described by Equation 2.5, widely known as Paris Law. According to this law the fatigue crack growth rate depends on only the range of the stress intensity factor, ΔK, so it is insensitive to the stress ratio, R, where $R= K_{min} / K_{max}$. In the equation, C and m, which are determined experimentally, are material constants [2, 19].

$$da/dN = C*\Delta K^m \qquad (2.5)$$

Briefly, according to the Paris law when the stress intensity factor, which involves the applied stress and the crack length, increases the crack propagation rate will also increase.

2.6 Previous Research

For many years there have been many researches, experiments, efforts dedicated to understand the concept of corrosion and fatigue. These experiments have been performed with many different materials under different loading conditions.

First, McEvily developed a wide range of cracks growth in aluminum alloys 7075-T6 and 2024-T3 by using fatigue testing machine in 1958 [4, 33]. Then Paris firstly employed the stress intensity factor range, ΔK, versus the crack propagation rate, da/dN, as the primary parameters [4, 27]. After these steps in fracture mechanics, many experiments have been performed in different aspects of the issue recently. With the development of technology in every area, researchers now seek deeper understanding of the parameters and the reasons of the crack behavior.

There has been large number of studies dealing with fatigue crack growth behavior of metals in the salt water environments. Gangloff, highlighted modern laboratory methods for characterizing the corrosion fatigue behavior of metals [17]. He summarized the principles and mechanisms of corrosion fatigue, and discussed experimental methods, i.e. specimen design, loading, environment control, crack size measurement etc. He emphasized that corrosion fatigue experiments are difficult to perform due to several factors, for instance aggressive environments are difficult to contain at a constant condition, and hinder precise measurements of specimen

displacement, load, and crack size [17]. Wei et al. conducted a 3-year research to develop a basic understanding of the material degradation processes of localized corrosion and corrosion fatigue crack nucleation and growth in aluminum alloys [50]. They used 2024-T3 and 7075-T651 aluminum alloys, which are widely used in aircraft construction. They tried to characterize beginning of localized corrosion damage, transition from pitting to fatigue crack growth, and corrosion fatigue crack growth. Experiments were performed at room temperature in 0.5M NaCl solutions. Pitting was strongly dependent on temperature and solution pH. The crack nucleation size was found to depend on the cyclic-load frequency, was larger at lower frequencies. Experiments to study the fatigue crack growth were carried out in 1.6 mm thick 2024-T3 specimens at room temperature in 0.5M NaCl solutions at ΔK of 4 to 10 $MPa*m^{0.5}$ with R = 0.1 at 10 Hz. The crack growth rates showed a strong influence of environment and were nearly 10 times faster than in air [50].

The effect of pitting and corrosion on fatigue life has also been investigated by many researchers. Wang et al. investigated the effect of pre-existing corrosion pits on the fatigue behavior of 7075-T6 aluminum alloy [49]. To create corrosion pits, they immersed specimens in salt water solution (3.5% NaCl) for 1, 4, and 7 days. The maximum pit sizes were 30, 50, 60 μm, respectively. Fatigue tests were performed in a piezoelectric resonance system. Their results indicated that the presence of corrosion pits notably reduces the fatigue life of the aluminum alloy by a factor of 10–100 [49]. Sankaran et al. also investigated the effects of pitting corrosion on the fatigue behavior [45]. They used 150 mm long, 75 mm wide, and 2 mm thick rectangular specimens made of 7075-T6 aluminum alloy. After the corrosion exposure in a chamber for different

duration, the specimens were tested. Pitting corrosion reduced the fatigue life by a factor of 6 to 8. The fatigue life of the 7075-T6 specimens with different sizes of pits was predicted using the fatigue crack growth software, AFGROW. The measured fatigue lives generally agreed with the predictions using the average pit size as the initial crack size [45]. In another study, Chlistovsky et al. also examined the corrosion fatigue behavior in the presence of the corrosive environment [10]. The specimens made of 7075-T651 aluminum alloy were fatigue tested in 3.5% NaCl solution. Then they compared the results of the corrosion fatigue tests with the ones performed in laboratory air. They found that due to corrosion pit formation, the fatigue life was reduced in the corrosive environment [10]. Similarly, Kim et al. investigated the effect of pre-corrosion on the fatigue life of aluminum alloy 7075-T6511, and they also found that fatigue life is reduced significantly by pre-corrosion [24].

The transition from pit to crack is another aspect of the area. Pao et al. performed studies of the effects of pre-existing pits on fatigue crack initiation [39]. They tried to characterize the influences of corrosion pits on fatigue crack initiation on 7075-T7351 aluminum alloy, using fracture mechanics approach. They employed 12.7 mm thick 63 mm long 64.8 mm wide blunt-notch wedge-opening-load type specimens in the fatigue crack initiation experiments. Corrosion pits were produced by immersion of the specimens in 3.5% NaCl solution. Fatigue crack initiation tests were carried out at different stresses in ambient air at R =0.1 and 5 Hz on specimens with and without corrosion pits. After the tests and analyses they concluded that corrosion pits shorten the fatigue crack initiation life in ambient air by a factor of two to three and decrease the fatigue crack initiation threshold by about 50 percent. And they emphasized that for the

specimens containing pre-existing corrosion pits, cracks always initiate from these corrosion pits [39]. In their study, Nan et al. analyzed the corrosion pit and fatigue characteristics of magnesium alloy AZ31 [38]. They did corrosion fatigue experiments on 100 mm long 12 mm wide specimens in 3% NaCl solution using a cantilever-type rotating bending fatigue machine. During the tests, at some numbers of cycles they stopped the tests to investigate the pit and the crack initiation, and they replicated the specimen surfaces. Then they measured pit diameters or crack lengths by observing the replicas by optical microscope. They also used scanning electron microscope for fracture surfaces. After these tests they concluded that at the lower stress levels 70–80% of the corrosion fatigue life is the corrosion pit growth period. They also stated that corrosion fatigue life is significantly decreased in comparison with the laboratory air [38]. Another study concerning about transition from pit to crack was conducted by Ro et al. [40]. They investigated the mechanisms of corrosion fatigue in aluminum samples. They performed their experiments on two alloys, C47A and C433, using a computer controlled servo-hydraulic machine. Their results showed that the fatigue crack growth rate is strongly affected by ΔK and R, environment, and microstructure of the material [40]. Xu-Dong et al. examined the effect of prior corrosion state on fatigue crack initiation and propagation behavior of aluminum alloy [51]. They used 45 mm long 12 mm wide dog-bone shaped specimens made of 6151-T6 aluminum alloy. Before tests the specimens were corroded in a environmental chamber with a corrosive solution. They carried out the fatigue tests in high vacuum environment by a servo-hydraulic testing system. And the crack length was measured directly with scanning electron microscopy (SEM). They observed that

cracks always initiate from corrosion pits. Other results may be summarized as followings:

(1) Corrosion time is the main parameter for the pit size and distribution. The pit depth can be used to characterize the damage of prior corrosion,

(2) The distribution of the pits strongly affect on the fatigue crack propagation behavior and direction [51].

Lukas and Kunz studied the mechanisms of the crack nucleation from pit and transition to propagation in micro level [30]. They aimed to overview present knowledge about this mechanism. They stated that the initiation and early propagation of fatigue cracks can occupy a major part of the fatigue life of materials. Quantitative descriptions of these phenomena are not sufficient for now. And finally they also concluded that the fatigue cracks always initiate from corrosion pits [30]. Burns et al. also examined the effect of existing corrosion pits on the fatigue cracking [7]. They tried to establish the mechanisms of initial crack growth using fracture mechanics approach. They used 30.5 mm long, 19.1 mm wide, and 7.6 mm thick specimens made of 7075-T6511 aluminum alloy. The specimens were exposed to EXCO solution for different durations. They carried out fatigue tests according to ASTM E466. They concluded that fatigue life of 7075-T6511 is decreased significantly by pre-corrosion, and pit size scales this reduction. Their experiments also showed that the geometry near the pits edges effects the crack initiation rate considerably [7]. In a research conducted by the Air Force Institute of Technology, Hunt investigated the fatigue crack initiation and growth behaviors from corrosion pits in 7075-T6 aluminum alloy under uniaxial loading, with stress ratio R=0.5 [20]. He studied both through and corner corrosion pits. He performed his experiments in

both ambient air and saltwater environments. The uniaxial specimens with 6.28 mm diameter center holes were cut from 3.22 mm thick 7075-T6 aluminum alloy sheets. Then corrosion pits were created by electrochemical reaction. He employed a high resolution camera to observe and measure the crack growth. And he concluded the followings:

(1) Corrosive environment decreases the required cycles for crack initiation in both types of corrosion pits, as shown in Figure 2.8.

(2) Corrosive environment reduces the fatigue life of specimens under cyclic uniaxial loading in comparison to ambient laboratory air for both through and corner corrosion pits.

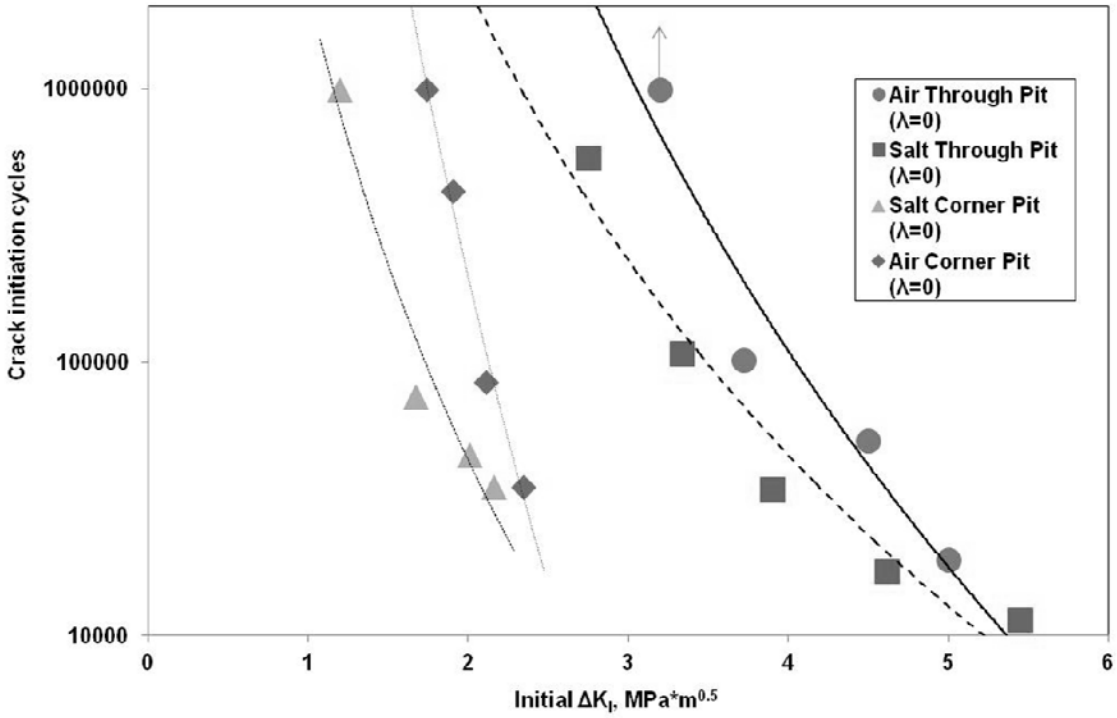

Figure 2.8: Crack initiation cycles vs. initial stress intensity factor [20].

Like the examples above, most fatigue data have been generated on test specimens of subjected to uniaxial loading [18]. Much is currently known about how a crack propagates and how different environments change the crack growth behavior under the uniaxial fatigue condition [2, 11]. Current research focuses on the characterization of the transition from corrosion pit to fatigue crack behavior of 7075-T6 aluminum alloy under biaxial loading in both ambient air and the salt water (3.5%) environment, using a fracture mechanics approach. Thus, studies about biaxial loading conditions need to be mentioned in detail.

In 1978, Liu and Dittmer introduced their study about the effect of multiaxial loading on the fatigue crack growth behavior [29]. Their report covered their two-year-tests carried out between 1976 through 1978. Experiments and analyses were performed on the cyclic crack growth behavior of center-cracked cruciform type of specimens made of either 7075-T7351 or 2024-T351 aluminum alloys under biaxial loading conditions with different biaxial stress ratios. Their results are summarized as followings:

(1) The crack will grow straight when the stress component parallel to the crack direction is equal or smaller than the stress component normal to the crack direction,

(2) For both straight and curved cracks, stress intensity factors may be calculated and these factors are enough to correlate the crack growth rate data,

(3) The stress parallel to the crack has small or negligible effects on crack growth rates depending upon the biaxial ratio. The larger biaxial stress component controls the crack growth rate,

(4) The crack growth rates and crack growth directions In Mode III loading conditions are the same with the ones in the Mode II loading conditions,

(5) For the variable amplitude tests, they found that cracks grow faster at positive biaxial stress states and slower at negative biaxial loading conditions,

(6) At a given stress intensity factor, the crack growth rates are the same under all biaxial constant amplitude loading conditions, which means that biaxiality does not affect crack growth rates under constant amplitude loading [29].

Hopper and Miller studied the propagation of fatigue cracks in notched and un-notched plates under biaxial stresses [18]. Their experimental work consisted of tests on a high-strength aluminum alloy, RR 58. They examined the fatigue crack propagation under different biaxial stress conditions in un-notched plate specimens and specimens with central circular notches, by using a servo-hydraulic testing machine. Due to the capability of the machine, they couldn't have the cycling loading on both the horizontal and the vertical component at the same time, hence they kept the horizontal load constant and had cycling vertical loading with biaxiality ratio, λ, -1, 0, and +1. They used a travelling microscope to measure the crack length, and curve-fitting technique for readings of crack length and number of cycles to calculate crack growth rates, similar to the present research. Their results showed that the additional loading parallel to the crack causes crack growth rates differing from those under uniaxial loading for both un-notched and notched specimens; tensile loads lead to decrease in crack growth rates and compressive loads result in increase in crack growth rates. Briefly, they found that, the fatigue crack propagation rate is affected by stress biaxiality, and there is a retarding effect of tensile transverse stress on crack growth rate [18].

In their study, Anderson and Garrett examined the influence of biaxial stress fields on the crack growth behavior [1]. Their changeover tests were carried out on steel

cruciform specimens with a 6 mm thick, 68 mm diameter central test section, and a 14 mm central crack. In the changeover tests, procedure starts at one particular biaxial ratio and changes to another in the middle of the test, and then any inflection in crack growth rate is recorded. In their experiments a cyclic load P_x was applied normal to the crack direction, and P_y parallel to it. The biaxiality ratio, λ, was defined as P_x/P_y. Crack length was measured optically along with the number of cycles. They employed a universal servo-hydraulic testing machine. Anderson and Garrett observed that biaxial stress field causes change in crack growth rate [1].

Their results relevant to the present research can be summarized as follows:

(1) Equal biaxial tensions reduces the fatigue crack growth rate, comparing to the uniaxial condition at the same nominal applied stress (P_y) normal to the crack line.

(2) Compressive stresses superimposed parallel to the crack growth direction cause a large increase in fatigue crack propagation rate in comparison to the uniaxial conditions, equal biaxial tension-compression cause almost three times increase in crack growth rate [1].

Sunder and Ilchenko attempted to investigate fatigue crack growth under biaxial loading condition, particularly for pressurized transport aircraft fuselage panels under the combined action of strong wind loading and internal pressurization that causes a biaxial cyclic loading action [48]. They also aimed to develop an easy to use digitally controlled biaxial test system for cruciform specimens. Their experiments were carried out on cruciform test coupons using a digitally controlled four actuator biaxial testing system. Steel specimens of 1 mm thickness and 2.7 mm thick 2024-T3 aluminum alloy specimens were used in the tests. They performed two sets of tests. The first set was performed

under constant amplitude loading on 1 mm thick steel specimens. The goal of these tests was to investigate the feasibility of the testing system and process. The second set of experiments was performed on aluminum alloy specimens under Marker-TWIST, which is described elsewhere [47]. After all these tests and analyses they concluded that the rates of fatigue crack growth are obviously sensitive to load biaxiality under both constant amplitude and spectrum loading [48].

Shanyavskiy also performed fatigue crack growth experiments [46]. His investigations were developed on the cruciform specimens made of materials AK4-1T1 and Al-alloy D16T, the range of thickness 1.2–10 mm. He used biaxial cyclic loadings in the biaxiality ratio, λ , between -1.4 and +1.5, and R-ratios from 0.05 to 0.8. Different cases for crack closure effects are examined in his study. He performed crack growth simulation under constant and variable amplitude of cyclic loads to characterize the crack closure effects under plane-stress condition, under plane-strain condition, under out-of-phase loading, because of plastic zone re-orientation, and because of overloads. He concluded that in aluminum based alloys subjected to biaxial loading, fatigue cracks grow faster with the larger applied stress ratios [46] .

Lee and Taylor conducted a study to investigate the effect of biaxial stressing on the fatigue life, fatigue crack growth, and path [28]. They performed tests on cruciform specimens made of 2 mm thick sheets of aluminum alloys 1100-H14 and 7075-T651, containing a horizontal or a 45° inclined center notch respectively, subjected to biaxial loading with biaxiality ratio, λ, from 0 to 1.5, stress ratio R= 0.1 and loading frequency 15 Hz in air. They concluded that:

(1) At a given biaxiality ratio, a greater longitudinal stress shortens the fatigue life,

(2) The direction fatigue crack is influenced by biaxiality ratio, the path is horizontal for $\lambda = 1$ but deviated for $\lambda > 1$,

(3) The fatigue life is reduced for a greater biaxiality ratio [28].

Yuuki et al. examined the effect of biaxial loading on the fatigue crack growth [52]. They conducted their fatigue tests on SUS 304 stainless steel using a servo-hydraulic biaxial fatigue testing machine. They carried out constant and changing biaxial stress condition tests to analyze the stress intensity factor for center cracks in the cruciform specimens with the biaxiality ratio, λ, -1, 0, and +1 and the stress ratio, R=0.1. They employed a travelling microscope to measure the crack length. From the experiments, they observed a considerable biaxial stress effect on crack growth when the stress level was high and the crack was short, but negligible effect at low stress levels in comparison to uniaxial fatigue [52].

The Air Force Institute of Technology has also performed some fatigue tests. Misak et al. investigated effects of in-plane biaxiality fatigue on the crack growth behavior of aluminum alloy 7075-T6 in their studies [35, 36]. They examined the biaxial and uniaxial fatigue crack growth under ambient laboratory air and salt water (3.5% NaCl) environments in one study [35], and only in air in the other [36]. They carried out the biaxial tests on cruciform specimens cut from the 3.18 mm thick plates, with a center hole of 6 mm diameter. They machined a 1 mm long and 0.25 mm wide notch by the electro-discharge method at an angle 45° to horizontal and vertical arms. Next, a pre-crack from the notch was created under the biaxial fatigue loading condition. The pre-

crack and the notch were perpendicular to the rolling direction of the specimen. They performed the tests under the biaxiality ratios, λ=1 and 1.5, and the stress ratio, R=0.5. They used a servo-hydraulic biaxial testing machine for their tests. An environmental chamber containing salt water was used to create the corrosive environment. Crack lengths were measured with an optical microscope system. They used a finite element analysis program to calculate the stress intensity factors, K_I and K_{II}. The uniaxial fatigue crack growth tests were also conducted in the same configuration, i.e. pre-crack and notch. Their results may be summarized as followings:

(1) Cracks grew parallel to the notch under uniaxial and biaxial fatigue for λ =1, while the path was not parallel to the notch for λ = 1.5 [35, 36], as shown in Figure 2.9,

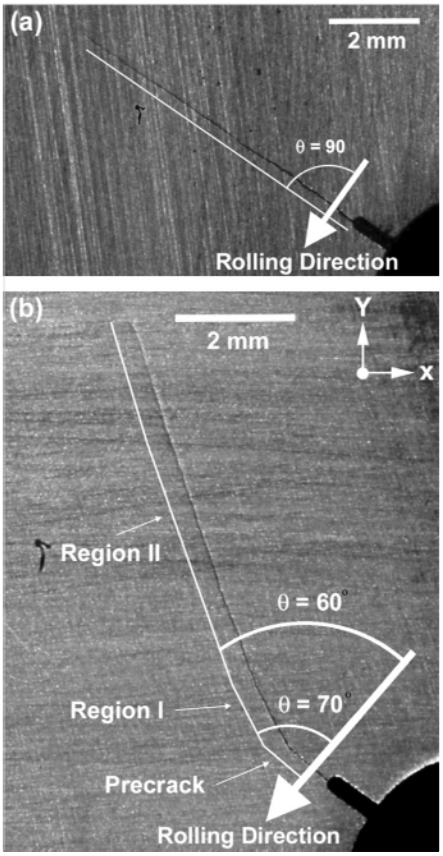

Figure 2.9: Crack propagation paths, (a) biaxial λ =1, (b) λ =1.5 [36].

(2) Biaxial fatigue increased crack growth rate in region I in comparison to uniaxial fatigue under both environments. Biaxial fatigue increased crack growth rate in region II relative to uniaxial fatigue under salt environment. Crack growth rates in region II were faster in salt water than air environment [35],

(3) Fatigue crack growth rates are affected by biaxial fatigue, and it increases with increase of biaxiality ratio [36].

In Figure 2.10 crack growth data from their experiments can be seen as a function of the range of stress intensity factor.

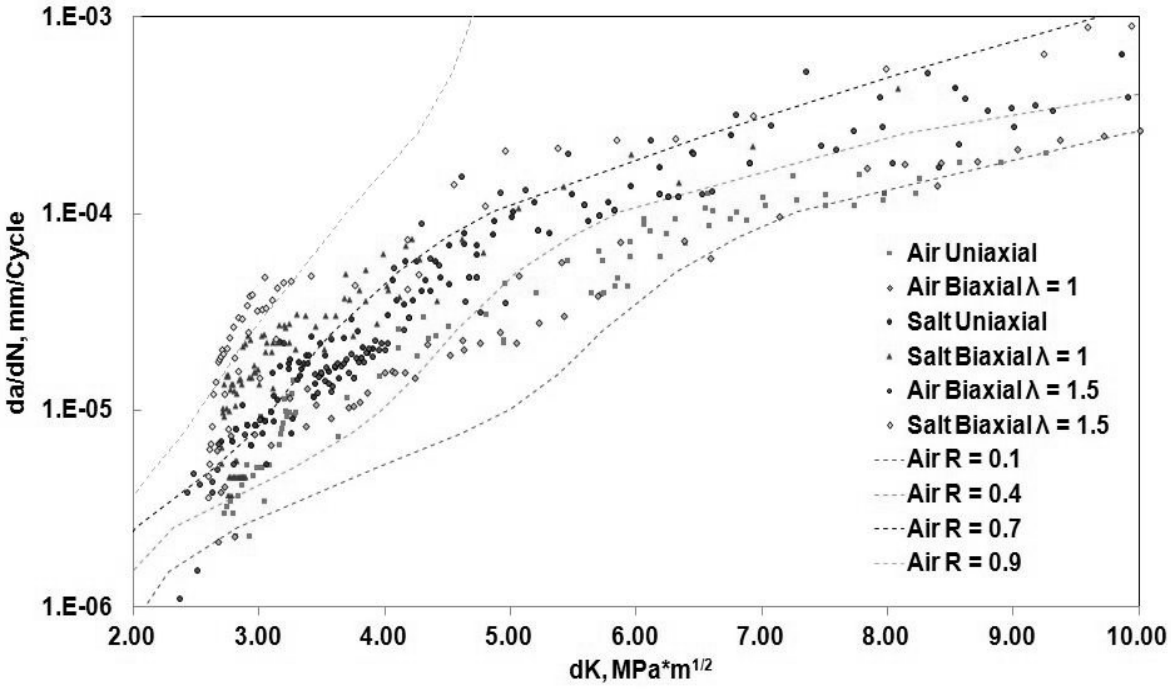

Figure 2.10: The plot of crack growth rate as a function of the range of stress intensity factor [35, 36].

2.6 Why This Thesis?

Much is known about fatigue crack growth under uniaxial loading condition, but there are limited numbers of studies under biaxial loading condition. These studies have shown that biaxial fatigue has an effect on the crack growth rate. But up to now there is no experiment on both fatigue crack initiation and growth behavior of materials under biaxial loading conditions. The present research is a unique study where fatigue crack initiation and growth behaviors in air and salt water environments under uniaxial and biaxial fatigue loading conditions were investigated and fracture mechanics was used to explain and predict the results. The test material was the aluminum alloy 7075-T6 since it is widely used as a structural material in aviation industry. This research presents the details and results of these experiments.

3. Methodology

3.1 Material

The material used in this research was 7075-T6 aluminum alloy. This alloy is a very high strength material used for highly stressed structural parts with improved stress-corrosion cracking resistance. It is also used in various applications; aircraft fittings, gears and shafts, fuse parts, meter shafts and gears, missile parts, regulating valve parts, aircraft, aerospace and defense applications, etc. The chemical composition and the mechanical properties of the alloy are shown in Tables 3.1 and 3.2, respectively.

Table 3.1: Chemical composition of 7075-T6 aluminum alloy [3].

Component	Wt. %
Al	87.1 - 91.4
Cr	0.18 - 0.28
Cu	1.2 - 2
Fe	Max 0.5

Component	Wt. %
Mg	2.1 - 2.9
Mn	Max 0.3
Other, each	Max 0.05
Other, total	Max 0.15

Component	Wt. %
Si	Max 0.4
Ti	Max 0.2
Zn	5.1 - 6.1

Table 3.2: Mechanical Properties of 7075-T6 aluminum alloy [3].

Hardness (Rockwell A)	53.5	Modulus of Elasticity	71.7 GPa
Hardness (Rockwell B)	87	Poisson's Ratio	0.33
Hardness (Brinell)	150	Fatigue Strength	159 MPa
Hardness (Vickers)	175	Fracture Toughness	20-29 MPa*$m^{0.5}$
Hardness (Knoop)	191	Shear Modulus	26.9 GPa
Ultimate Tensile	572 MPa	Shear Strength	331 MPa
Tensile Yield Strength	503 MPa		

7075-T6 is in the wrought alloy families [11]. In general 7xxx represents the alloys in which zinc is the principal alloying and other elements such as copper, magnesium, chromium, and zirconium can be specified. 7xxx series alloys are the strongest aluminum alloys and are used in aircraft structural components and other high-strength applications. And the designator after dash (i.e., H, T, O, and F) stands for the sequences of mechanical or thermal treatments. T6 indicates that the material is solution heat treated and artificially aged [11].

3.2 Test Specimens

The fatigue tests were conducted on cruciform and uniaxial specimens made of the aluminum alloy 7075-T6. Both types of specimens were cut from 3.18 mm thick plates by the AFIT machine shop using a water-jet machine. Each arm of the cruciform specimen had a length and width of 120 mm and 45 mm, respectively, as shown in Figure 3.1. The radius of curvature at the junction of the arms was 45 mm. And the uniaxial specimen had a simple geometry of a rectangle, with 203.2 mm length and 50.8 mm width, as shown in Figure 3.2. A 6 mm hole was machined at the center of both cruciform and uniaxial specimens.

Thereafter, the corrosion pits were created perpendicular to the rolling direction, at 45° to horizontal and vertical arms for cruciform specimen and 90° to applied load for uniaxial specimen. To create corrosion pit the electrochemical corrosion procedure was followed as outlined by Burns [6]. Firstly small chips were removed from the hole with a sharp blade to obtain a smooth surface, and whole surface was cleaned with acetone and methanol. Then to create the through pit shape, E-470 electroplating tape was used.

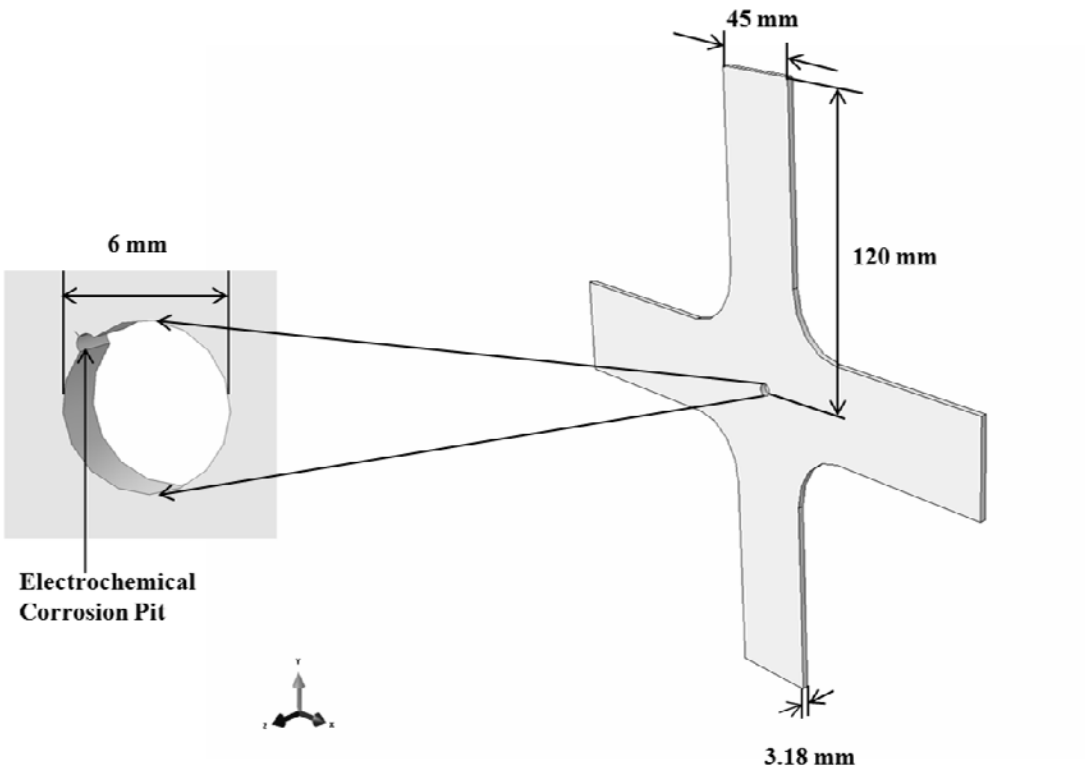

Figure 3.1: Diagram of the cruciform specimen with dimensions.

Two 2.0 mm wide strips of tape was placed more or less 0.25 mm apart on the edge of the hole at 45° to horizontal and vertical arms for cruciform specimen and perpendicular to the loading direction for uniaxial specimen, as shown in Figure 3.3. The area between these two tapes would be exposed to the electrochemical solution and therefore would be corroded [20].

After the application of the tape, the areas other than the area between tapes were painted with XP 2000 Stop-off lacquer in a circular shape with a radius of approximately 2 cm around the hole and let to dry for 3-4 hours. Then a small plastic cylinder was stuck to one side of painted region using silicone. This plastic cylinder was employed as a

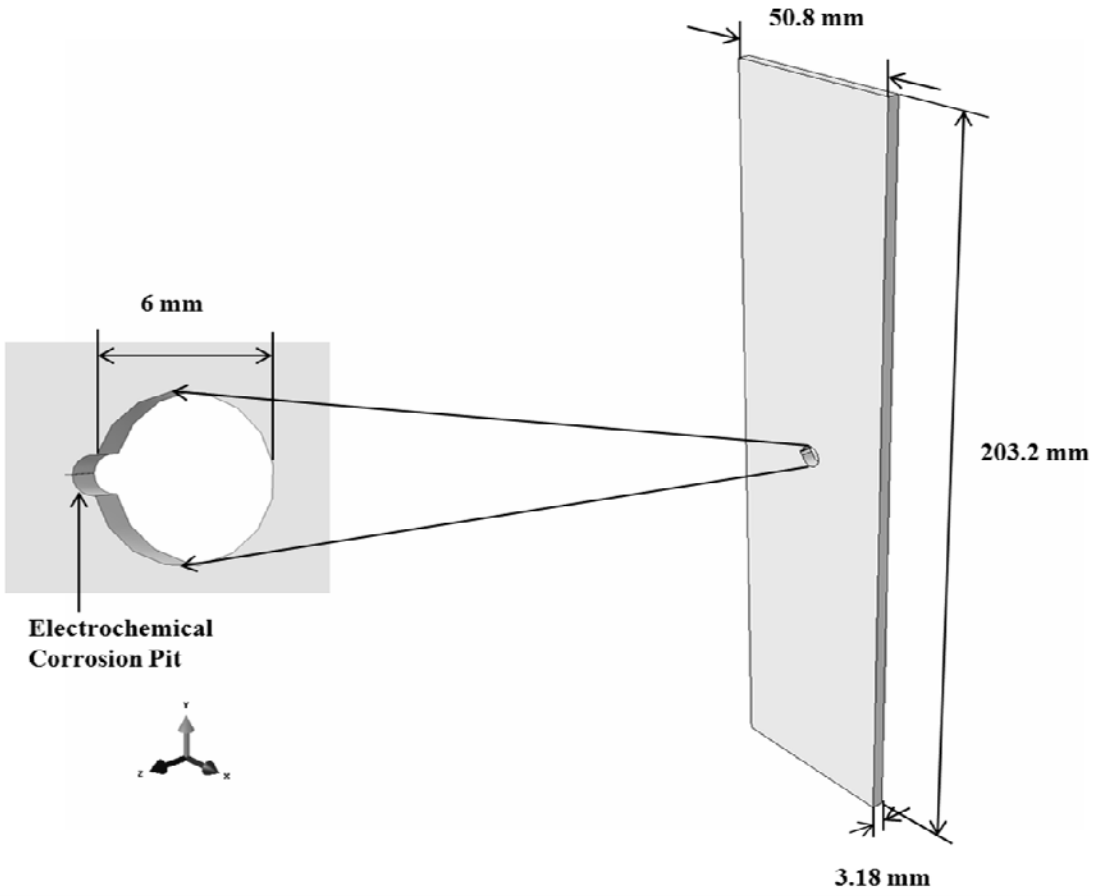

Figure 3.2: Diagram of the uniaxial specimen with dimensions.

container for the chemical solution. The silicone was allowed to dry for another 3-4 hours before electrochemical reaction. And to prevent the solution leakage a piece of tape was applied to the opposite side of the hole. For chemical reaction to corrode the specimens, a special corrosive solution of 0.1MAlCl3 + 0.86MNaCl + HCl (pH =2) was used [20]. The reaction was forced by 6 VDC. A triple output DC power supply was used to provide this potential. The negative output clip was attached to a platinum electrode immersed in the chemical solution, and the positive output clip was attached to the specimen.

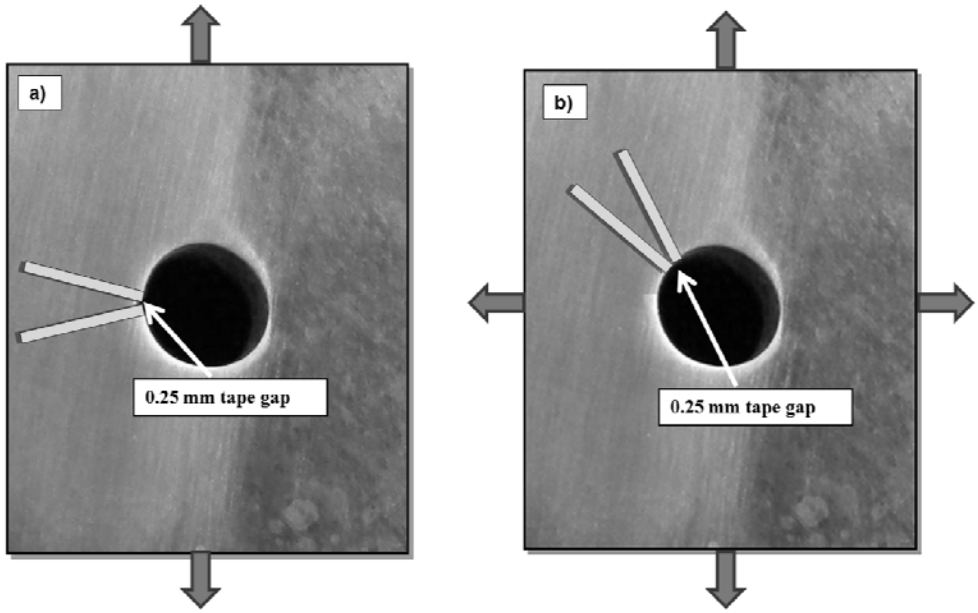

Figure 3.3: a) Tape placement for creating a through pit on uniaxial specimen b) Tape placement for creating a through pit on cruciform specimen.

Hydrogen bubbles, which might slow or stop the reaction, would form around the corrosion area throughout the chemical reaction. A pipette was employed to remove the bubbles. The chemical reaction lasted 10 minutes, which was calculated in the previous experiments. Thereafter the solution was emptied, and the plastic cylinder, stop-off lacquer, and tape were removed from the specimen to see the corrosion pit. Then the specimen was rinsed with pure water and dried to stop any ongoing reaction. Figure 3.4 shows an example of through corrosion pit formed after the reaction. The size of the pit was measured by using the Zeiss optical microscope. These pit sizes were used in a commercially available software for finite element analysis, Abaqus, to model the specimens and analyze the tests for the calculations to estimate the stress intensity range, ΔK, for the experiments. To calculate the stress intensity factor, the path of crack was

reproduced in Abaqus, and a realistic smallest visible crack length, 0.25 mm, was assumed to be the initiation point. The pit sizes and estimated range of stress intensity factors for each experiment are shown in Table 3.3. These measurements of pit sizes were supplemented by scanning electron microscope (SEM) after the tests by means of SEM images of the fracture surfaces taken by a SEM Quanta 450.

A three letter code was used to label the specimens. The first letter refers to the specimen types, (X) for cruciform specimens and (S) for uniaxial specimens. The second letter refers to environments, either air (A) or salt (S). And the third letter, (I), refers to the through pit. $_{max}$

After all these steps the surface around the hole was polished by using 1000 grit sandpaper. This provided a smooth and uniform surface for easier identification of the crack initiation.

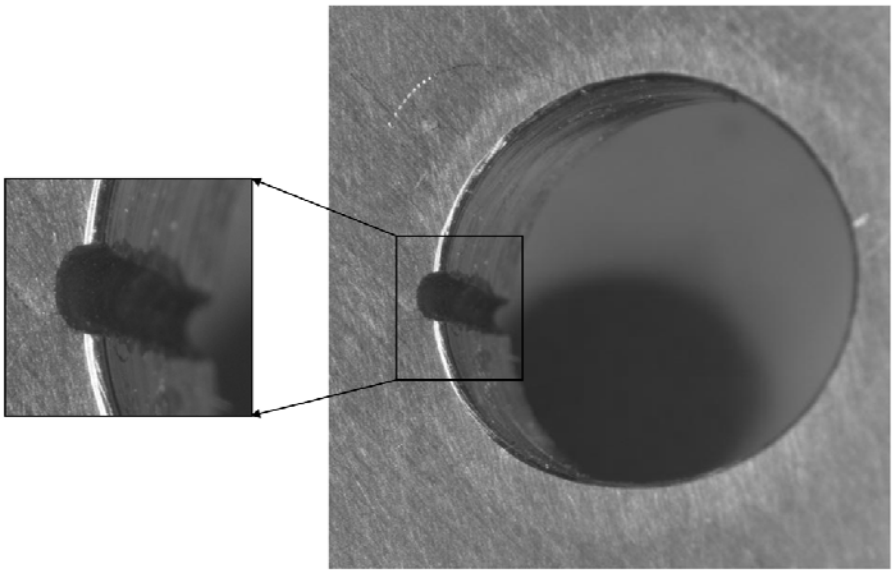

Figure 3.4: Example of through corrosion pit.

Table 3.3: Specifications for test specimens.

Specimen	Stress Ratio	Radius of Pit (mm)	Environment	Initial ΔK ($MPa*m^{0.5}$)	σ_{max} (MPa)	F_{max} (N)
SAI-01	0.1	0.4425	Air	3.77	40	6462
SAI-02	0.1	0.41	Air	18.45	196	31663
SAI-03	0.1	0.39	Air	12.27	129.7	20952
SAI-04	0.1	0.365	Air	10.69	113.5	18338
SAI-05	0.1	0.345	Air	6.55	69.45	11219
XAI-01	0.1	0.366	Air	9.47	211	29993
XAI-02	0.1	0.633	Air	3.89	86.2	12253
XAI-03	0.1	0.418	Air	5.63	125	17768
XAI-04	0.1	0.405	Air	6.93	154.8	22004
SSI-01	0.1	0.345	Saltwater	4.52	47.9	7732
SSI-02	0.1	0.482	Saltwater	5.97	63.27	10220
SSI-03	0.1	0.4	Saltwater	3.59	38	6139
SSI-04	0.1	0.491	Saltwater	3.31	35.1	5670
XSI-01	0.1	0.37	Saltwater	6.83	211	29993
XSI-02	0.1	0.329	Saltwater	4.53	140	19900
XSI-03	0.1	0.358	Saltwater	2.77	85	12082
XSI-04	0.1	0.39	Saltwater	2.26	70.4	10007

***Initial ΔK values are computed by Abaqus.**

3.3 Test Procedures

All tests for this research were conducted in the AFIT mechanics of materials laboratory. MTS Planar Biaxial Testing machine was used for the experiments. The System consisted of four actuators and load cells, hydraulic grips and fixtures, rubber isolation mounts and a hydraulic power unit. The system supports 100 kN, 250 kN and 500 kN actuators to perform static testing and dynamic testing to 20 Hz. MTS Model 793 Software was used to enter the test inputs and to control the load cells. FlexTest GT digital control box acted as an interface, interpreting signal from the computer to the load frame [37]. The machine was capable of applying cycling biaxial loads in the horizontal and vertical directions independently. This enabled to have different biaxial stress ratios. The biaxiality ratio in this research is defined as $\lambda = F_x / F_y$, where F_x and F_y are the fatigue loads in horizontal and vertical directions, respectively. All biaxial tests in this research were under the in-phase loading condition with the biaxiality stress ratios, λ equal to 1 and the stress ratio, R equal to 0.1. Further, uniaxial fatigue crack tests were conducted with the same stress ratio, R equal to 0.1 by employing rectangle specimens with a center hole and corrosion pit. The time dependence of the applied fatigue loads was sinusoidal with a frequency of 20 Hz for all tests. All tests were carried out until either the fatigue crack initiated and grew to a length of approximately 17 mm or 1 million cycles without crack initiation.

Initially, the applied loads for experiments were calculated using closed form solutions from the paper written by Kaminskii and Sailov [22], as shown in Equations 3.1, 3.2, and 3.3, where a is the crack length, r is radius of the hole, σ_y and σ_x are principal stresses, α is the angle between the principal stresses and the crack, K_I is the

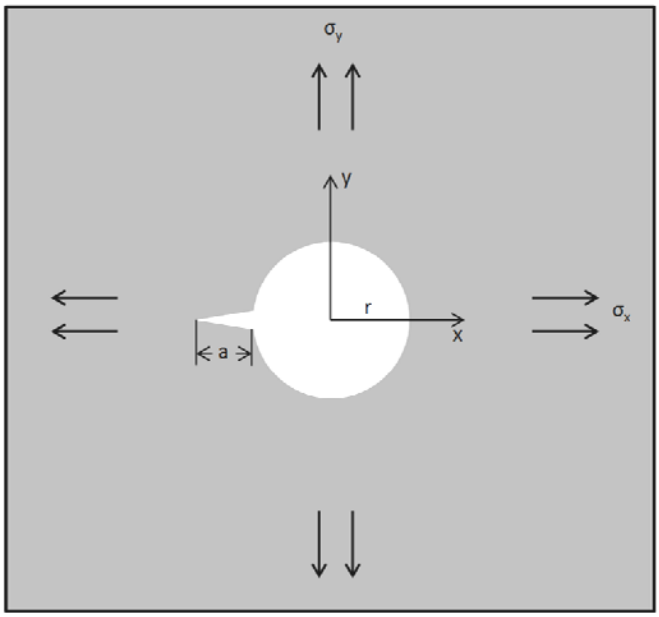

Figure 3.5: Configuration for Kaminskii and Sailov's solution.

stress intensity factor, and ΔK_I is the range of stress intensity factor for mode I loading. Configuration for their solution is shown in Figure 3.5. These equations used the crack length, other geometric properties and applied loads to calculate the stress intensity factor for a crack originating from a circular hole.

In their paper, in case of a circular hole and an arbitrary angle α between the principal stresses and the crack, the solution for stress intensity factors can be summarized as follows:

$$K_1 = \frac{\sigma_y \sqrt{\pi r}}{2\sqrt{2}} \sqrt{\frac{l_0 \left(l_0 + 2\right)^3}{\left(l_0 + 1\right)^3}} \left(1 + \frac{\sigma_x}{\sigma_y} - \left(1 - \frac{\sigma_x}{\sigma_y}\right) \cos 2\alpha\right) \qquad (3.1)$$

where,

$$l_0 = \frac{1}{2}\left(-1 + \frac{a}{r} + \sqrt{2\frac{a}{r} + \frac{a^2}{r^2} + 1}\right) \tag{3.2}$$

If the hole is circular and the angle α between the principal stresses and the crack is α= π /4 rad =45° then the solution for stress intensity factor becomes the following:

$$K_1 = \frac{\sqrt{\pi r}}{2\sqrt{2}}\sqrt{\frac{l_0\,(l_0+2)^3}{(l_0+1)^3}}\,(\sigma_y + \sigma_x) \tag{3.3}$$

$$\Delta K_I = (1\text{-}R) * K_I \tag{3.4}$$

For the tests these equations were used because it was thought to be accurate enough to give approximate values to be used in the calculation of the experimental loads. After then it was verified that the results from the equations were similar with values computed from Abaqus. The comparison is given in the Finite Element Analysis section of this thesis. After the completion of the experimental tests, the ranges of stress intensity factor were modified to represent the values from Abaqus.

During the tests the crack initiation and growth were observed carefully at all times. A high magnification optical microscope system consisted of a PixeLink camera with an AF Micro Nikkor 200 mm lens was used to photograph the crack growth during the fatigue tests. Photographs of the crack were recorded as the number of cycles progressed. These photographs were imported in PixeLink uSCOPE software and the

lengths were measured. The software uses the pixels in the image to calculate a length. For calibrating PixeLink uSCOPE, the camera was put in front of the machine and specimen was in focus and a picture including the hole was taken. Since the diameter of the hole could be measured accurately by external means, the software was then easily calibrated so that the number of pixels across the diameter of the hole corresponded to the actual diameter of the hole. To provide good illumination for the picture, a bright light bulb was used. The test setup is shown in Figure 3.6.

If the crack initiated during the test, the test was stopped when the crack reached a length of about 17 mm to protect the fracture surfaces. Having a crack length more than this might cause specimen break into two pieces, which would damage the fracture surfaces.

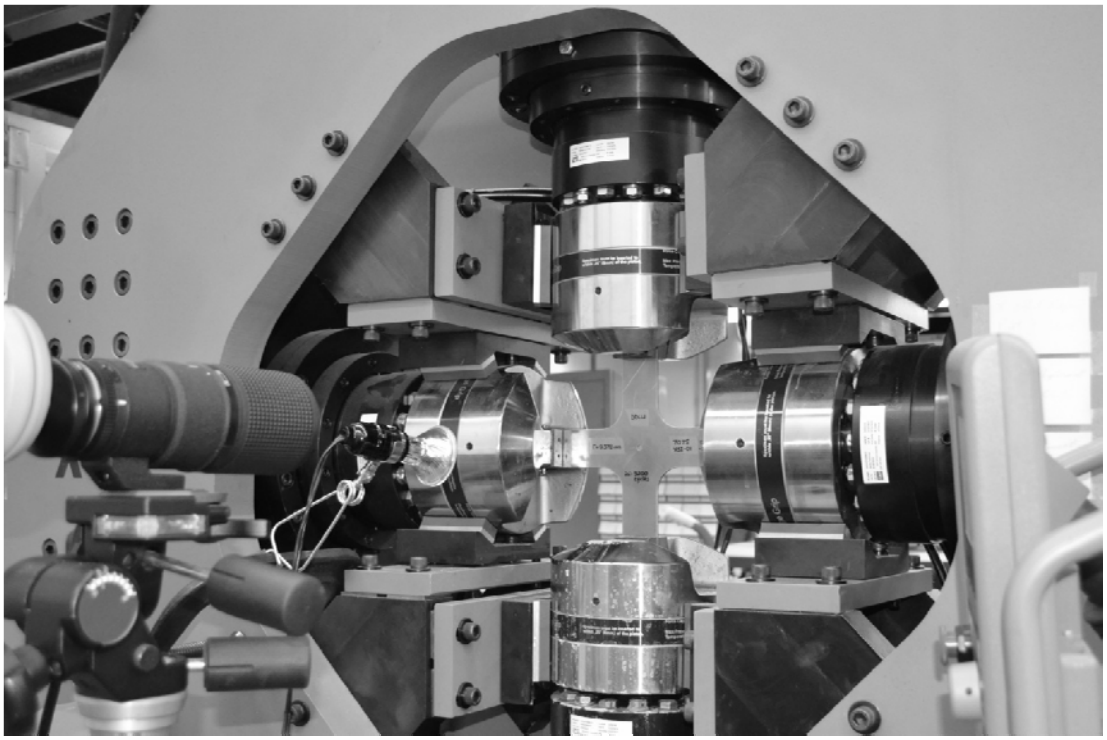

Figure 3.6: The test setup.

In the experimental part of this research some of the specimens were tested in ambient laboratory air, and some other tests were conducted in saltwater environment. To create this environment, a portion of the specimen, containing the hole and the corrosion pit, was put inside a special environmental chamber containing 3.5% NaCl water solution, as shown in Figure 3.7. The test specimen was placed between two stainless steel chambers. These chambers were connected together using screws, and were sealed with rubber gaskets to prevent leakage. Then the saltwater was added through the holes at the top of the chambers. The hole, the corrosion pit, and the crack growth could be easily monitored during the experiments, by means of front and back polycarbonate screens.

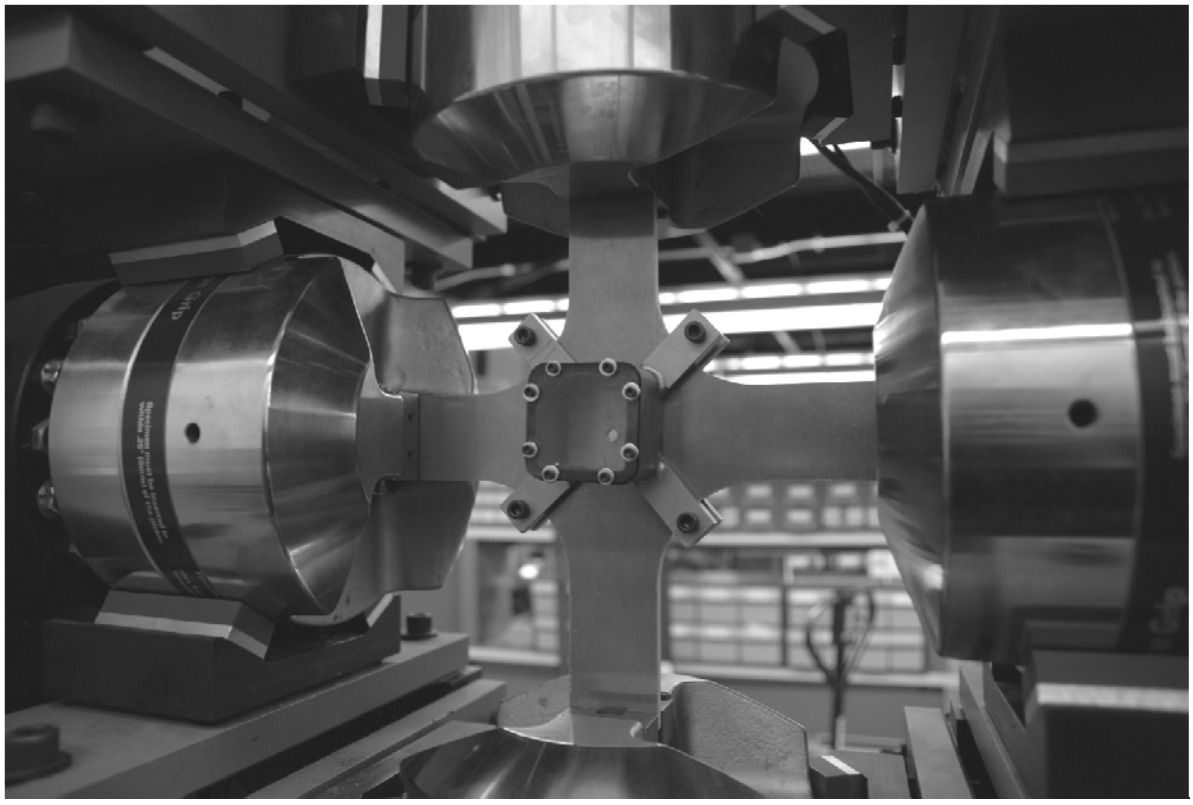

Figure 3.7: The water chamber used to expose the specimens to a saltwater environment.

After the tests the fracture surfaces were cut from specimen as shown in Figure 3.8 by using a band saw with the intention that the surfaces could be examined by a scanning electron microscope (SEM). SEM images of fracture surfaces were taken by FEI Quanta 450. A fractographical analysis was performed on the fractured specimens and the images were compared to the experimental data. During the examination, the acceleration voltage was set to 5.00 kV. The fracture surfaces from all tests were analyzed with different magnification, by changing horizontal field width (HFW). Microstructure was examined in detail, throughout the fracture surface. Especially microstructures at the crack initiation at the through pit were examined for all four cases to see the differences. In addition, by using scanning electron microscope striation measuring was performed to evaluate the accuracy of da/dN values at selected crack lengths.

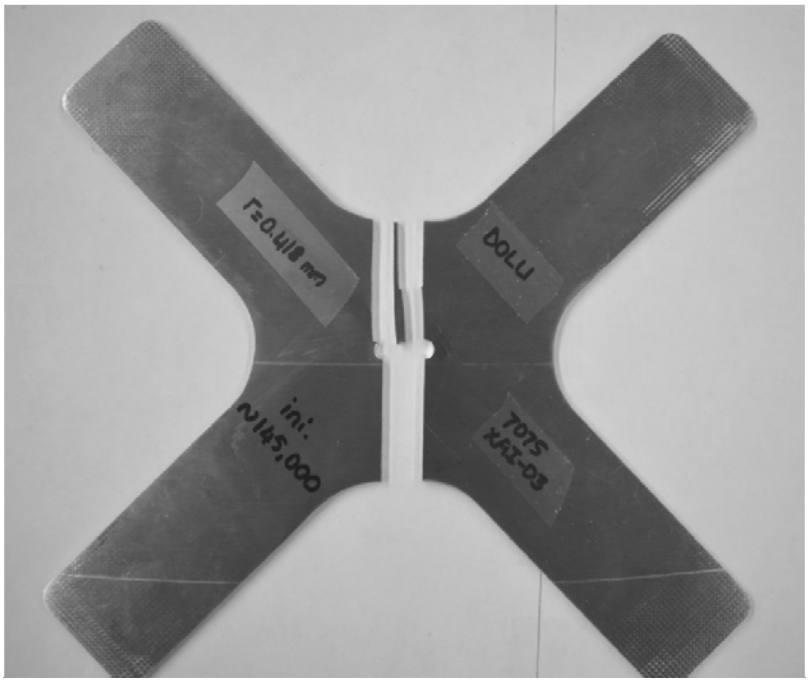

Figure 3.8: The cut of the fracture surface from the specimen.

3.4 Finite Element Modeling

As mentioned in Section 3.3, there is a closed form solution for calculating stress intensity factors for a crack originating from a circular hole under biaxial stress as given in equations 3.1, 3.2, and 3.3. For the experimental tests the results from these equations were used, after then to verify the results from the equations a finite element analysis was used. The specimens were analyzed by Abaqus, which is widely used software for finite element analysis. The analysis provided the range of stress intensity factor, ΔK_I. For modeling specimens, quadrilateral plane stress elements with quadratic interpolation and linear static stress analysis finite element modeling, which is the most common type of FEA, were used. Throughout the modeling procedure of biaxial and uniaxial specimens in Abaqus, the following assumptions were made [20]:

(1) The material was homogeneous and isotropic.

(2) The mechanical properties of the aluminum alloy given in Table 3.2 were constant.

(3) There were no flaws other than the corrosion pit.

(4) For all specimens the crack initiated from the corrosion pit.

(5) For the cruciform specimens the applied loads were 45° to the crack path.

(6) For the uniaxial specimens the applied loads were perpendicular to the crack path.

(7) Specimens were in plane stress condition.

(8) There was no variation in the applied loads [20].

Models of cruciform and uniaxial specimens were created using Abaqus graphical user interface, in the light of a very simple model involved; a flat plate with a centered hole like the specimen, shown in Figure 3.9. Dimensions of these models match the ones shown in Figures 3.1 and 3.2. After that finite element models, involving the corrosion pit and the crack profile from the edge of the hole, were produced. The radius of corrosion pit in the model was set at 0.4 mm for uniaxial specimen, and 0.36 mm for cruciform specimen, because these were the average values of the experimentally created pits. To reduce the complexity of the finite element models, the pits, used in the models, were assumed uniform half-circles. In the next step, the crack, originating from the edge of the pit, was created. For both specimens, i.e. cruciform and uniaxial, firstly two cases were modeled. To calculate the initial range of stress intensity factor, a realistic smallest

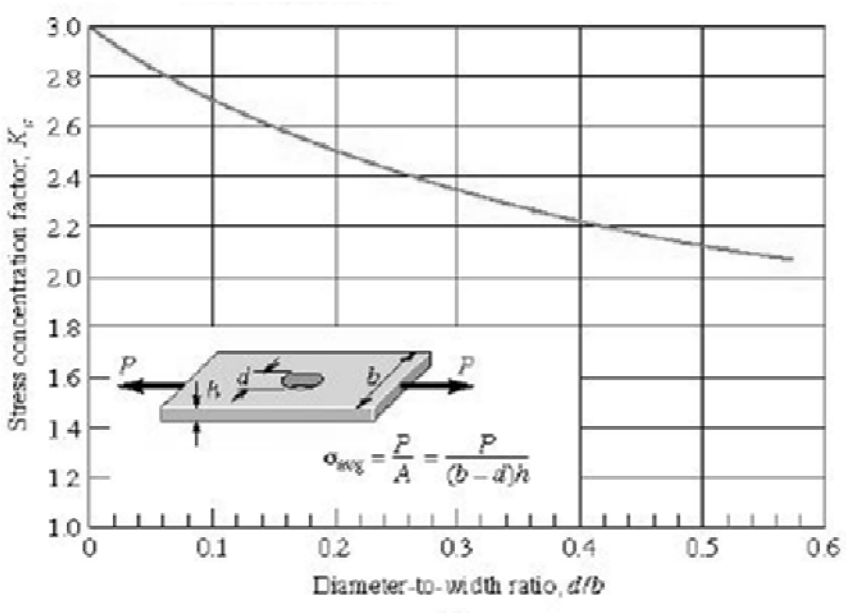

Figure 3.9: Specimen geometry used as the reference for the finite element model of the stress concentration caused by the circular hole [13].

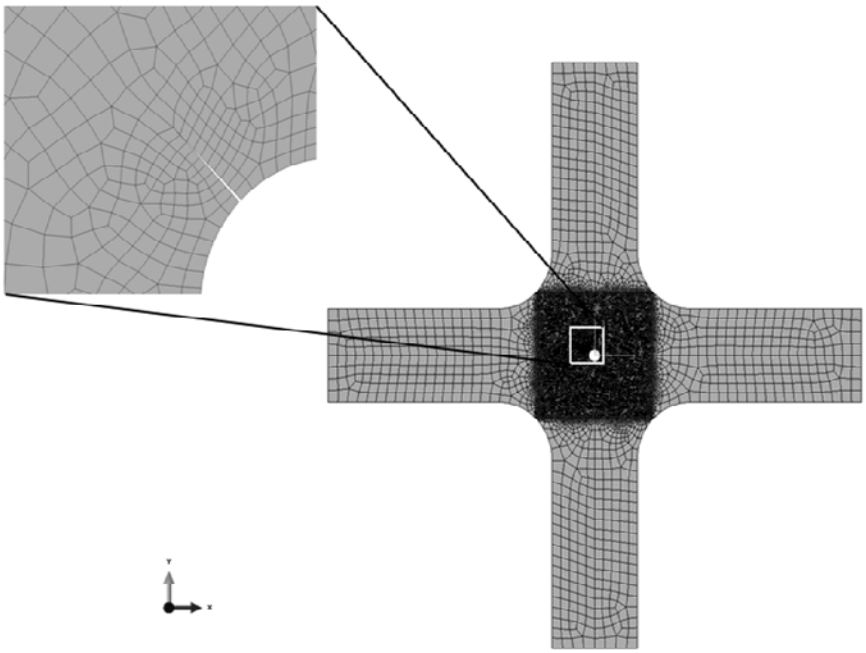

Figure 3.10: Cruciform specimen with global finite element mesh, and detail of the mesh in the vicinity of the crack tip.

visible crack length, 0.25 mm from the pit, was assumed to be the initial crack length. A cruciform specimen with global finite element mesh along with a detail of the mesh in the vicinity of the crack tip is shown in Figure 3.10. As shown in Simandjuntak's study [44], the mesh near the crack was refined so that accurate results were achieved.

A uniaxial specimen with global finite element mesh along with a detail of the mesh in the vicinity of the crack tip is shown in Figure 3.11.

After the initial conditions for each specimen were modeled, crack length of 15 mm from the pit were also modeled for both specimens. Once the first and the last conditions, several stress intensity factors were calculated for several crack lengths.

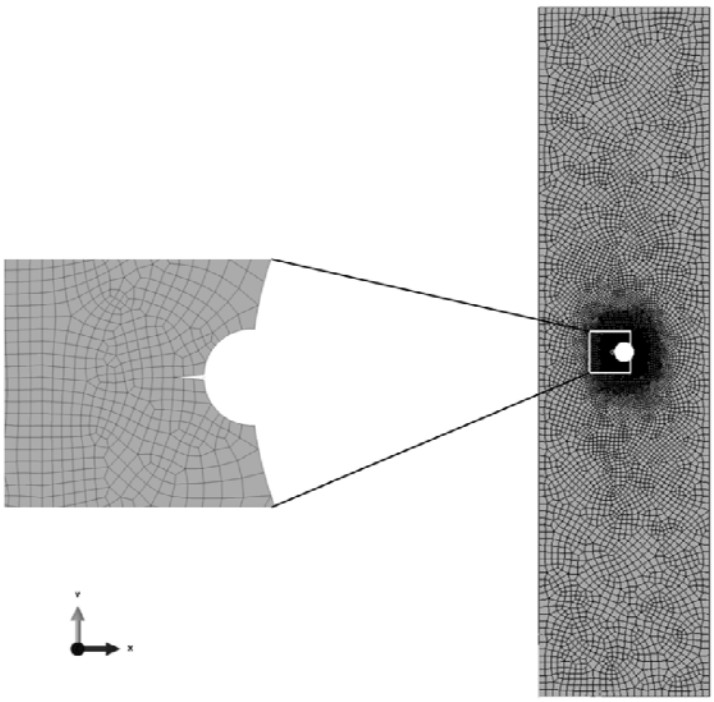

Figure 3.11: Uniaxial specimen with global finite element mesh, and detail of the mesh in the vicinity of the crack tip.

Interpolation was used to fill in the values between these data points. It was thought to be unnecessary and time consuming to create an Abaqus model for each of the crack sizes throughout the experiments.

For each experiment, these models were used to calculate the range of stress intensity factor, ΔK. To do this, applied stresses, $\Delta\sigma$, were entered as the loading conditions. The initial ranges of stress intensity factor from the Abaqus model were within 6% of the value given by equations 3.1, 3.2, 3.3, and 3.4 under the same loading and geometric conditions, as shown in Table 3.4. The small differences in the results between the closed form and finite element analyses solution is probably a result of the

Table 3.4: ΔK values predicted by Kaminskii's solution and the ΔK values calculated by Abaqus for biaxial loading condition.

Specimen	Initial ΔK (Kaminskii's Solution) ($MPa*m^{0.5}$)	Initial ΔK (Abaqus Model) ($MPa*m^{0.5}$)
XAI-01	10.0	9.47
XAI-02	4.1	3.89
XAI-03	5.95	5.63
XAI-04	7.36	6.93
XSI-01	10.0	9.47
XSI-02	6.66	6.28
XSI-03	4.04	3.84
XSI-04	3.35	3.14

assumption of the equation: the equation assumes infinitely wide plates. The experimental specimens do not meet this assumption, thus, minor deviation from the equation is likely.

In Appendix A, Figures A.1 to A.16 show the final meshes of the following four models, which were developed to calculate the range of stress intensity factor, ΔK:

(1) Uniaxial specimen having a crack length of 0.25 mm,

(2) Uniaxial specimen having a crack length of 15 mm,

(3) Cruciform specimen having a crack length of 0.25 mm,

(4) Cruciform specimen having a crack length of 15 mm.

4. Results and Discussion

4.1 Chapter Overview

This chapter presents the results from all experiments conducted for this research. The results include pictures of crack propagation path for all four cases, plots relating the range of stress intensity factor to the required number of cycles for a fatigue crack to initiate, plots of the crack growth rate as a function of stress intensity range, in addition to the analysis of the SEM images. The crack paths for uniaxial and biaxial loading conditions in ambient air and salt water environments are discussed in section 4.2, the results for the biaxial fatigue tests on the cruciform specimens with through pits are mentioned in section 4.3, the results for the uniaxial tests on the uniaxial specimens with through pits are discussed in section 4.4, and fractographical results are presented in section 4.5.

Table 4.1: Summary of all test results.

Specimen	R	Δσ (MPa)	a (mm)	$N_{initiation}$ (cycles)	Initial ΔK ($MPa*m^{0.5}$)	F_{max} (N)
XAI-01	0.1	190	0.353	17,006	9.47	29,993
XAI-02	0.1	78	0.633	1,000,000	3.89	12,253
XAI-03	0.1	113	0.418	140,000	5.63	17,768
XAI-04	0.1	139	0.405	45,000	6.93	22,004
XSI-01	0.1	190	0.378	8,698	6.83	29,993
XSI-02	0.1	126	0.329	50,480	4.53	19,900
XSI-03	0.1	77	0.358	203,218	2.77	12,082
XSI-04	0.1	63	0.33	1,000,000	2.26	10,007
SAI-01	0.1	36	0.4425	1,000,000	3.77	6,462
SAI-02	0.1	176	0.41	1,929	18.45	31,663
SAI-03	0.1	117	0.39	5,828	12.27	20,952
SAI-04	0.1	102	0.365	10,493	10.69	18,338
SAI-05	0.1	62.505	0.345	51,000	6.55	11,219
SSI-01	0.1	43.078	0.345	88,977	4.52	7,732
SSI-02	0.1	56.94	0.482	24,854	5.97	10,220
SSI-03	0.1	34.2	0.4	160,000	3.59	6,139
SSI-04	0.1	31.59	0.491	770,000	3.31	5,670

4.2 Crack Path

Figure 4.1 shows the crack paths for all four cases in ambient air and salt water environments. In the ambient air environment, the uniaxial fatigue case had a crack in x-direction or horizontal direction. The biaxial fatigue tests had also essentially similar crack paths as in the case of uniaxial fatigue i.e. along x-axis with a slight deviation from the center line. In the case of salt water environment, crack paths for uniaxial and biaxial cases were also along the x-axis with negligible deviation from this straight path in comparison to the corresponding cases in ambient air environment.

The direction of resultant force in biaxial fatigue tests was $\pm 45^0$. Uniaxial fatigue has the resultant force in the y-direction. Thus, the crack path is expected to be

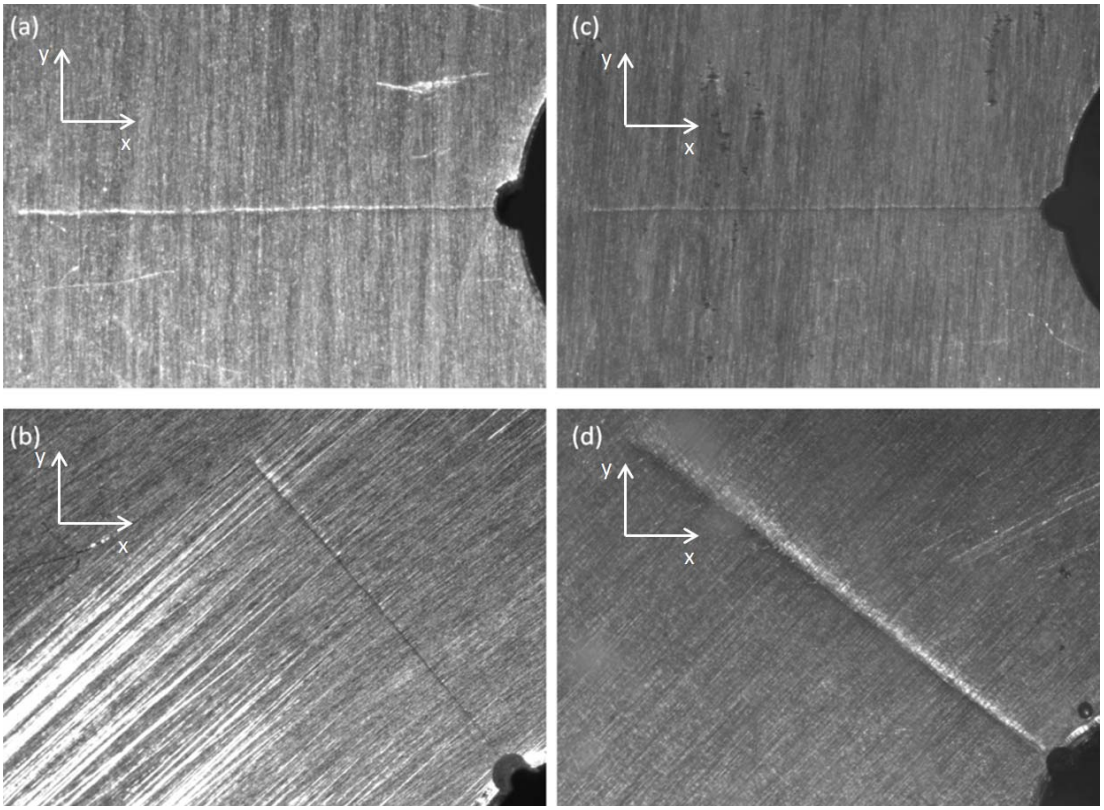

Figure 4.1: Crack propagation paths for all four cases; in ambient air (a) uniaxial, (b) biaxial (λ=1) , and in salt water environment (c) uniaxial, (d) biaxial (λ = 1).

perpendicular to the resultant force, i.e. the uniaxial fatigue crack path will be along the x-axis. Any deviation from this direction can be due to the microstructural effects.

4.3 Results of Biaxial Fatigue with Through Pits

Biaxial tests on the cruciform specimens with through pits were conducted in the light of the previous studies by Misak et al. [34, 35, 36]. Fatigue crack initiated and grew for ΔK's of 5.63, 6.93, and 9.47 MPa*$m^{0.5}$ in ambient laboratory air, for ΔK's of 2.77, 4.53, and 6.83 MPa*$m^{0.5}$ in saltwater (3.5% NaCl) environment. On the specimen XAI-02 with initial ΔK = 3.89 MPa*$m^{0.5}$ in the air environment, and the specimen XSI-04 with initial ΔK = 2.26 MPa*$m^{0.5}$ in the saltwater environment crack did not initiate after 1 million cycles so these experiments were terminated. The crack length versus the number of cycles for the specimens that had crack initiation are shown in Figures B.1, B.2, B.3, B.4, B.5, and B.6 in Appendix B. Similarly, the da/dN vs. ΔK curves are shown in Figures B.7, B.8, B.9, B.10, B.11, and B.12 in Appendix B. The da/dN vs. ΔK curves were obtained from the experimental data. During the experiments, continuous monitoring of the crack length (a) as a function of the number of load cycles (N) was conducted. The crack length versus the number of cycles curve was plotted and a trend line was applied using Microsoft Excel [20]. Since during some experiments the cracks would be unnoticeable until a realistic visible length, with the help of trend line, crack initiation cycle was determined more accurately than the camera monitoring method. Using this accurate data, the number of cycles until initiation vs. initial ΔK was plotted as shown in Fig. 4.2.

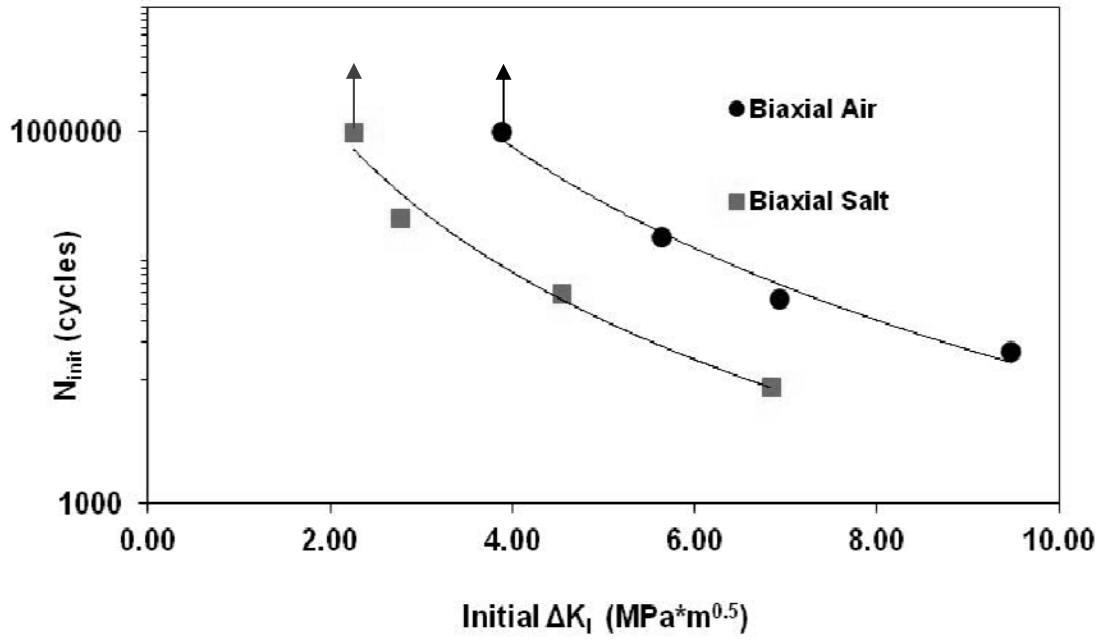

Figure 4.2: Plot of the number of cycles until initiation vs. initial ΔK for the cruciform specimens exposed to both air and saltwater (3.5 %) environments.

Furthermore, the crack growth rate curves were calculated by using the derivative of the trend line from the crack length versus the number of cycles curve. As trend line removed some of the data scatter, the derivate of this further reduced the data scatter of manual experimental measurements.

The combined da/dN data for all of the cruciform specimens is shown in Fig. 4.3a. In the figure, the trend lines stand for the data from Misak et al experiments [34, 35, 36] and the points are from the current experiments. The crack growth rate for R=0.5 was higher than the one with R=0.1.

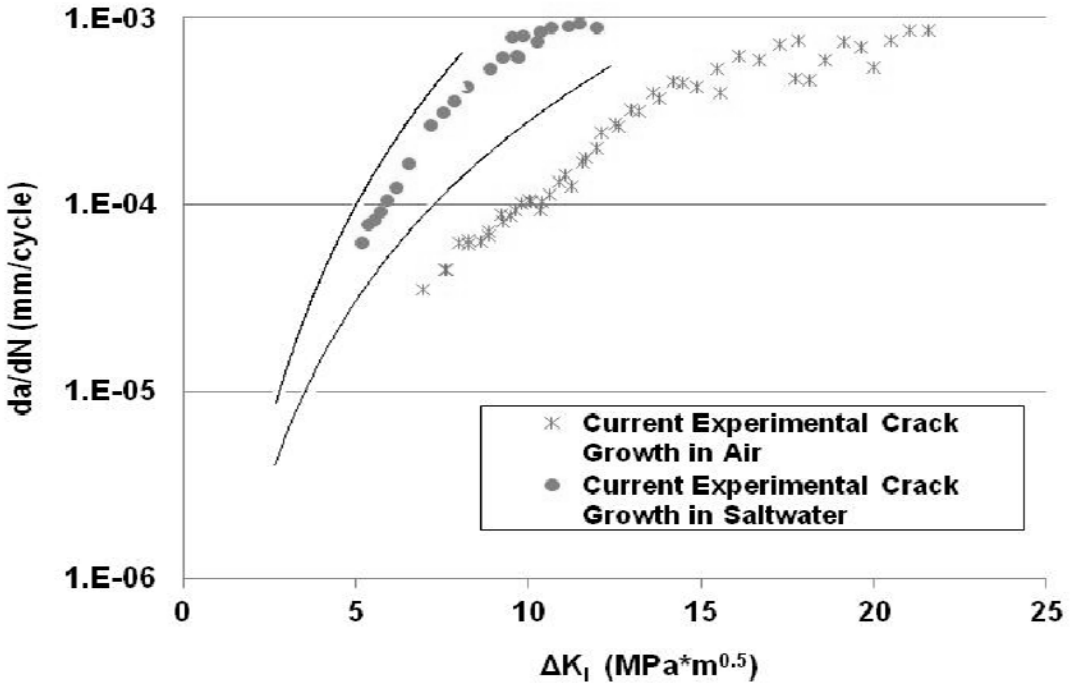

Figure 4.3a: The crack growth rate of the cruciform specimens as a function of the stress intensity range.

Figure 4.3b shows crack growth rate of the cruciform specimens as a function of the stress intensity factor in logarithmic scale for the present experiments. From these curves Paris constants, C and m, were calculated and compared with the ones from the experiments conducted by Misak et al. [34, 35, 36]. For the current experiments the constant were calculated as C= 1.09E-07, and m=3.01 in ambient air. For the previous experiments these constants were C= 2.28.E-07, and m=3.09.

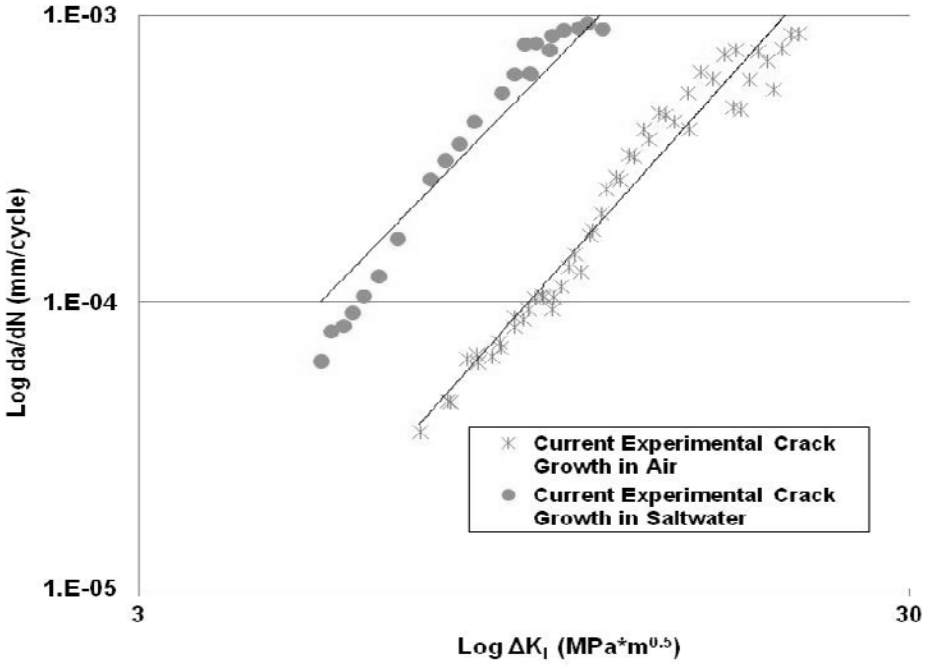

Figure 4.3b: The crack growth rate of the cruciform specimens as a function of the stress intensity range in logarithmic scale.

4.4 Results of Uniaxial Fatigue with Through Pits

In addition to experiments under biaxial fatigue condition in ambient air and salt water (3.5% NaCl) environments, for comparison fatigue crack initiation and growth behavior under uniaxial fatigue in ambient air and salt water environments was also characterized. During the uniaxial fatigue experiments, fatigue crack initiated and grew for ΔK's of 4.33, 6.55, 10.69, 12.27, and 18.45 MPa*m$^{0.5}$ in ambient laboratory air, for ΔK's of 3.31, 3.59, 4.52, and 5.97 MPa*m$^{0.5}$ in saltwater (3.5% NaCl) environment. For the specimen SAI-01 with initial ΔK = 3.77 MPa*m$^{0.5}$ in ambient air crack did not initiate after 1 million cycles so this test was terminated. The crack length versus the number of cycles for the uniaxial specimens that had crack initiation and growth are

shown in Figures C.1, C.2, C.3, C.4, C.5, C.6, C.7, C.8, and C.9 in Appendix C. Figure 4.4 shows the plot of the number of cycles until crack initiation vs. initial ΔK.

Similarly, the da/dN vs. ΔK curves are shown in Figures C.10, C.11, C.12, C.13, C.14, C.15, C.16, C.17, and C.18 in Appendix C. These plots were developed using the same trend line method described in Section 4.3.

Additionally a comparison of the effect of stress ratio on crack initiation is shown in Figure 4.5a. In the figure, the crack initiation data from the experiments with R=0.5 conducted by Hunt [20] and the current crack initiation data with R=0.1 are plotted. For uniaxial fatigue with the stress ratio of 0.1 crack initiated later than the one with R=0.5 for a given ΔK value because of the crack closure effect.

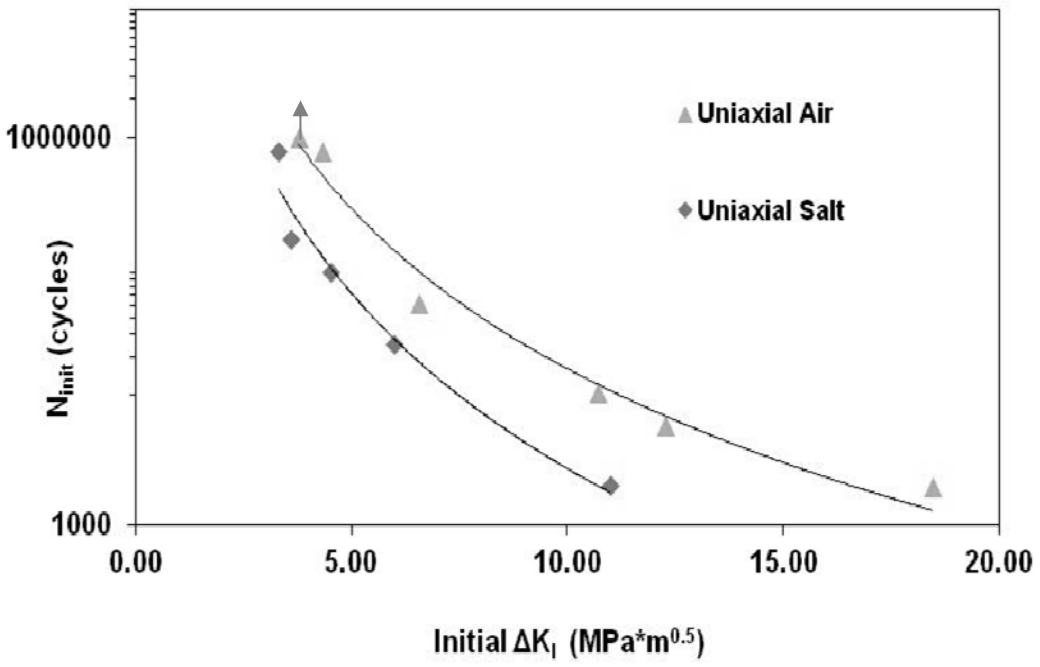

Figure 4.4: Plot of the number of cycles until initiation vs. initial ΔK for the uniaxial specimens exposed to both air and saltwater (3.5% NaCl) environments.

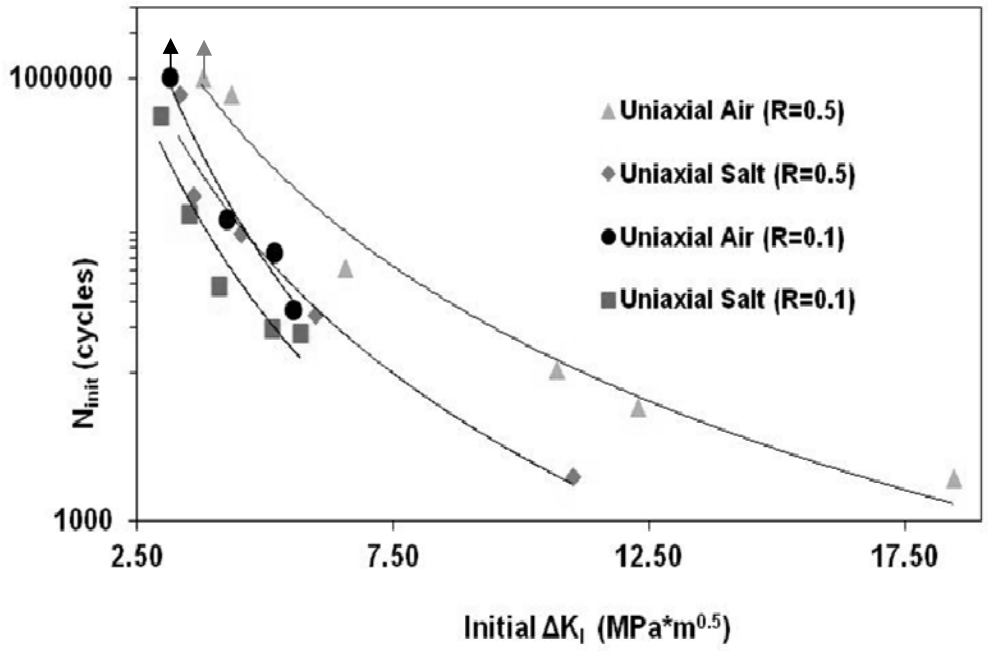

Figure 4.5a: Plot showing comparison of previous crack initiation data with current crack initiation data for uniaxial specimens with different stress ratios as a function of stress intensity range.

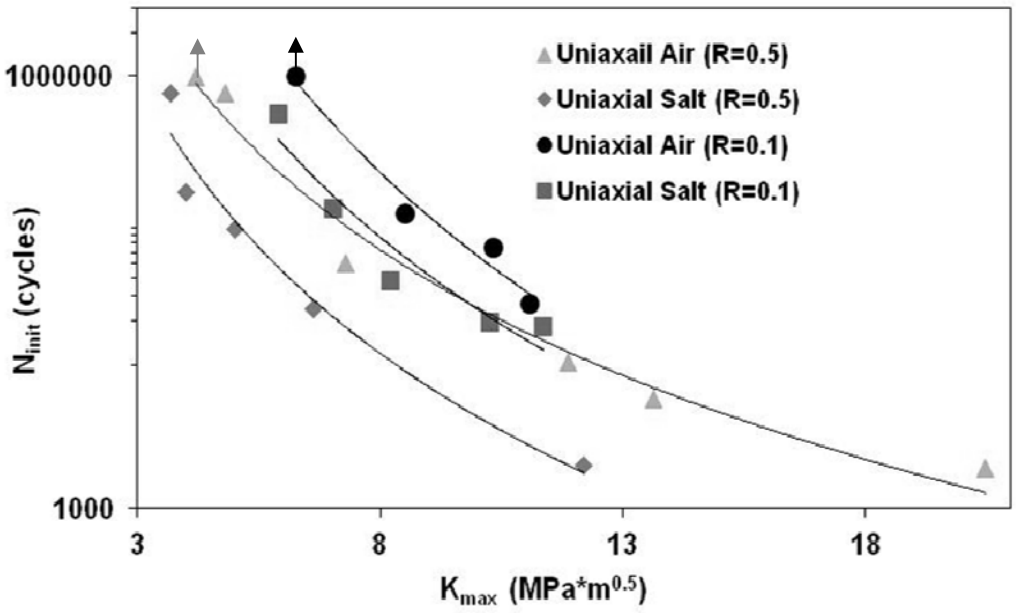

Figure 4.5b: Plot showing comparison of previous crack initiation data with current crack initiation data for uniaxial specimens with different stress ratios as a function of maximum stress intensity factor.

Furthermore crack initiation cycle data was drawn as a function of maximum stress intensity factor as shown in Figure 4.5b. This was done to see whether crack initiation cycle curves would tend to be similar or not. But the curves didn't coincide when the data was correlated to maximum stress intensity factor.

Figure 4.6a is a compilation of all of the crack growth rate data for uniaxial specimens. In this figure, the data points are from the current experiments, while the trend lines represent the data from the experiments carried out by Misak et al. [34, 35, 36]. The crack growth rate for R=0.5 was higher than the one with R=0.1.

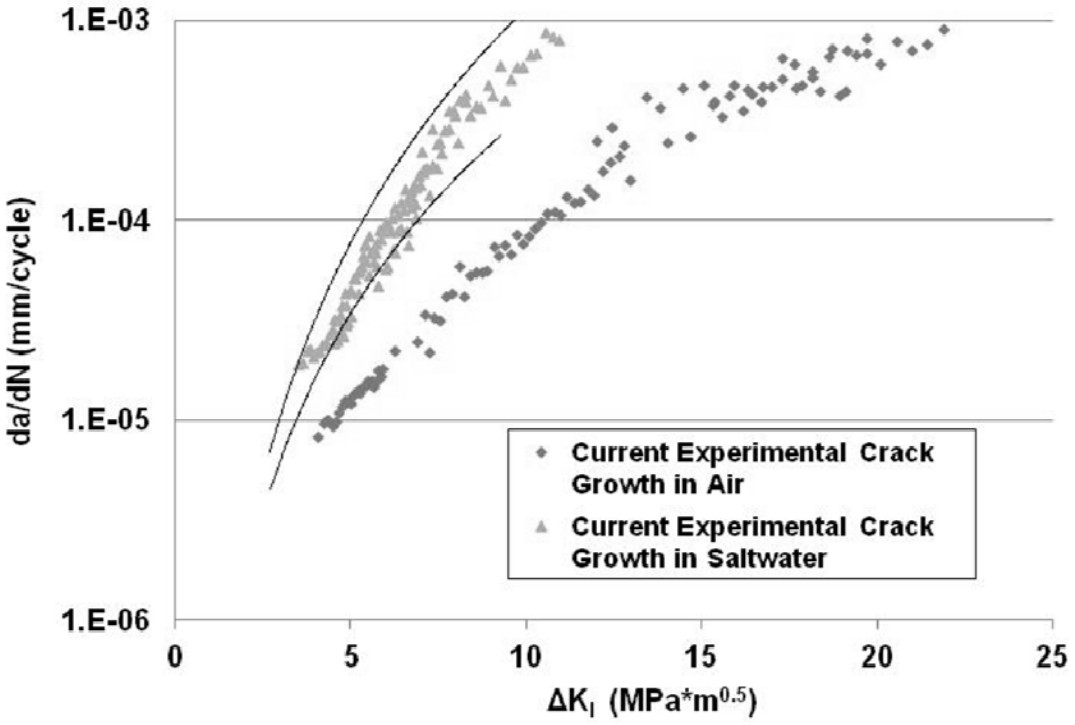

Figure 4.6a: The crack growth rate of the uniaxial specimens as a function of the stress intensity range.

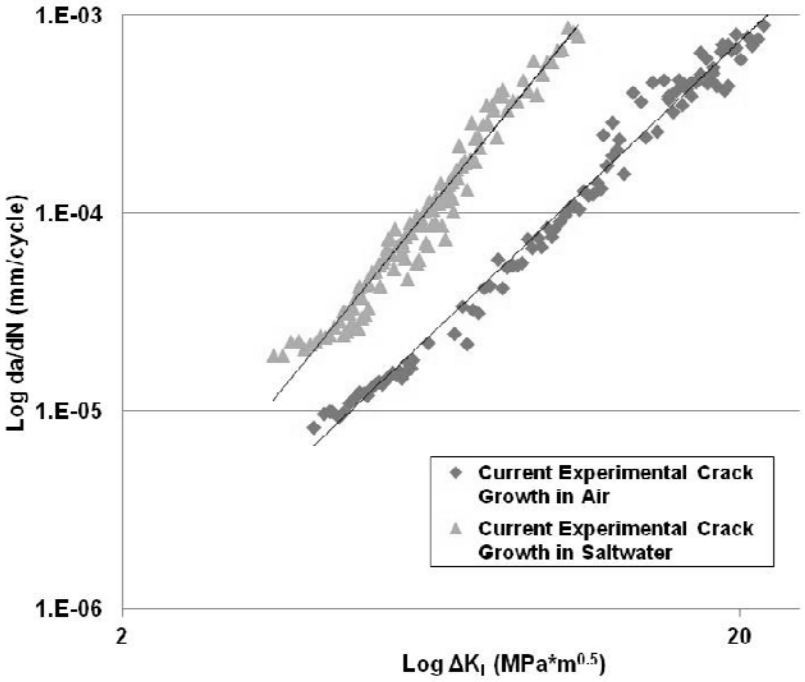

Figure 4.6b: The crack growth rate of the uniaxial specimens as a function of the stress intensity range in logarithmic scale.

Figure 4.6b shows crack growth rate of the uniaxial specimens as a function of the stress intensity factor in logarithmic scale for the present experiments. From these curves Paris constants, C and m, were calculated and compared with the ones from the experiments conducted by Misak et al. [34, 35, 36]. For the current experiments the constant were calculated as C= 1.03E-07, and m=2.96 in ambient air. For the previous experiments these constants were C= 2.28E-07, and m=3.11.

4.5 Fractography

After the tests, the fracture surfaces were cut from specimen by using a band saw. This allowed the fracture surfaces to be examined by a scanning electron microscope (SEM). Since the entire corrosion pit was visible, the actual pit size could be

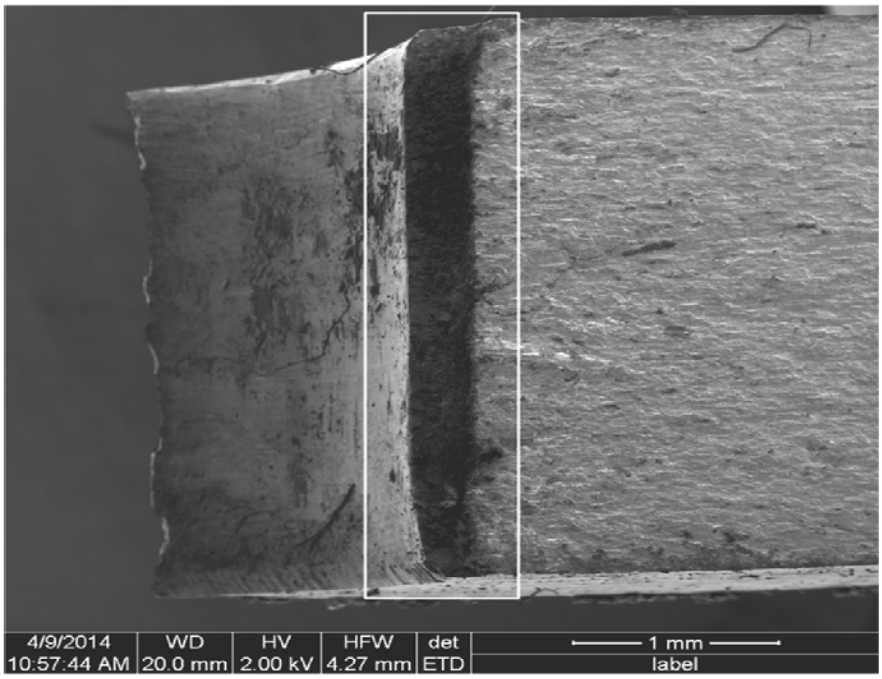

Figure 4.7: Top view of a through pit in air after the specimen was cut into two halves along the fatigue crack (4.27mm HFW).

measured with the SEM. An example of an entire through pit and a measurement example are shown in Figure 4.7 and 4.8, respectively. In addition to these examples, other SEM images of the fracture surfaces are shown in Appendix D.

As shown in Figure 4.8 several measurements along the length of the through pit were taken. The average pit size from each specimen was used in the related Abaqus model to compute the stress intensity factor. These updated ΔK values replaced the values previously calculated from the closed form solution of Kaminskii and Sailov [22] for biaxial loading condition.

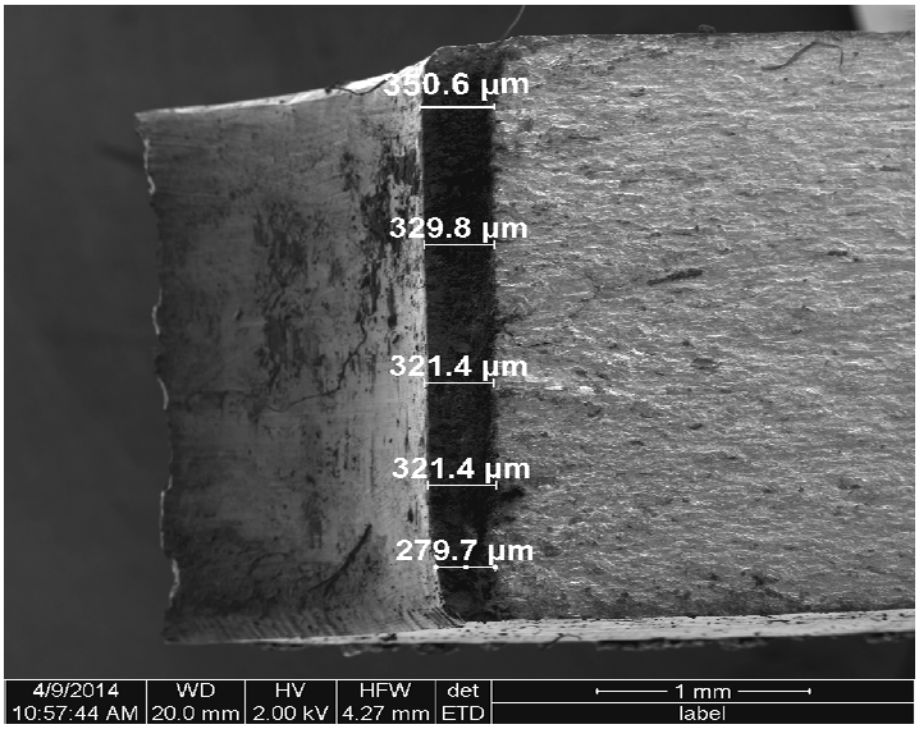

Figure 4.8: Top view of the through pit specimen SAI-05 using the SEM. Measurement of the pit was taken at several positions to calculate an average pit size.

The crack initiation and growth from the corrosion pit could be examined with significantly more detail using the SEM compared to optical microscope. Fracture surfaces with HFW of approximately 30 µm for all four cases are shown in Figure 4.9. In the case of uniaxial loading condition in ambient air, crack was along the plane of maximum mode I. The fracture surface was smooth, which is typical of planar slip dislocation mechanism. In biaxial loading condition in air there was smooth crack front but also there were some wavy slip dislocation mechanism and "v" shape formations as a result of biaxial force. In uniaxial loading condition in saltwater environment there were some oxide products, however majority of the surface showed planar slip. Finally in

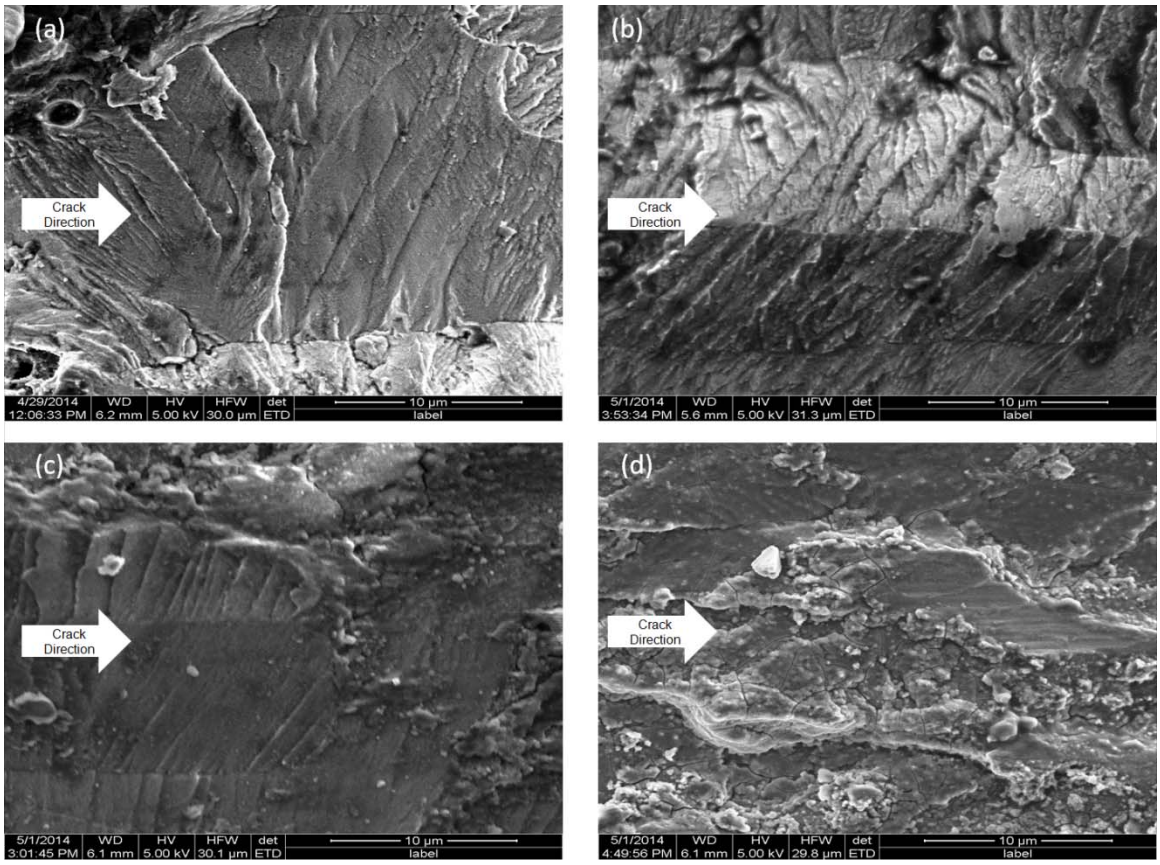

Figure 4.9: SEM images of crack surfaces for all four cases; in ambient air (a) uniaxial, (b) biaxial (λ=1), and in salt water environment (c) uniaxial, (d) biaxial (λ=1) with horizontal field width (HFW) of approximately 30 µm.

biaxial loading condition in saltwater environment, mud cracking occurred typically seen when the oxide layer is thick. The thicker oxide layer was a result of biaxiality: more corrosion products were developed and more hydrogen embrittlement occurred.

In addition, by using scanning electron microscope, striation measurements were performed to evaluate the accuracy of da/dN values at selected crack lengths. As shown in Table 4.1 and Figure 4.10 da/dN values was confirmed with striation measuring method which shows the accuracy of the calculations made during the research.

Table 4.2: Calculated da/dN values and the values from striation measuring method.

Specimen	Crack length (mm)	da/dN (mm/cycle)	Value from striation measuring method (µm)
SAI-05	5.738	8.36E-08	83.07
XAI-03	5.271	1.46E-07	142.2
SSI-03	11.74	1.43E-07	147.2
XSI-03	12.956	2.39E-07	249.4

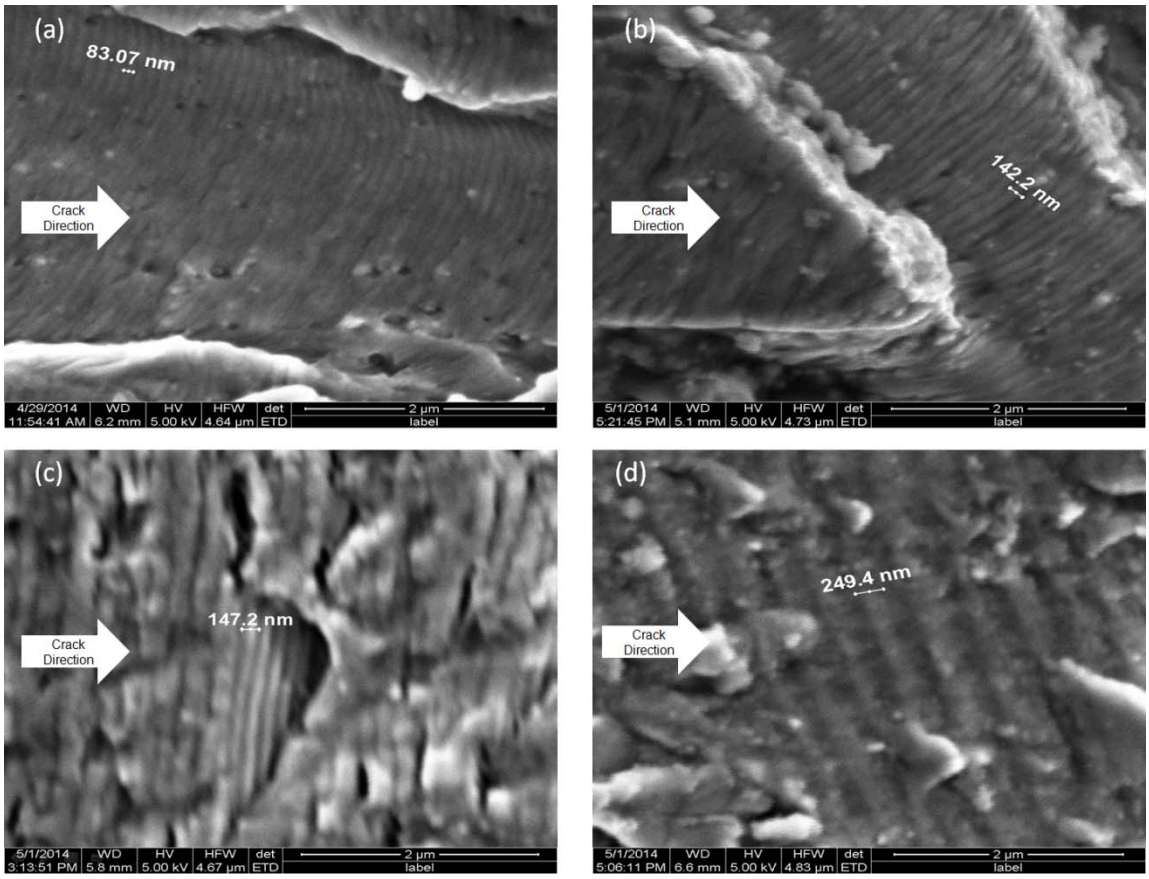

Figure 4.10: Striation details for all four cases; in ambient air (a) uniaxial, (b) biaxial (λ=1), and in salt water environment (c) uniaxial, (d) biaxial (λ = 1) with HFW of 4.6 µm.

4.6 Discussion of Results

As shown in Figure 4.11, as the stress intensity factor increases, the number of cycles until crack initiation decreases. The specimens that are exposed to saltwater environment build up fatigue cracks in lesser number of cycles than the ones that are exposed to laboratory air for both loading conditions. In ambient air number of cycles curves for biaxial and uniaxial loading conditions are almost equal, on the other hand in saltwater environment crack occurs in fewer cycles in biaxial loading condition comparison to uniaxial loading condition. This statement was justified by SEM examination, which was mentioned in the previous section.

The effect of stress ratio on crack initiation can be seen easily in Figure 4.5. Since with the R value of 0.5 the effects of crack closure was minimal, in the previous experiments with R=0.1 crack initiated earlier than present experiments for a given ΔK value.

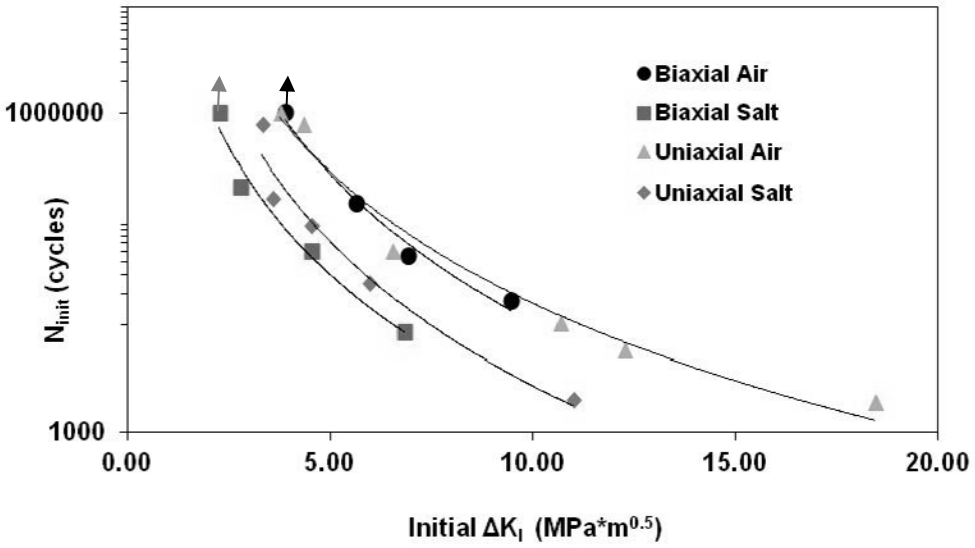

Figure 4.11: Plot showing required number cycles for fatigue crack initiation for all specimens.

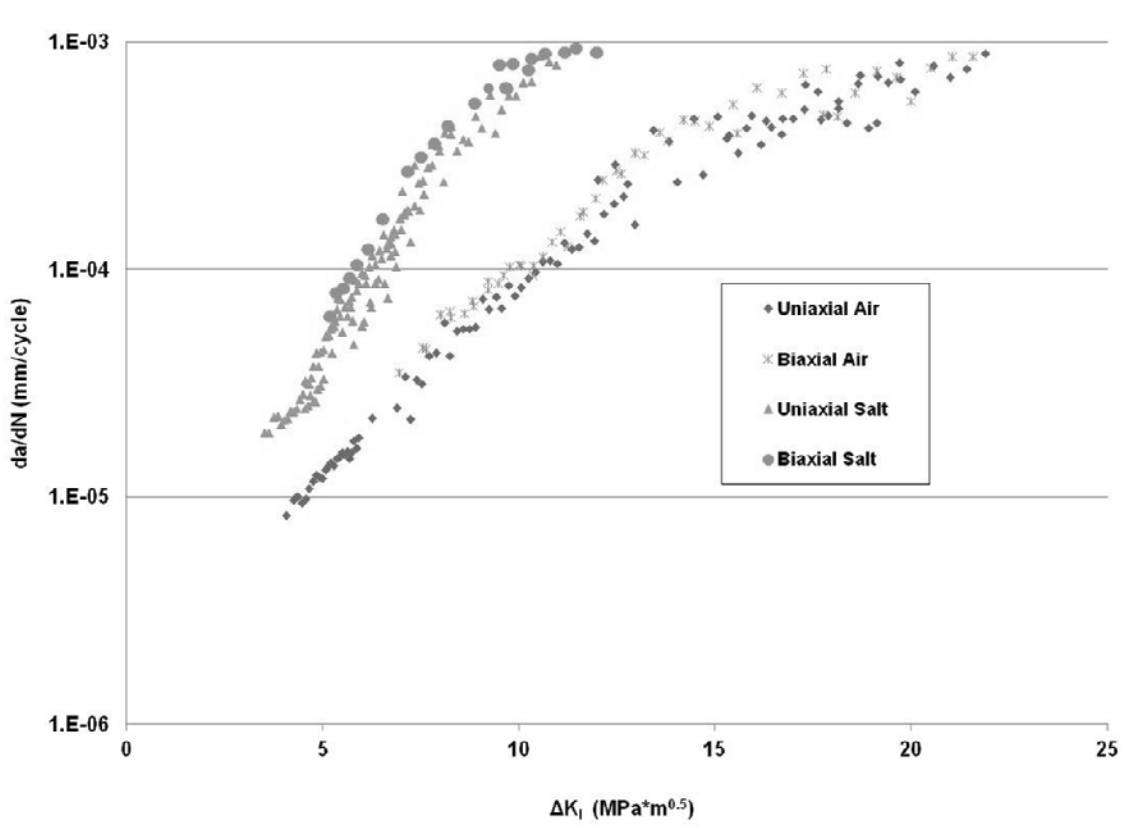

Figure 4.12: The crack growth rate of all specimens as a function of the stress intensity range.

Figure 4.12 shows the comparison of crack growth rates between air and saltwater environments for biaxial and uniaxial loading conditions. In ambient air environment biaxial and uniaxial crack growth rate curves almost coincide. But in saltwater environment biaxial specimens have faster crack growth rate than uniaxial specimens for a given ΔK value because of the biaxilality: more corrosion products go inside and more hydrogen embrittlement occur. Also, this figure shows that the crack growth rate is faster in the saltwater environment than the corresponding value in ambient air environment at a given ΔK in both loading conditions. This behavior is expected since saltwater environment is likely to cause the embrittlement at the crack tip. In general, there was

overall parallel shift of da/dN vs. ΔK relationship from right to left when test environment was changed from air to salt water in all tests [34]. Additionally, as shown in Figures 4.3 and 4.6, the crack growth rate for the experiments with R=0.5 is higher than the one with R=0.1 because the effects of crack closure.

5. Conclusions and Recommendations

5.1 Conclusions

In this study, the fatigue crack formation from a through corrosion pit at a circular hole in 7075-T6 aluminum subjected to biaxial loads in both an air and saltwater (3.5% NaCl) environment was investigated. Fracture mechanics approach was used to explore fatigue crack initiation and growth behaviors. The stress intensity range (ΔK) was the driving factor for determining the load applied to the specimens. These specimens were fatigued to failure using a MTS Planar Biaxial Testing machine. Number of cycles for crack initiation and fatigue crack growth rates were determined from these experiments. These results were compared to the data collected from the experiments conducted by Hunt [20] and Misak et al. [34, 35, 36]. Using a commercial finite element code, Abaqus, the models were created to determine the range of stress intensity factor (ΔK) for the test specimens accurately. Additionally, the SEM was used to examine the fracture surfaces of the specimens in detail.

Conclusions from this study may be summarized as followings:

(1) Under both uniaxial and biaxial loading conditions crack initiated and propagated coplanar with corrosion pit in ambient air and saltwater environments.

(2) Corrosive environment (3.5% NaCl) reduced the required number of cycles for crack initiation under uniaxial and biaxial loading conditions when compared to the ones in ambient laboratory air. This reduction ranged from 86% to 90% for biaxial loading condition and from 75% to 83% for uniaxial loading condition.

(3) In all tests corrosive environment (3.5% NaCl) shortened the fatigue life of the specimens under uniaxial and biaxial loading conditions.

(4) In ambient air required numbers of cycles for crack initiation under biaxial and uniaxial loading conditions were almost the same. On the other hand in saltwater environment crack occured in lesser number of cycles in biaxial loading condition in comparison with uniaxial loading condition. The reduction was around 33%.

(5) The crack growth rate was faster in the saltwater environment than the corresponding value in ambient air environment at a given ΔK in both loading conditions.

(6) In ambient air environment biaxial and uniaxial crack growth rates almost coincided. But in saltwater environment biaxial specimens had larger crack growth rate than uniaxial specimens.

(7) On the specimens with the stress ratio of 0.1 crack initiated later than the one with R=0.5 for a given ΔK value because of the crack closure effect. Also the crack growth rate for the experiments with R=0.5 was higher than the one with R=0.1.

(8) Abaqus provided an accurate method for modeling biaxial (cruciform) and uniaxial specimens because it included the pit and finite geometry in the analysis. The stress intensity factors from Abaqus and calculated by closed form solution (Equations 3.2 and 3.3) agreed within 6% for biaxial loading condition.

5.2 Recommendations for Future Research

There are a wide range of test variables that could be changed to provide useful information to fully characterize crack initiation and growth behavior from corrosion pit on 7075-T6 aluminum alloy. While the research objectives were met on the current study, another research might focus on crack initiation and growth behavior of 7075-T6 from corner corrosion pit under biaxial loading condition which is lacking in the field.

Further studies in fatigue crack growth from corrosion pits under biaxial loading on different materials should be conducted. Additionally, these experiments should be extended with different geometry of the test specimens, different phases, different stress ratios, as well as different biaxiality ratios.

Appendix A: Finite Element Data

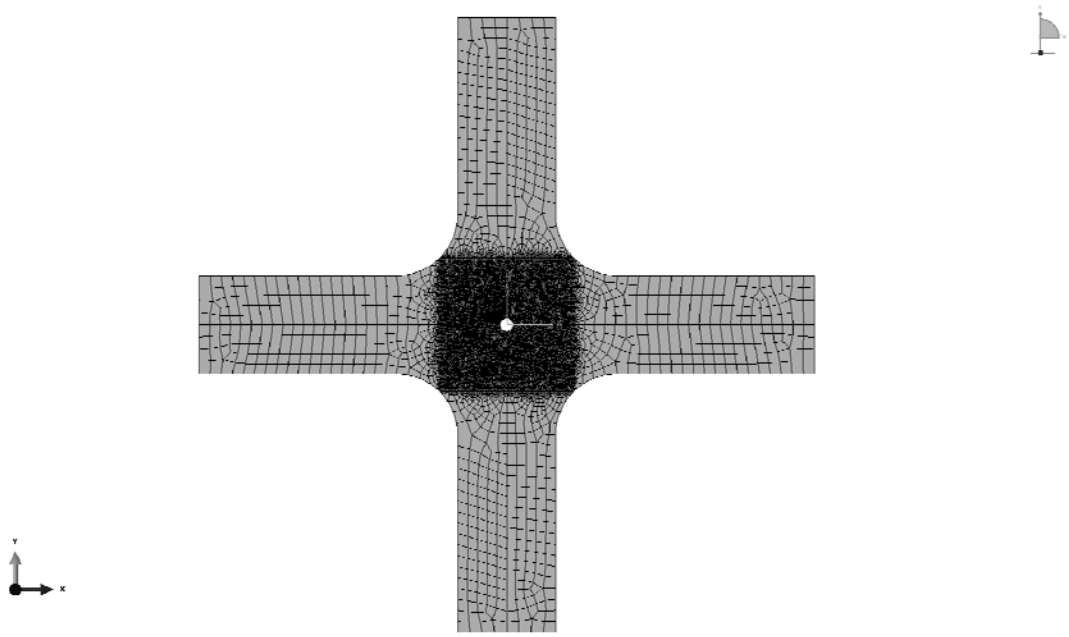

Figure A.1: Global finite element mesh of cruciform specimen (XAI-01) with the crack length of 0.25 mm.

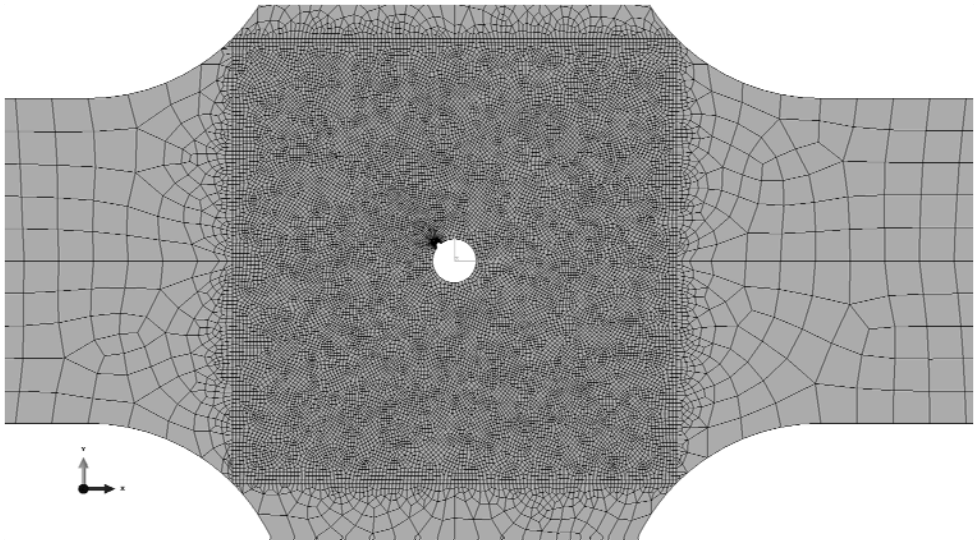

Figure A.2: Refined mesh of cruciform specimen (XAI-01) with the crack length of 0.25 mm in the vicinity of stress concentration.

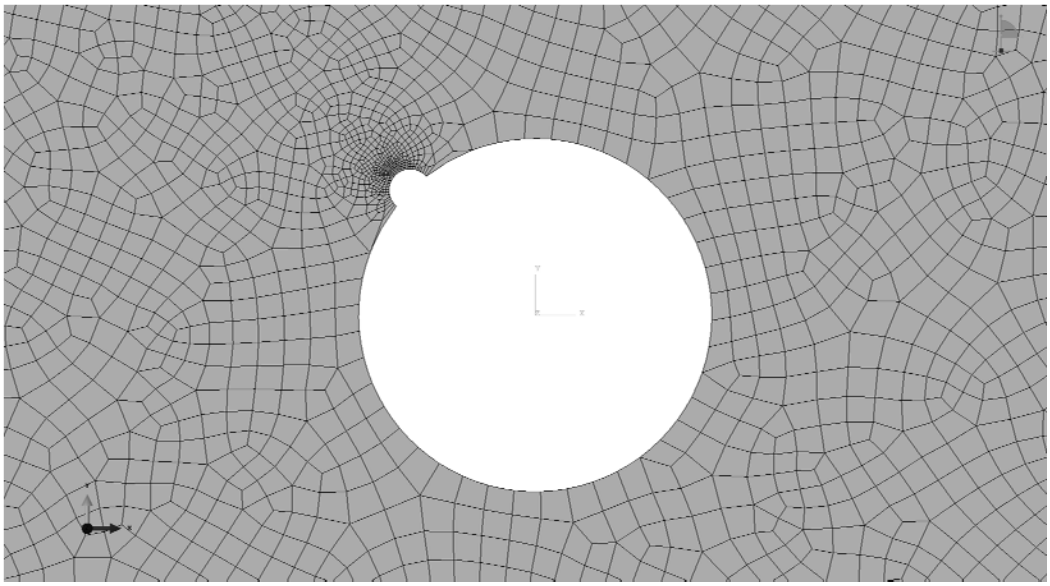

Figure A.3: Refined mesh of cruciform specimen (XAI-01) with the crack length of 0.25 mm in the vicinity of crack tip.

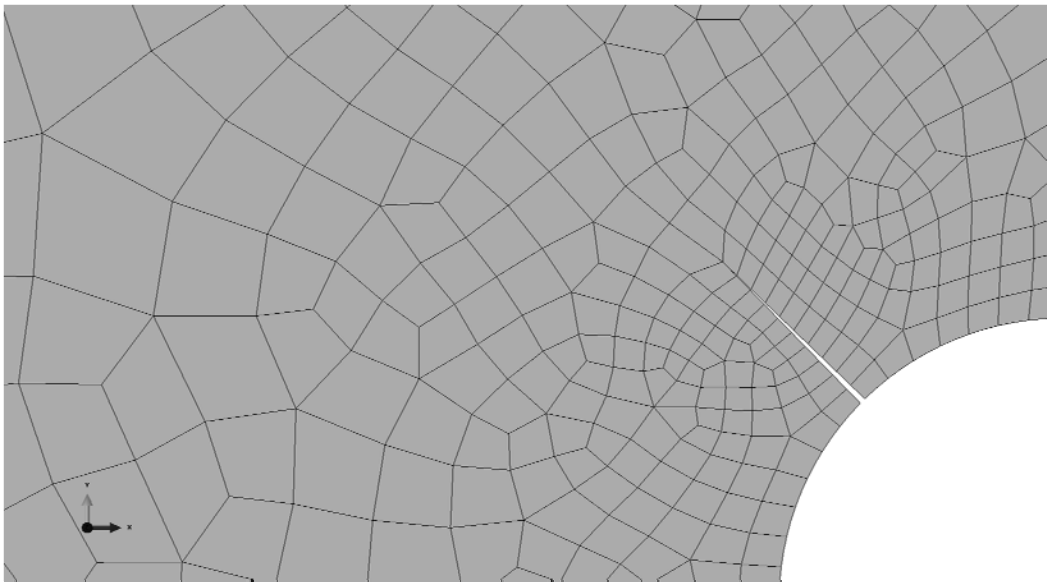

Figure A.4: Detail of the mesh of cruciform specimen (XAI-01) with the crack length of 0.25 mm in the vicinity of crack tip.

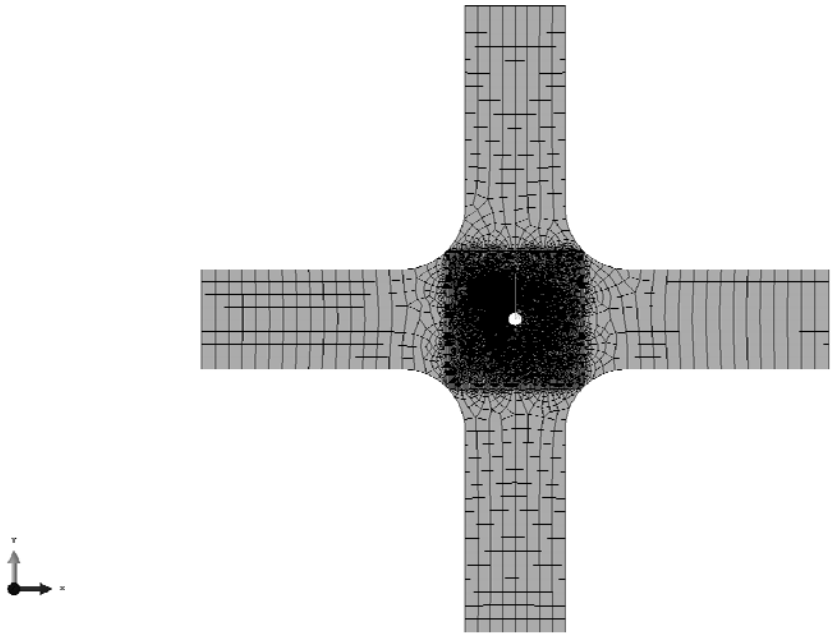

Figure A.5: Global finite element mesh of cruciform specimen (XAI-01) with the crack length of 15 mm.

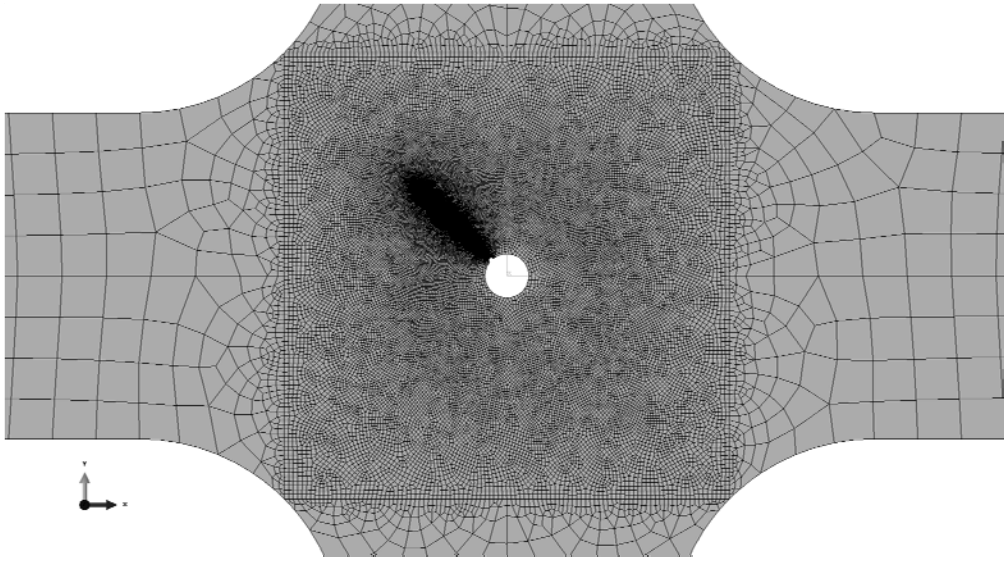

Figure A.6: Refined mesh of cruciform specimen (XAI-01) with the crack length of 15 mm in the vicinity of stress concentration.

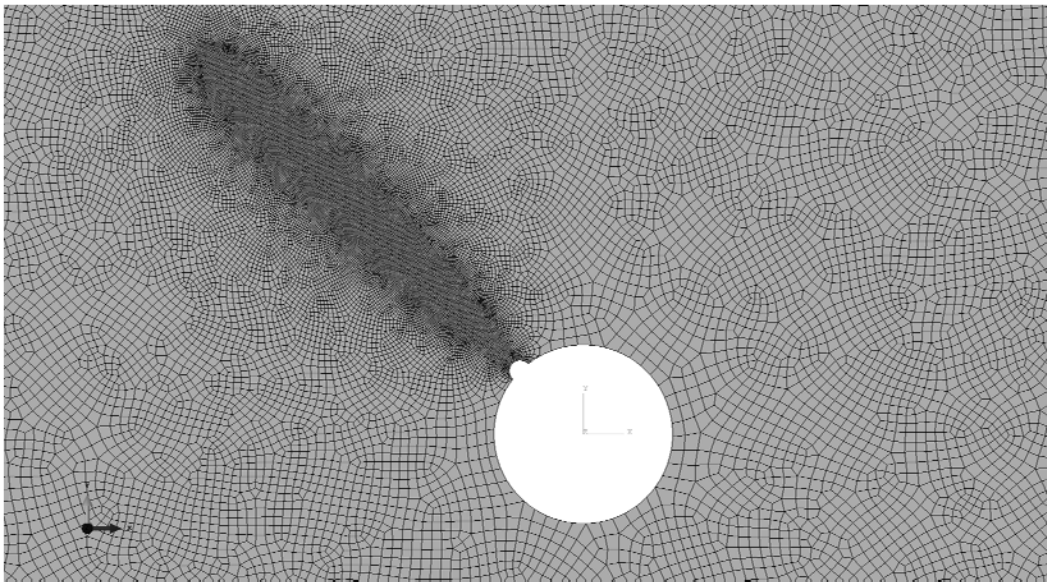

Figure A.7: Refined mesh of cruciform specimen (XAI-01) with the crack length of 15 mm in the vicinity of crack tip.

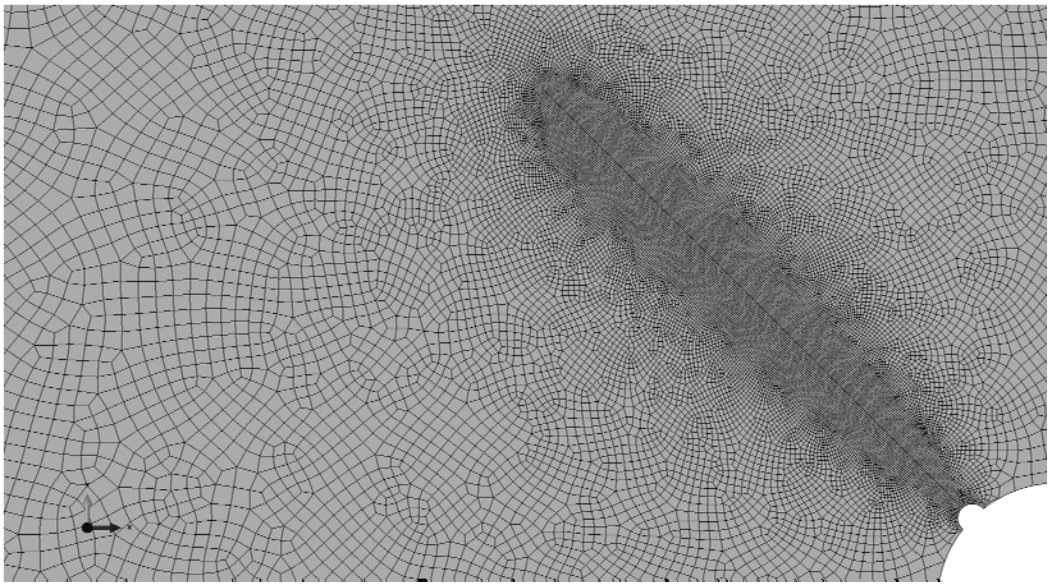

Figure A.8: Detail of the mesh of cruciform specimen (XAI-01) with the crack length of 15 mm in the vicinity of crack tip.

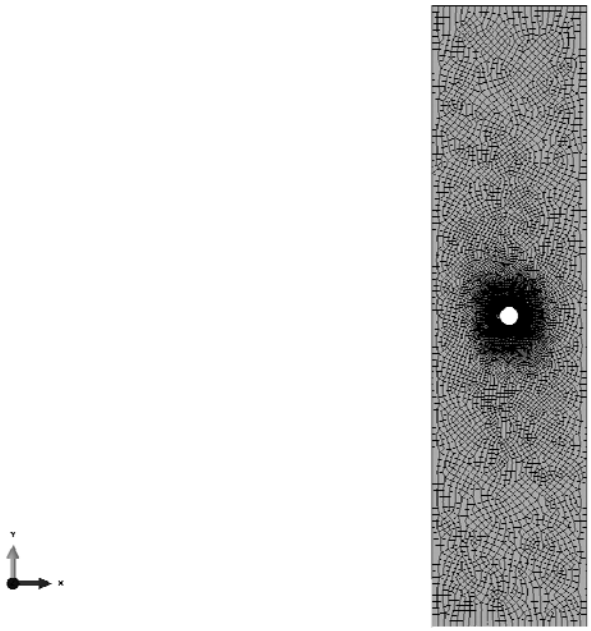

Figure A.9: Global finite element mesh of uniaxial specimen (SAI-01) with the crack length of 0.25 mm.

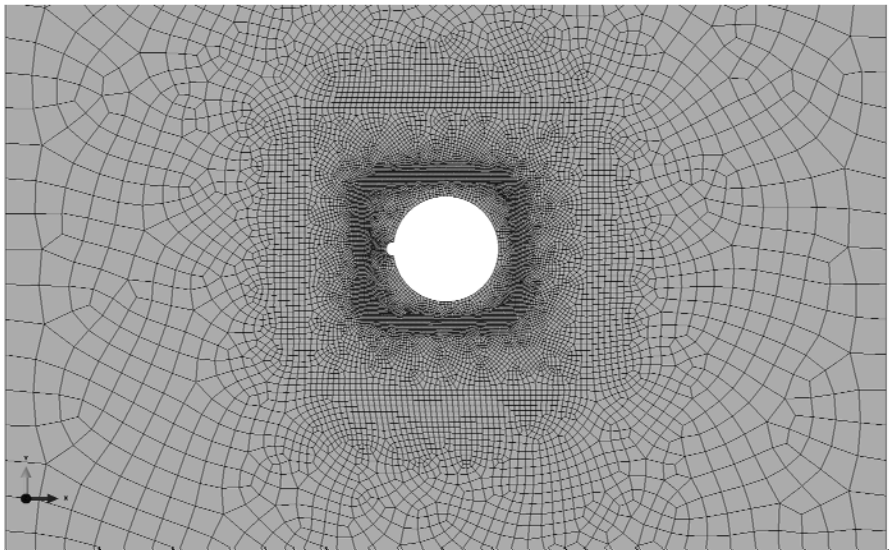

Figure A.10: Refined mesh of uniaxial specimen (SAI-01) with the crack length of 0.25 mm in the vicinity of stress concentration.

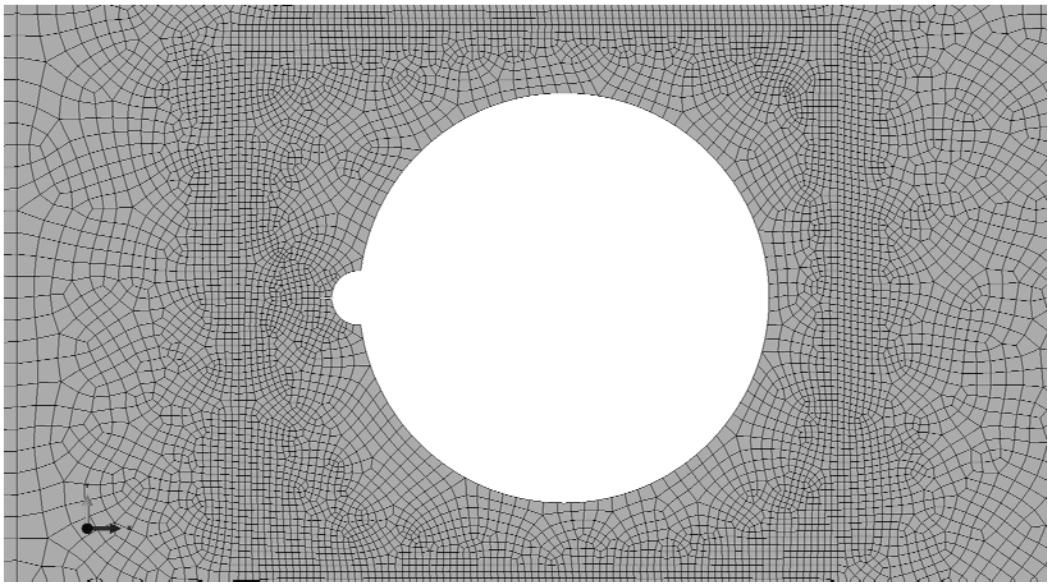

Figure A.11: Refined mesh of uniaxial specimen (SAI-01) with the crack length of 0.25 mm in the vicinity of crack tip.

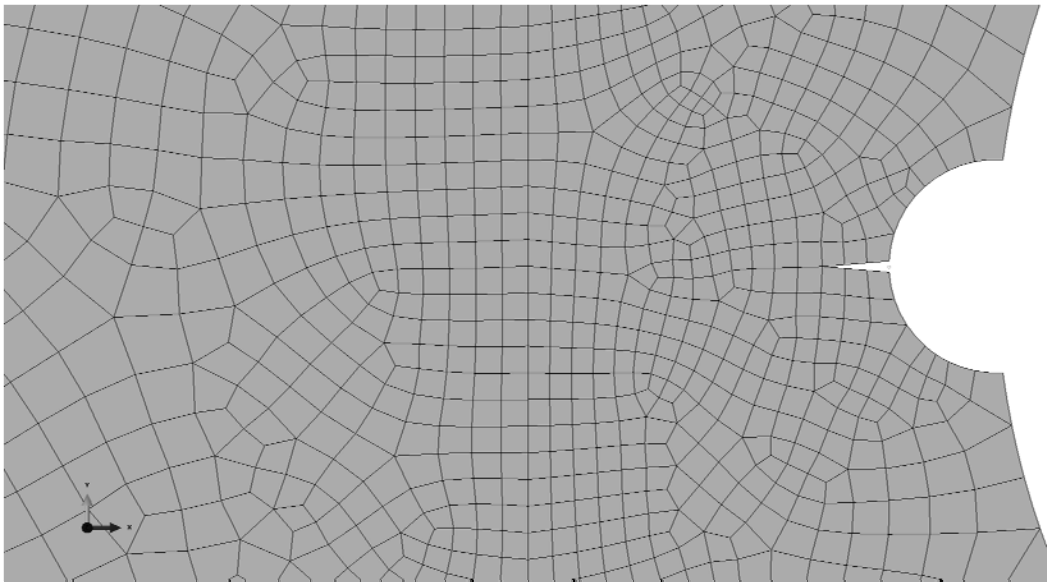

Figure A.12: Detail of the mesh of uniaxial specimen (SAI-01) with the crack length of 0.25 mm in the vicinity of crack tip.

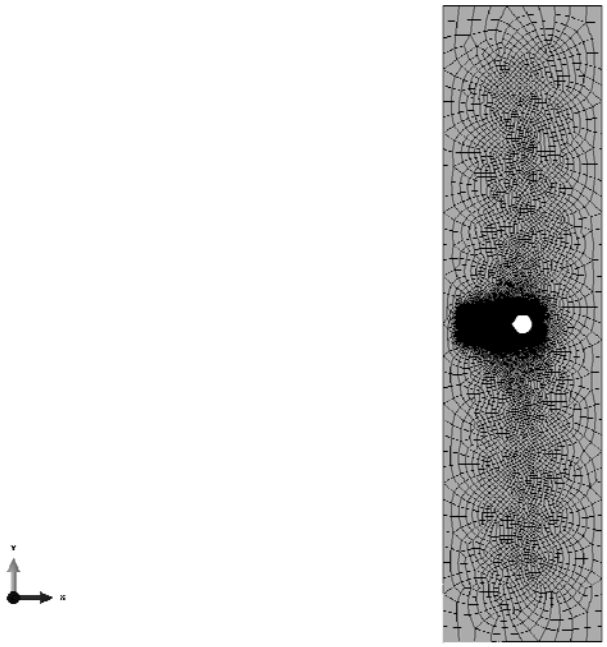

Figure A.13: Global finite element mesh of uniaxial specimen (SAI-01) with the crack length of 15 mm.

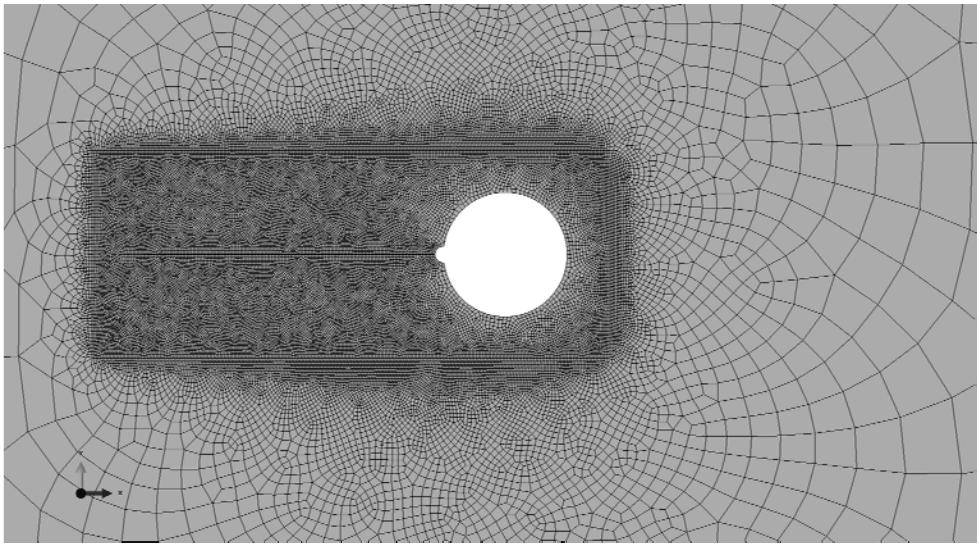

Figure A.14: Refined mesh of uniaxial specimen (SAI-01) with the crack length of 15 mm in the vicinity of stress concentration.

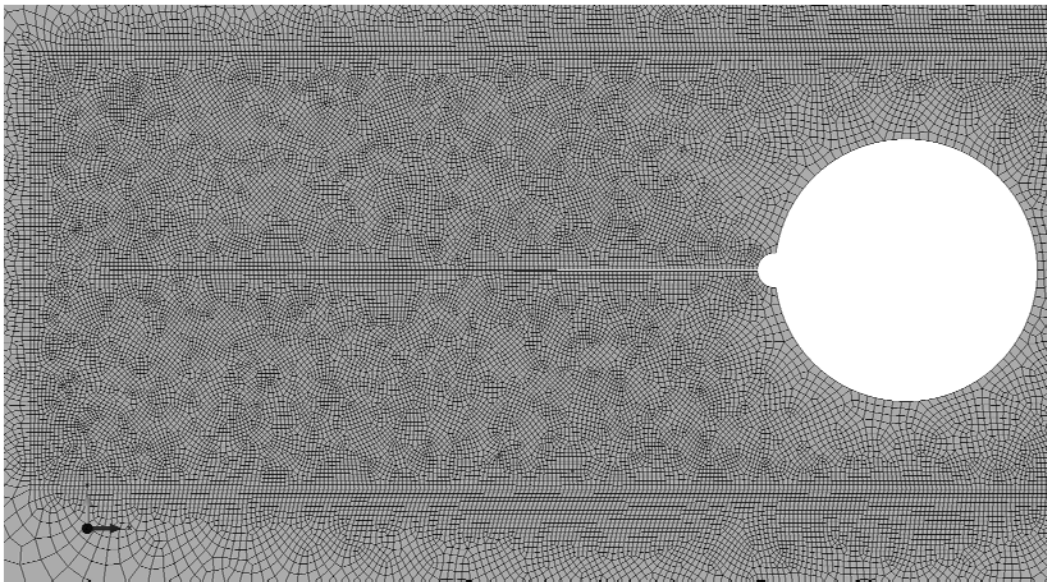

Figure A.15: Refined mesh of uniaxial specimen (SAI-01) with the crack length of 15 mm in the vicinity of crack tip.

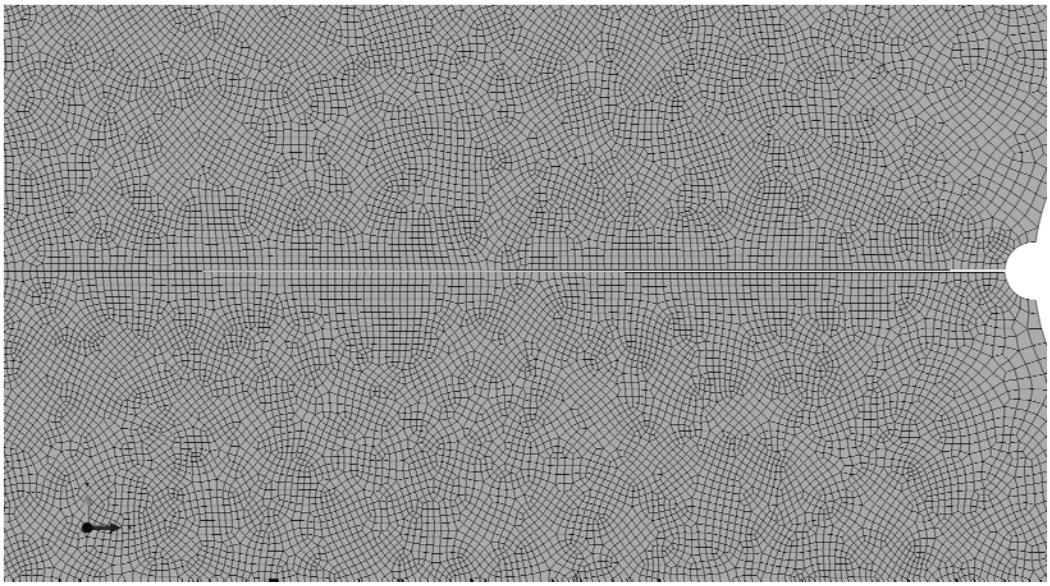

Figure A.16: Detail of the mesh of uniaxial specimen (SAI-01) with the crack length of 15 mm in the vicinity of crack tip.

Appendix B: Crack Growth Plots for Cruciform Specimens

(Specifications of the tests below are shown in Table 3.3.)

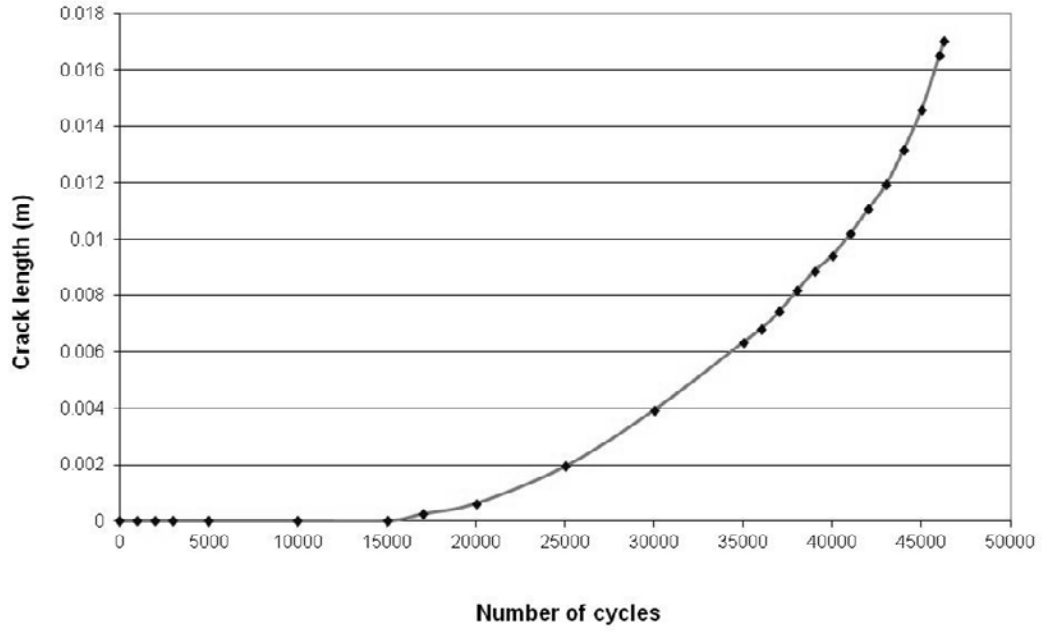

Figure B.1: Plot of the crack length vs. the number of cycles for XAl-01.

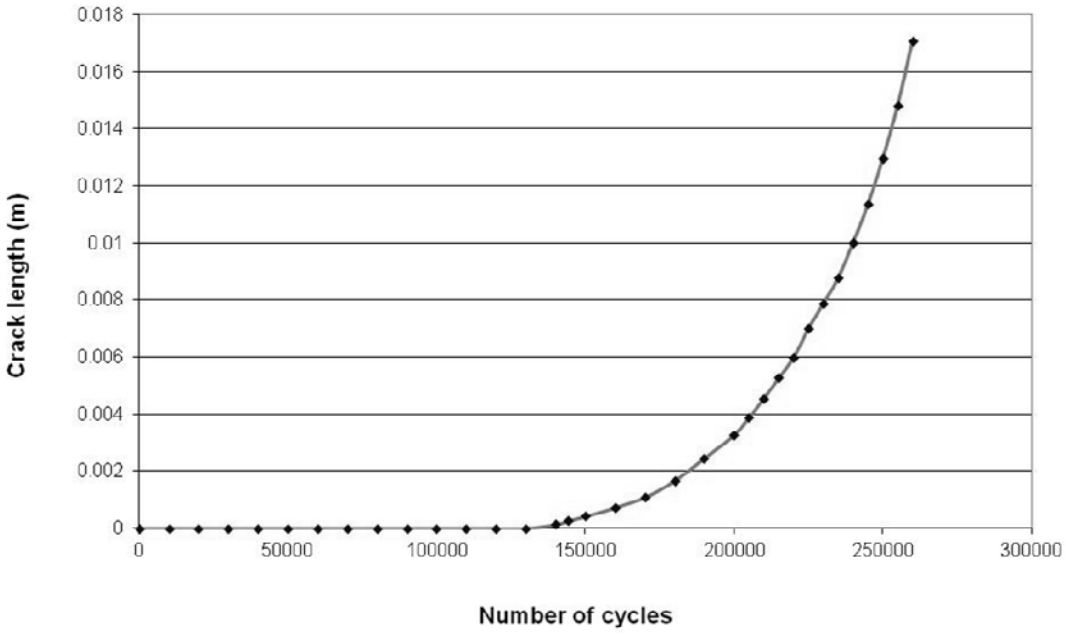

Figure B.2: Plot of the crack length vs. the number of cycles for XAl-03.

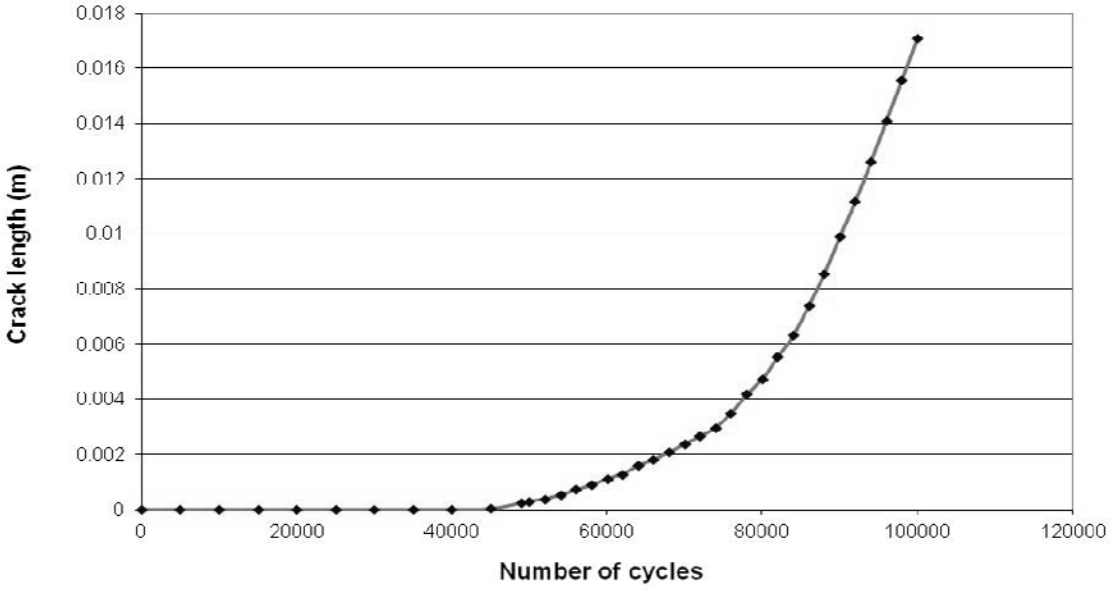

Figure B.3: Plot of the crack length vs. the number of cycles for XAl-04.

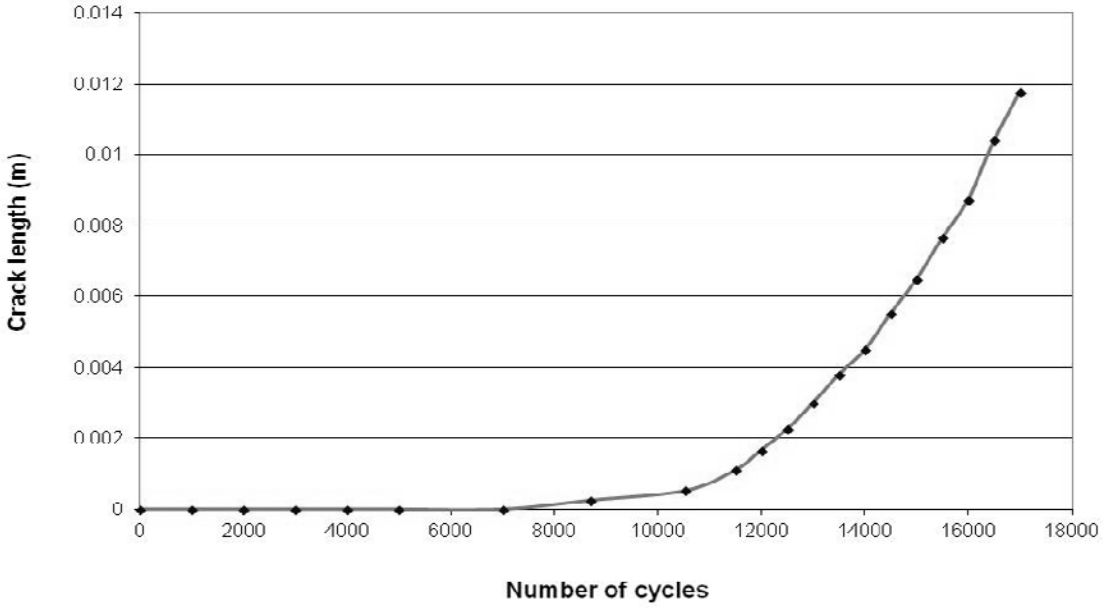

Figure B.4: Plot of the crack length vs. the number of cycles for XSl-01.

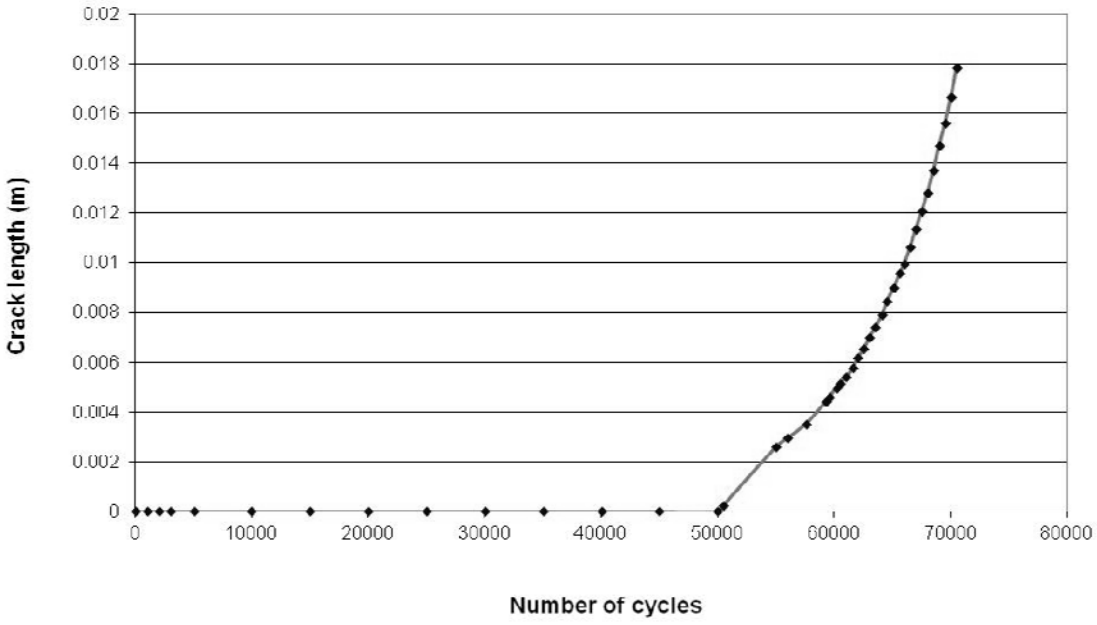

Figure B.5: Plot of the crack length vs. the number of cycles for XSl-02.

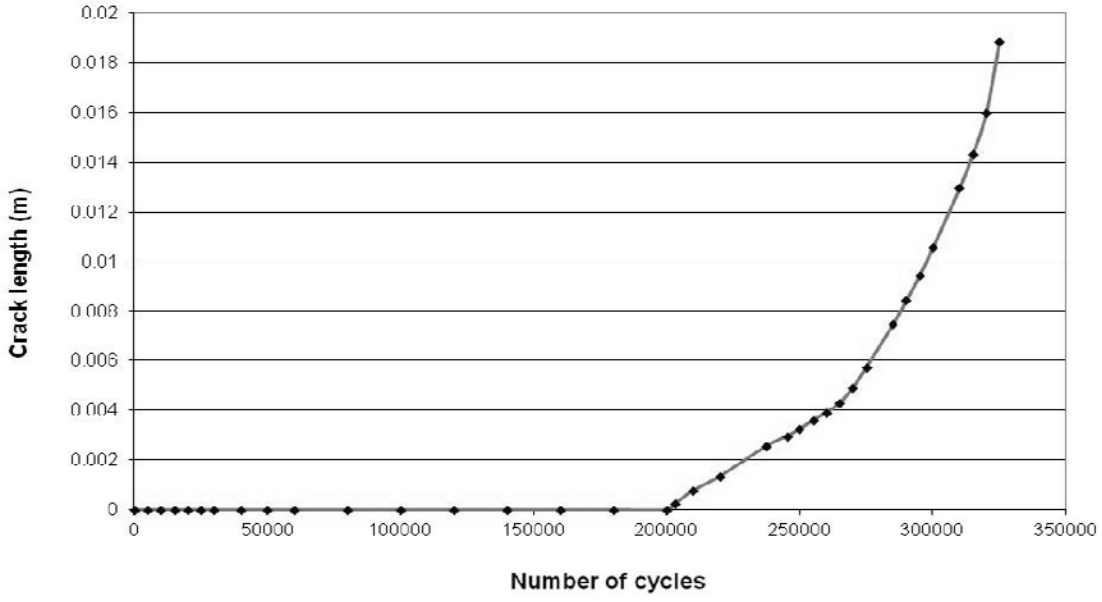

Figure B.6: Plot of the crack length vs. the number of cycles for XSl-03.

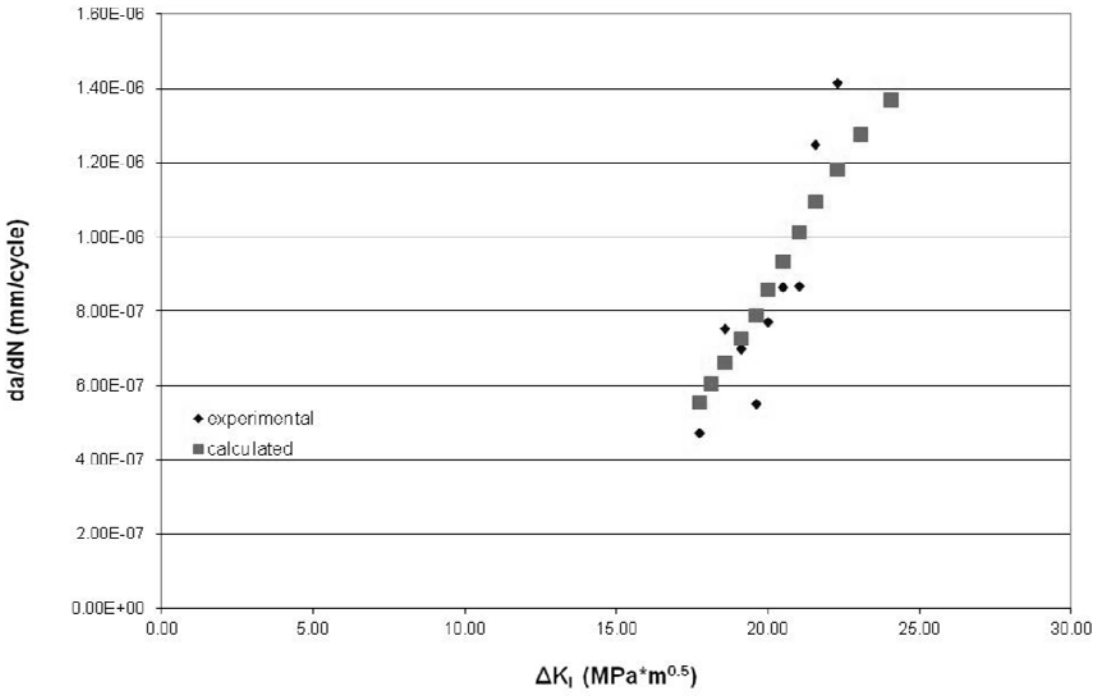

Figure B.7: Plot of the crack growth rate vs. the stress intensity factor for XAl-01.

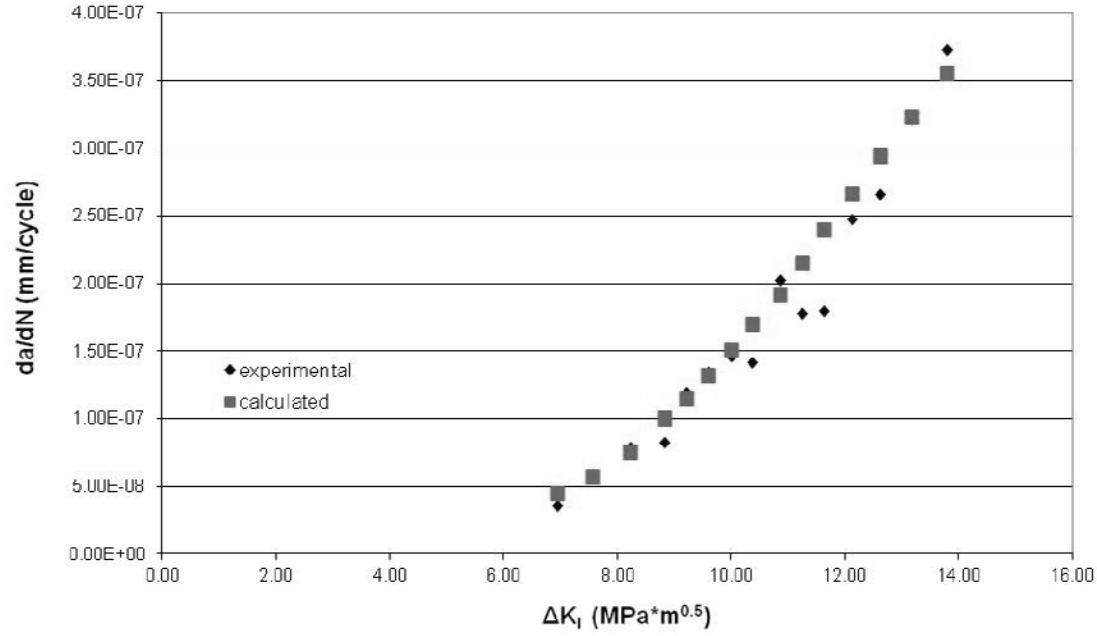

Figure B.8: Plot of the crack growth rate vs. the stress intensity factor for XAl-03.

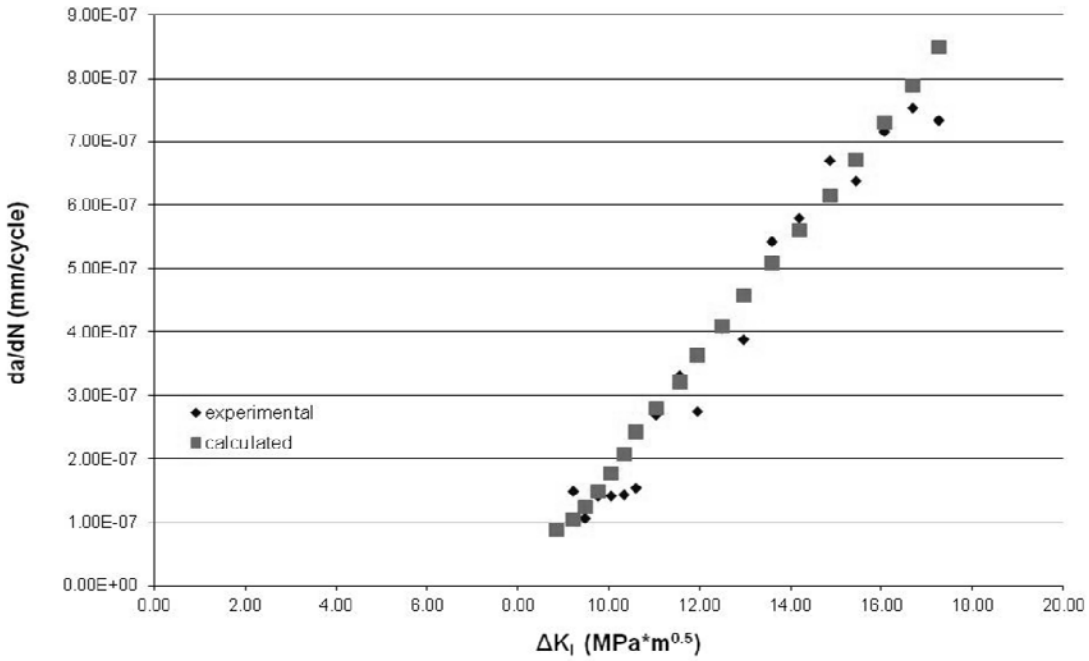

Figure B.9: Plot of the crack growth rate vs. the stress intensity factor for XAl-04.

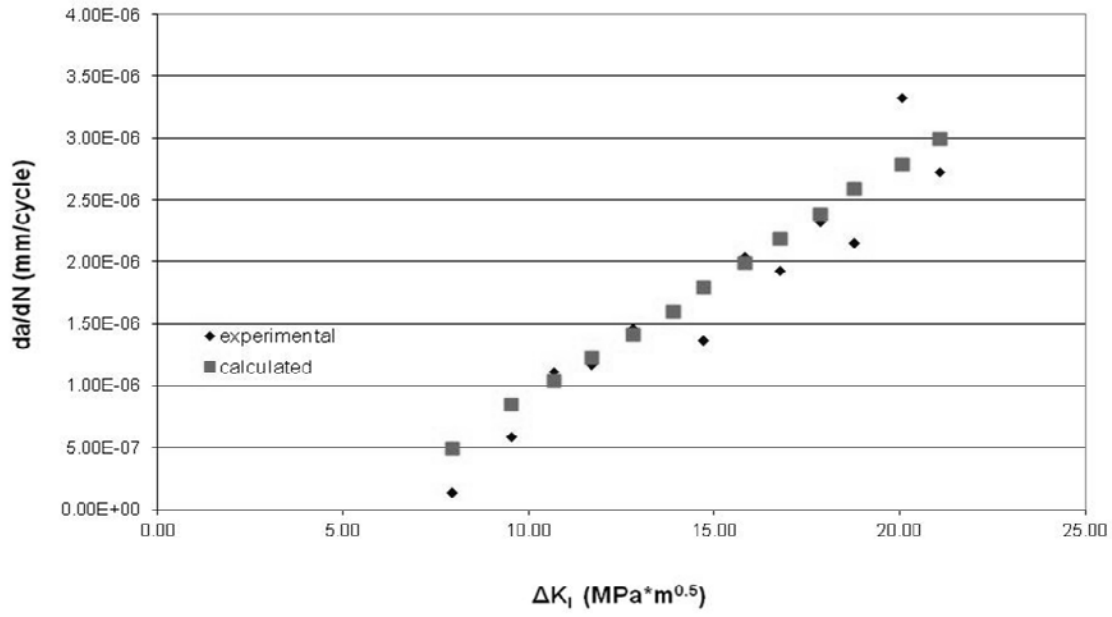

Figure B.10: Plot of the crack growth rate vs. the stress intensity factor for XSl-01.

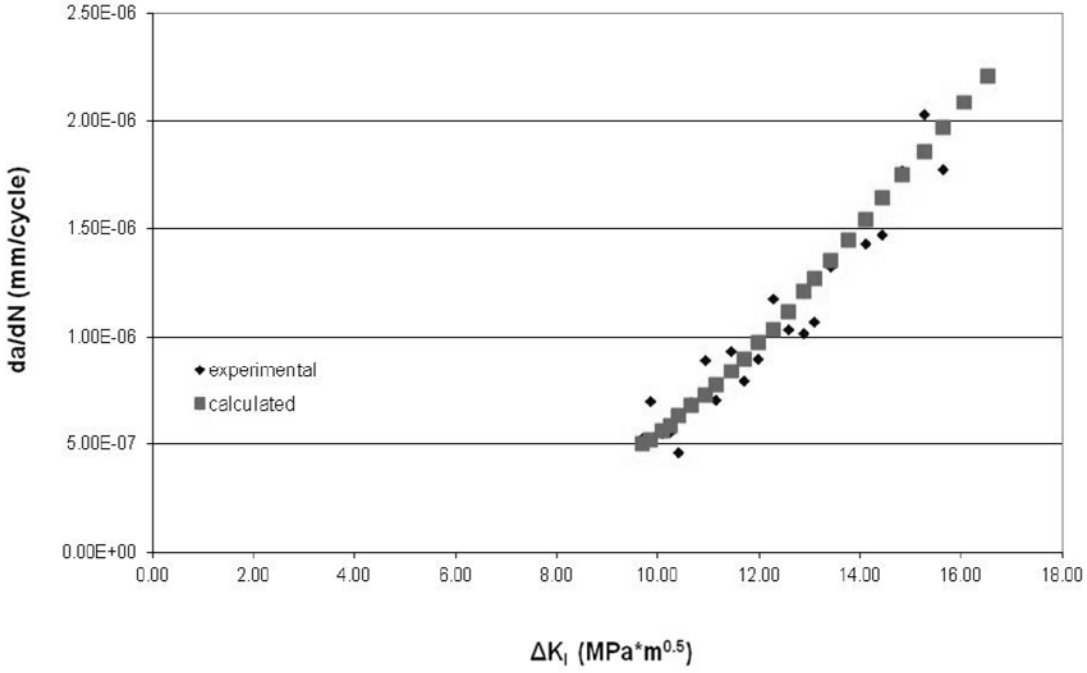

Figure B.11: Plot of the crack growth rate vs. the stress intensity factor for XSl-02.

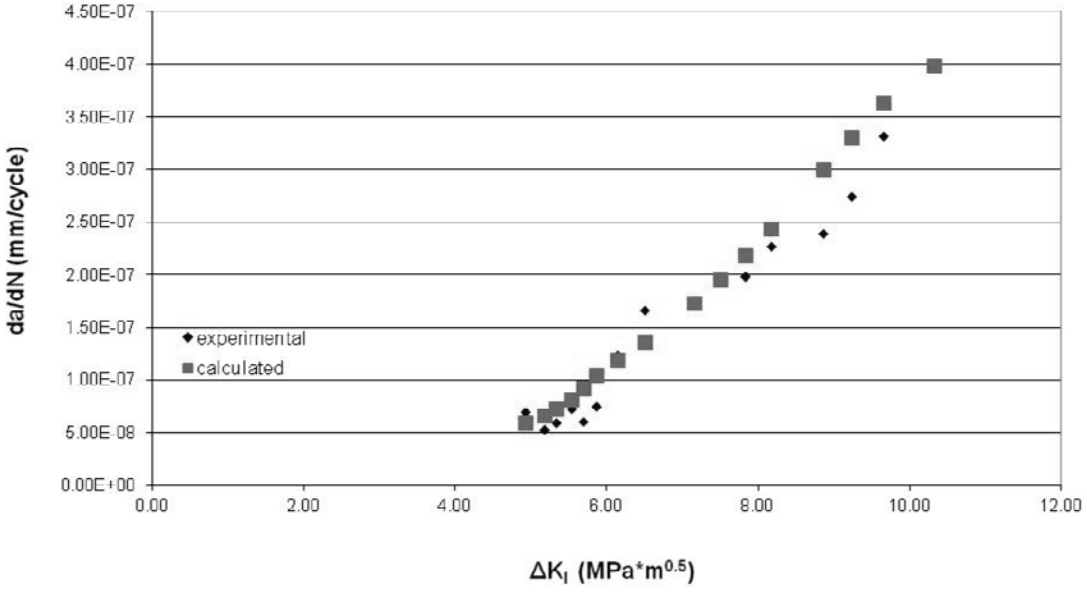

Figure B.12: Plot of the crack growth rate vs. the stress intensity factor for XSl-03.

Appendix C: Crack Growth Plots for Uniaxial Specimens

(Specifications of the tests below are shown in Table 3.3.)

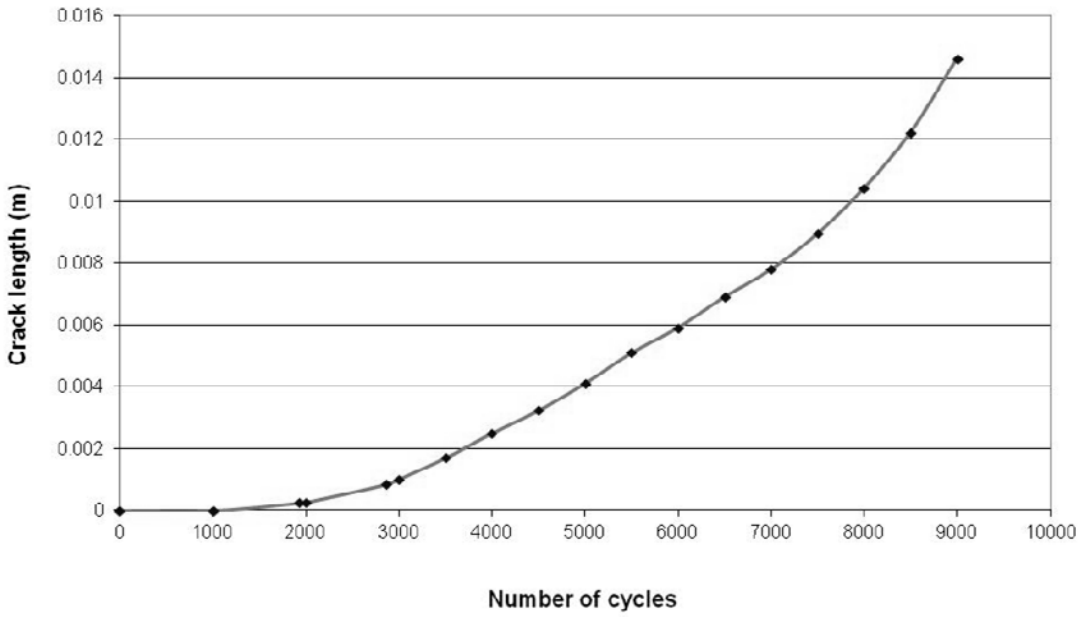

Figure C.1: Plot of the crack length vs. the number of cycles for SAl-02.

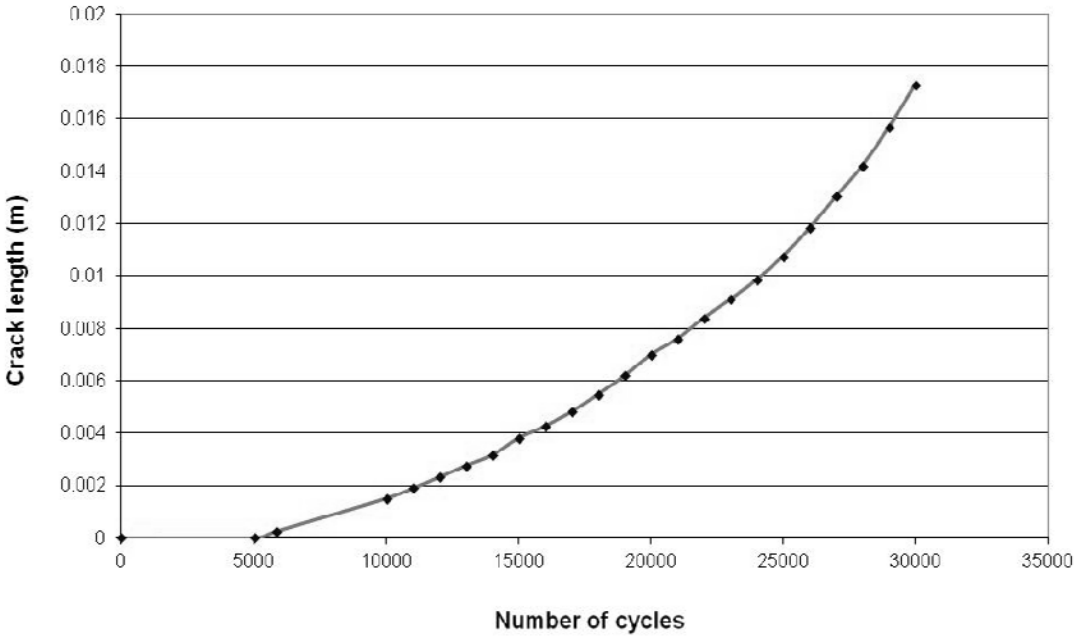

Figure C.2: Plot of the crack length vs. the number of cycles for SAl-03.

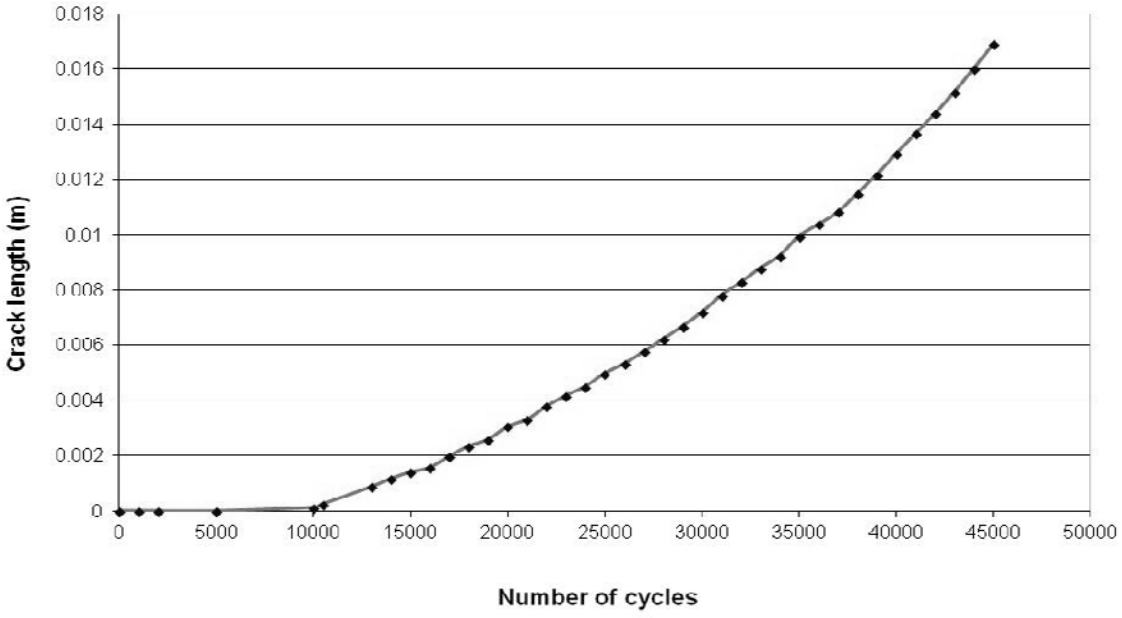

Figure C.3: Plot of the crack length vs. the number of cycles for SAl-04.

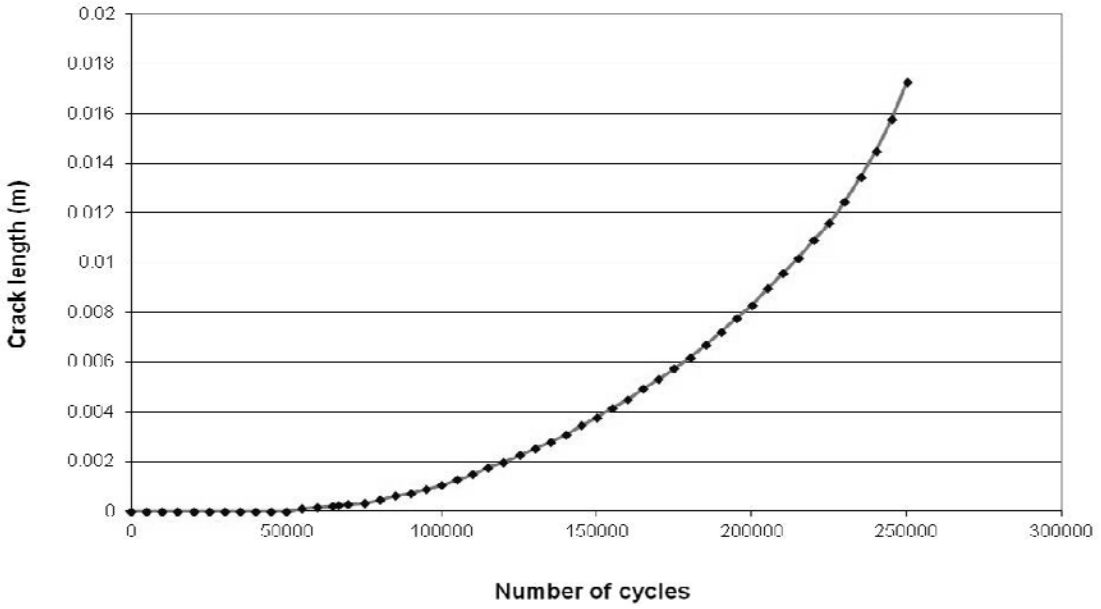

Figure C.4: Plot of the crack length vs. the number of cycles for SAl-05.

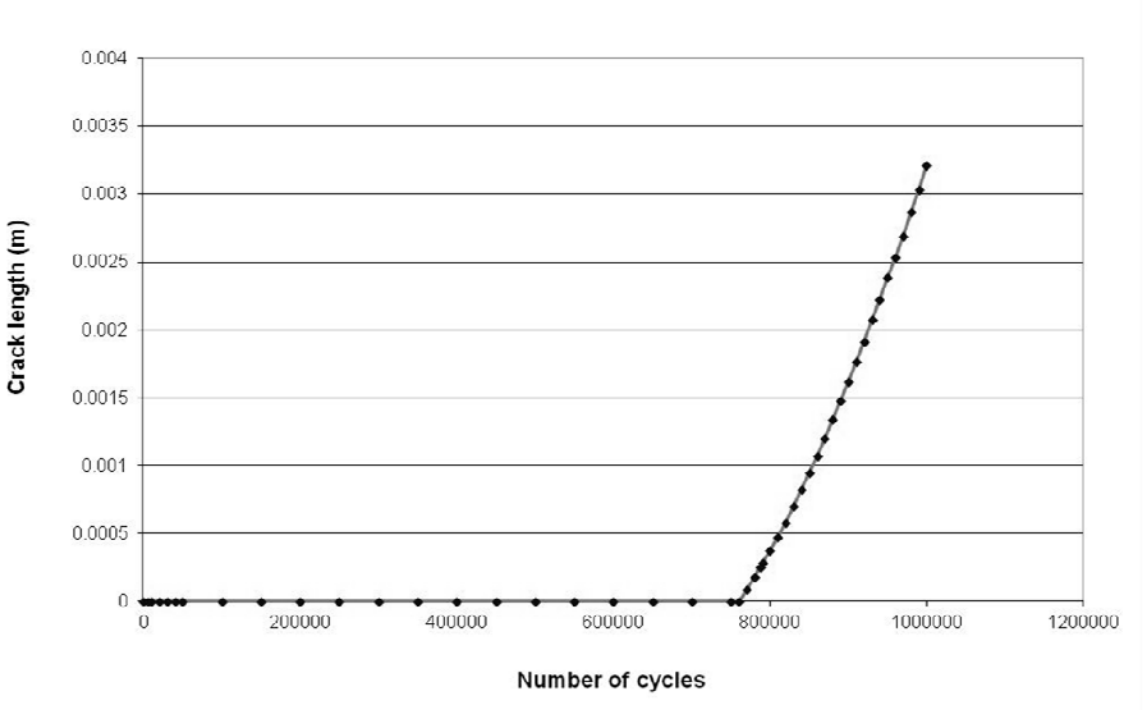

Figure C.5: Plot of the crack length vs. the number of cycles for SAl-07.

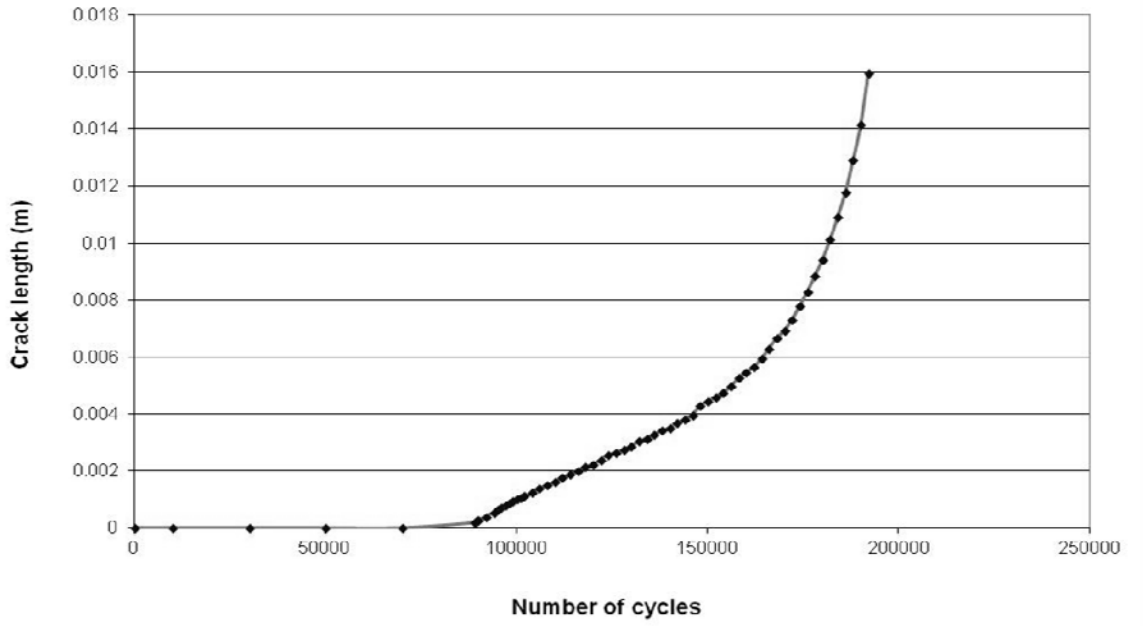

Figure C.6: Plot of the crack length vs. the number of cycles for SSl-01.

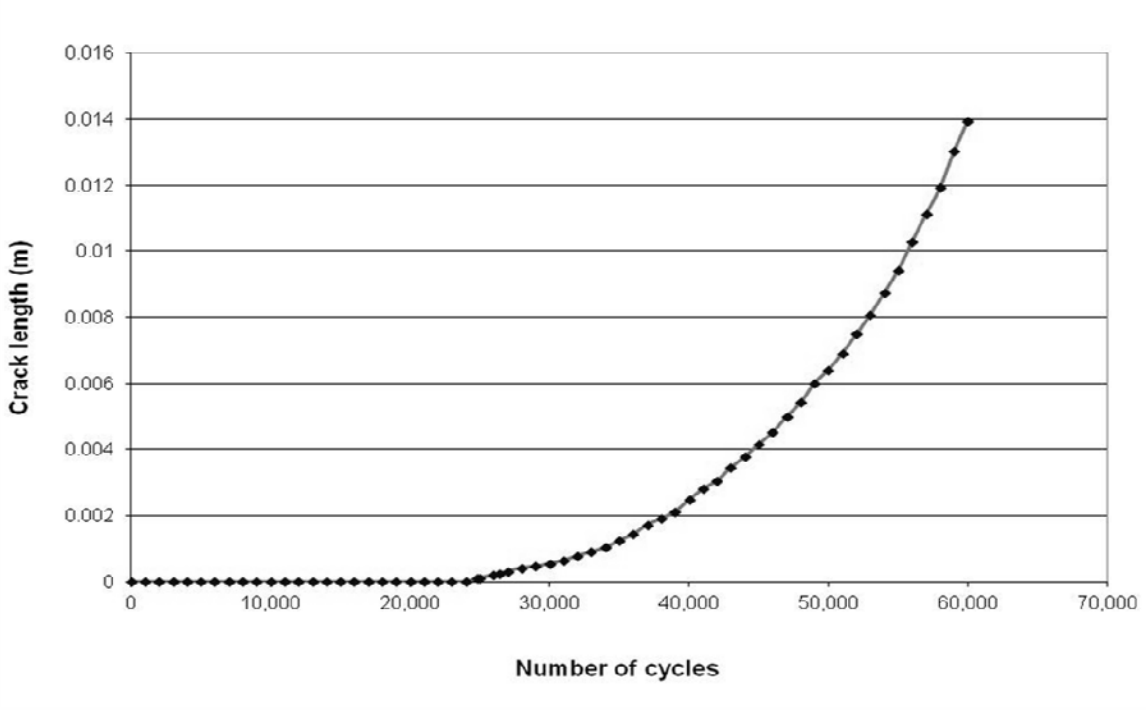

Figure C.7: Plot of the crack length vs. the number of cycles for SSl-02.

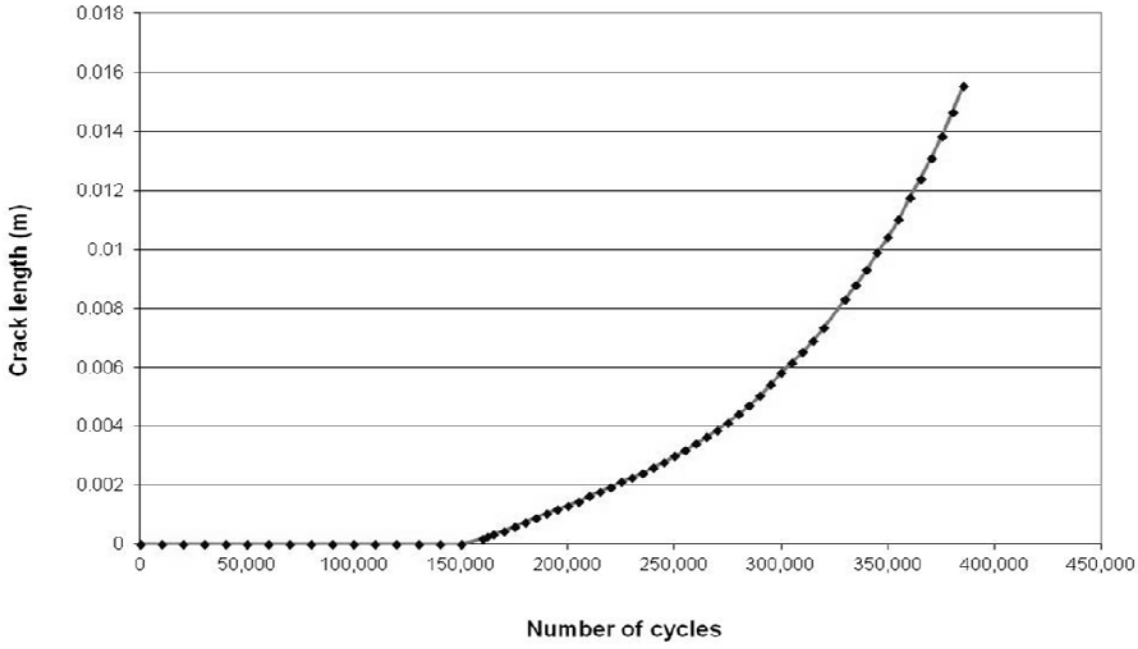

Figure C.8: Plot of the crack length vs. the number of cycles for SSl-03.

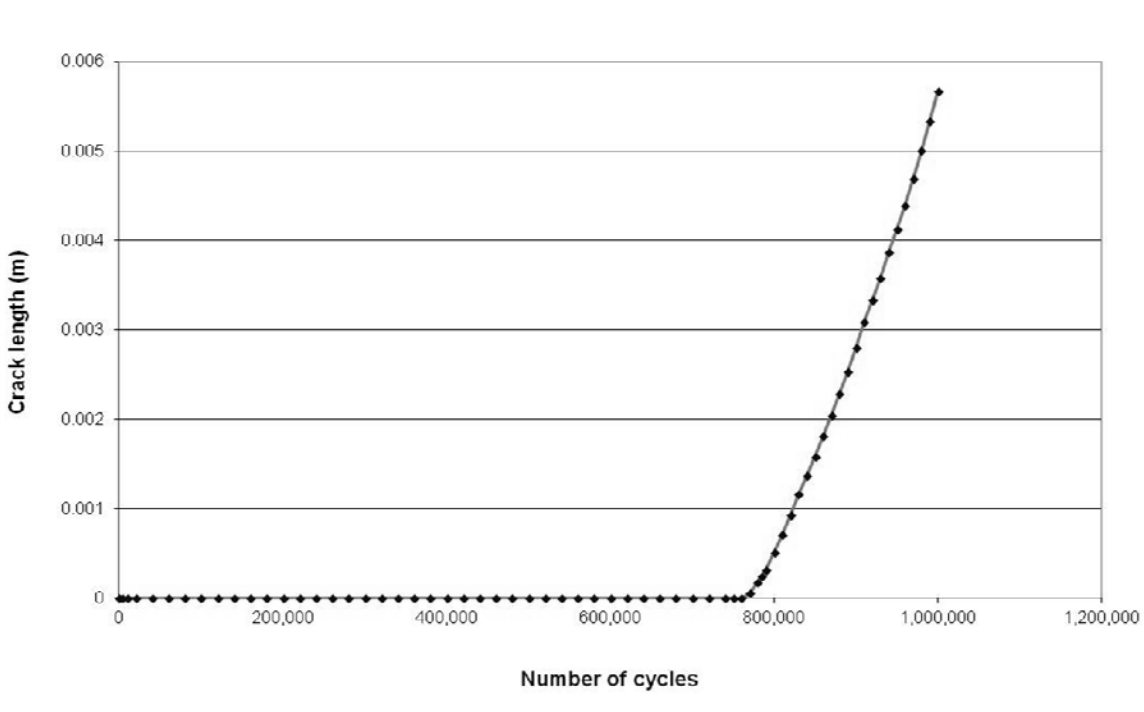

Figure C.9: Plot of the crack length vs. the number of cycles for SSl-04.

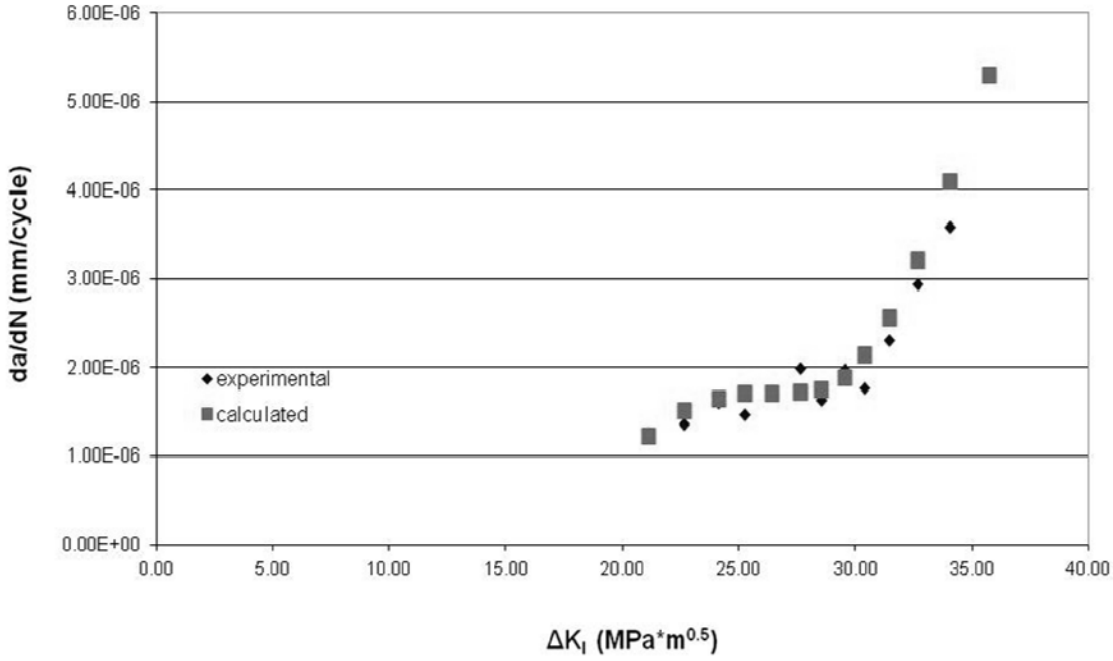

Figure C.10: Plot of the crack growth rate vs. the stress intensity factor for SAl-02.

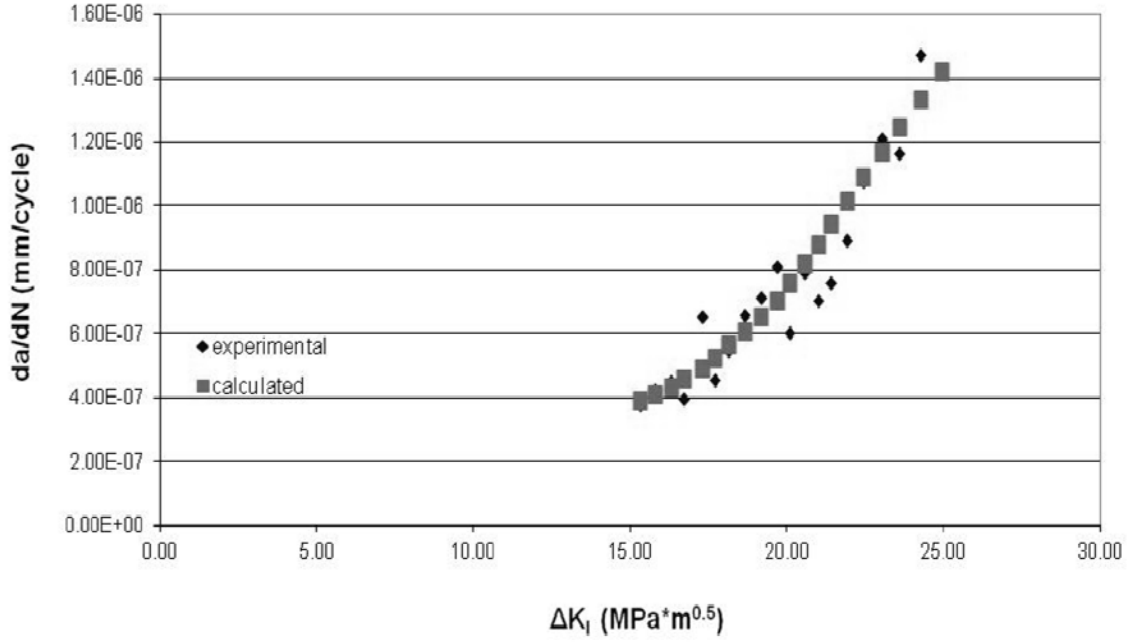

Figure C.11: Plot of the crack growth rate vs. the stress intensity factor for SAl-03.

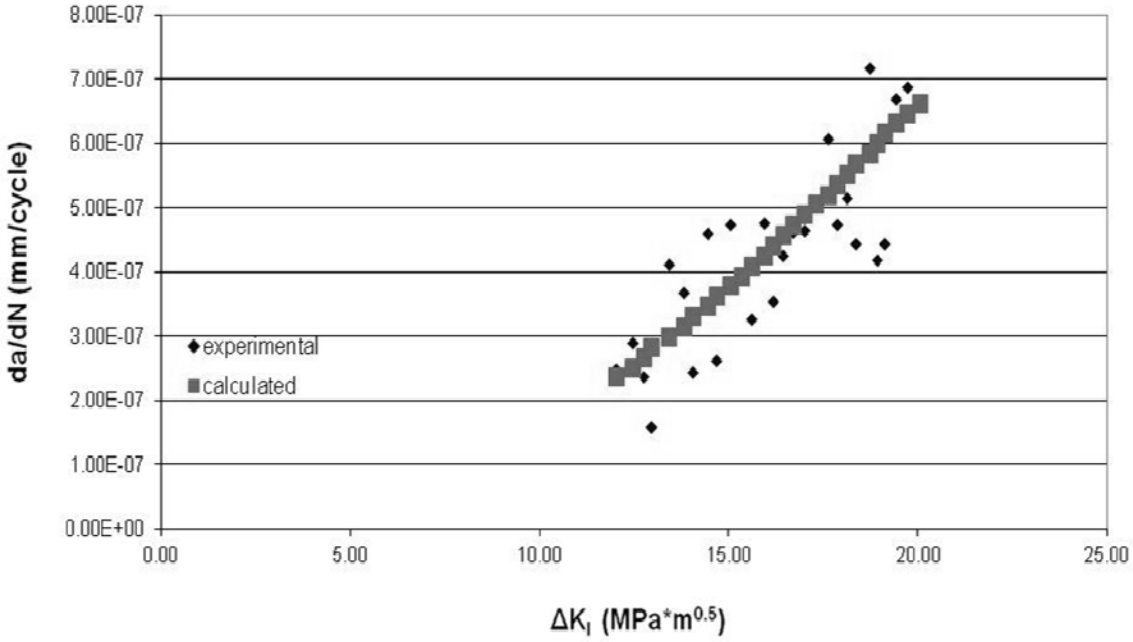

Figure C.12: Plot of the crack growth rate vs. the stress intensity factor for SAl-04.

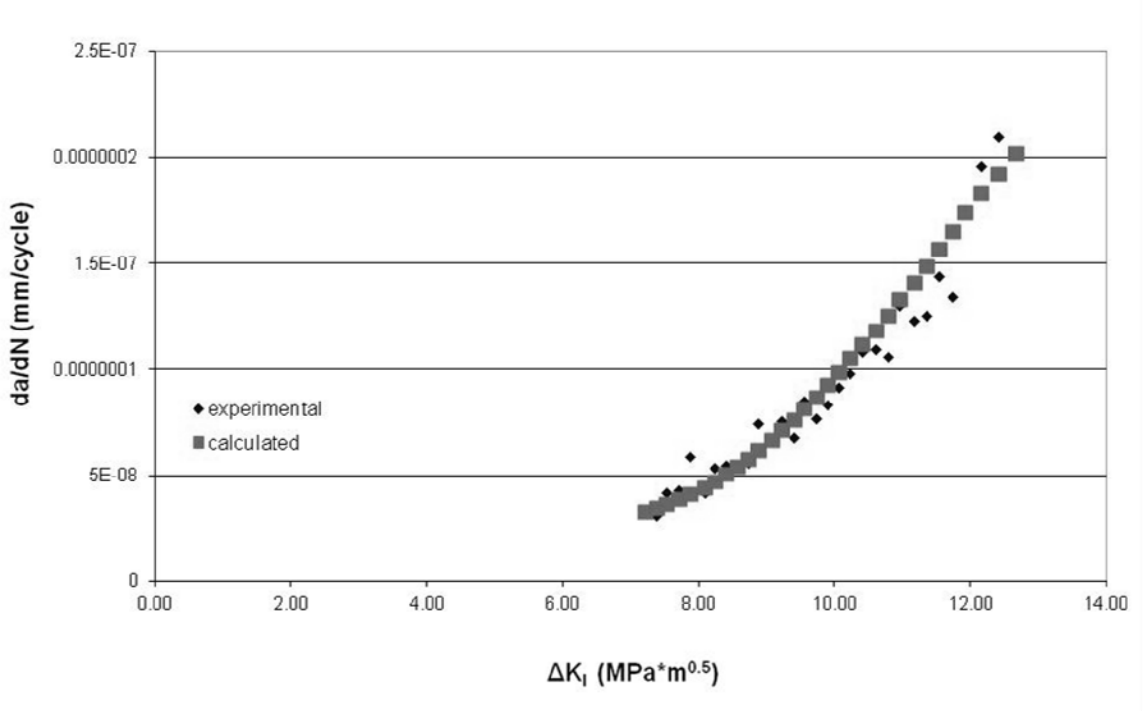

Figure C.13: Plot of the crack growth rate vs. the stress intensity factor for SAl-05.

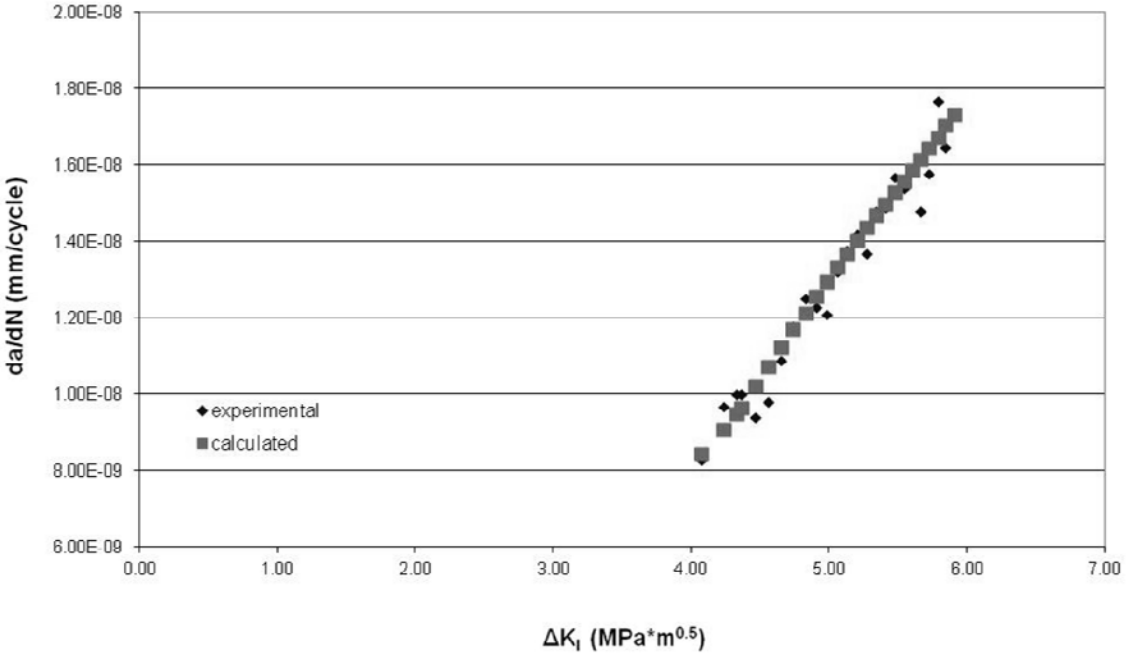

Figure C.14: Plot of the crack growth rate vs. the stress intensity factor for SAl-07.

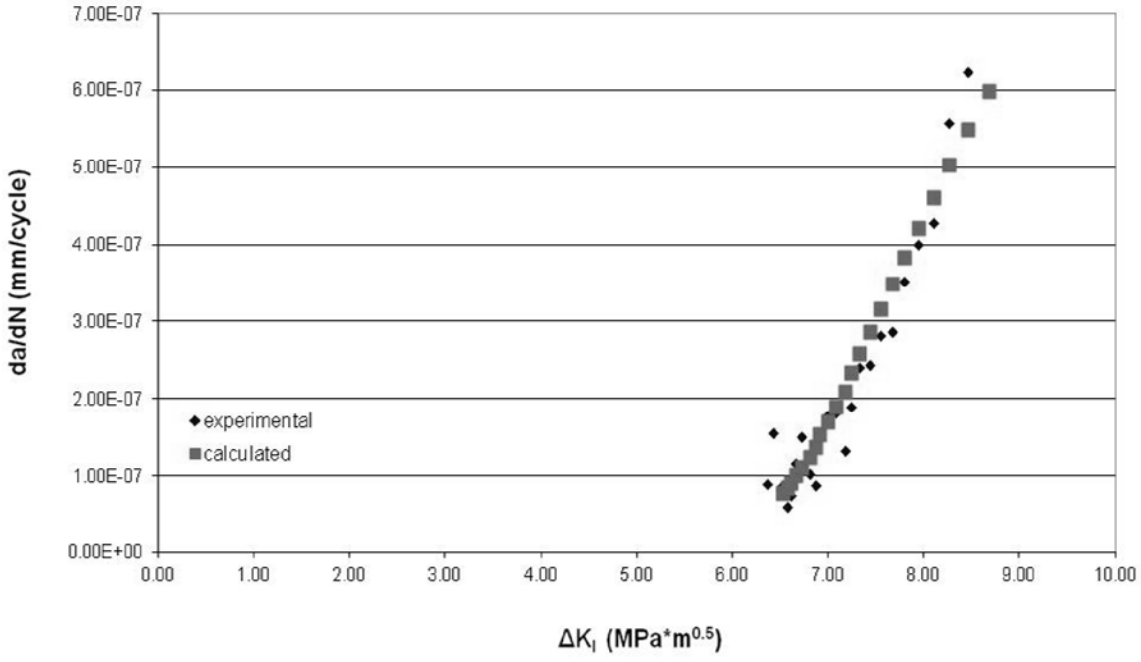

Figure C.15: Plot of the crack growth rate vs. the stress intensity factor for SSl-01.

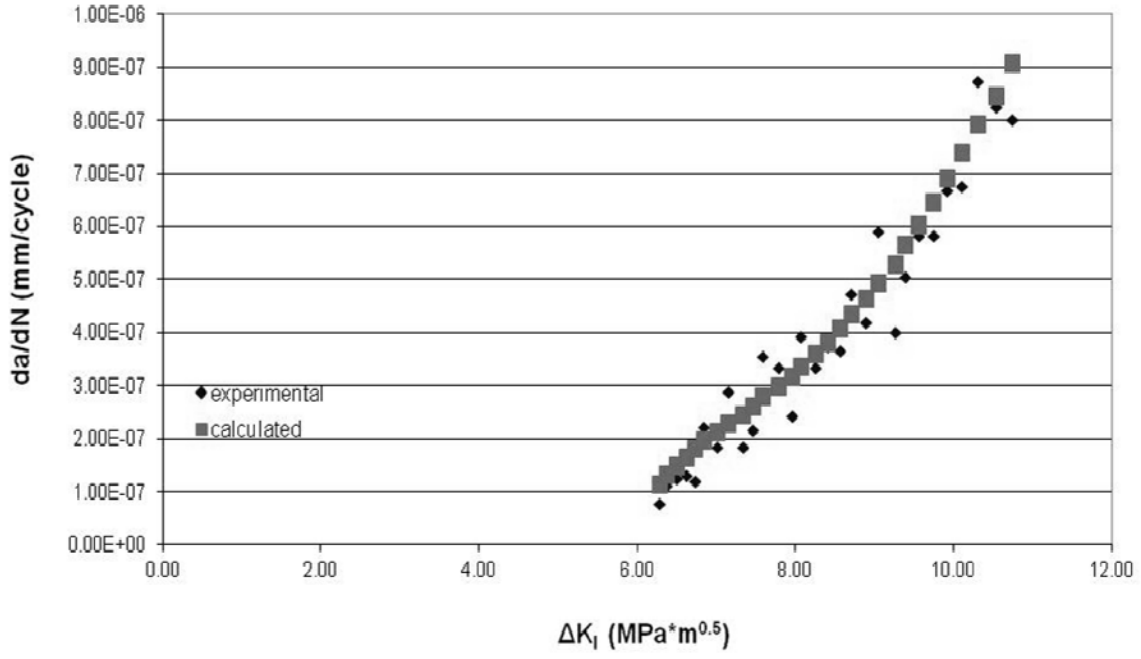

Figure C.16: Plot of the crack growth rate vs. the stress intensity factor for SSl-02.

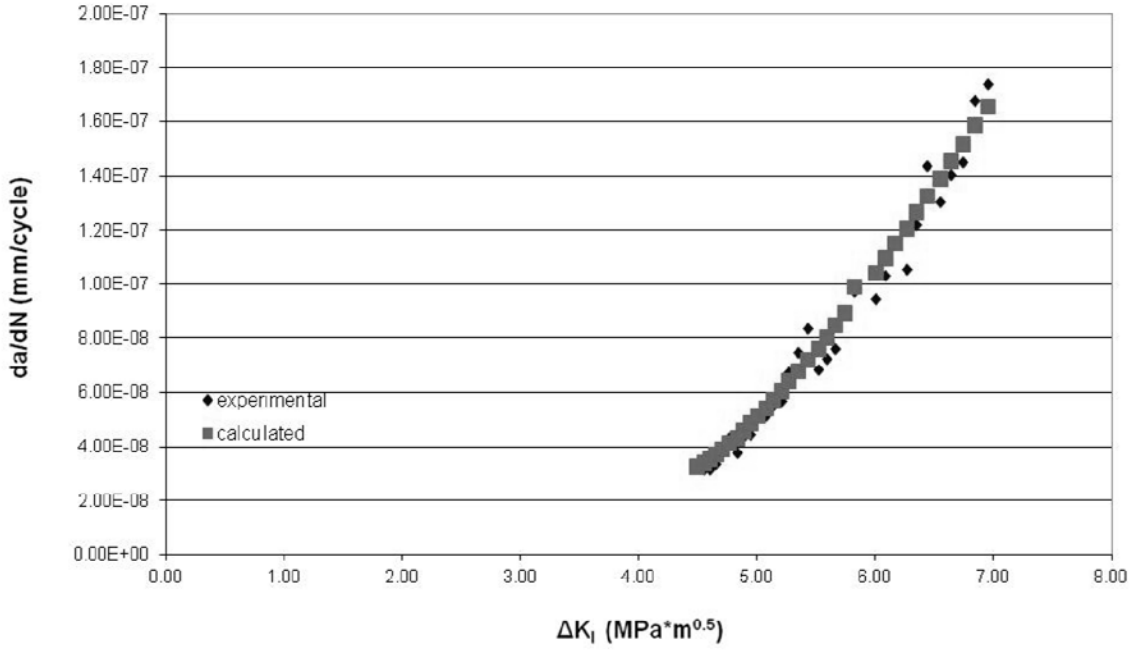

Figure C.17: Plot of the crack growth rate vs. the stress intensity factor for SSl-03.

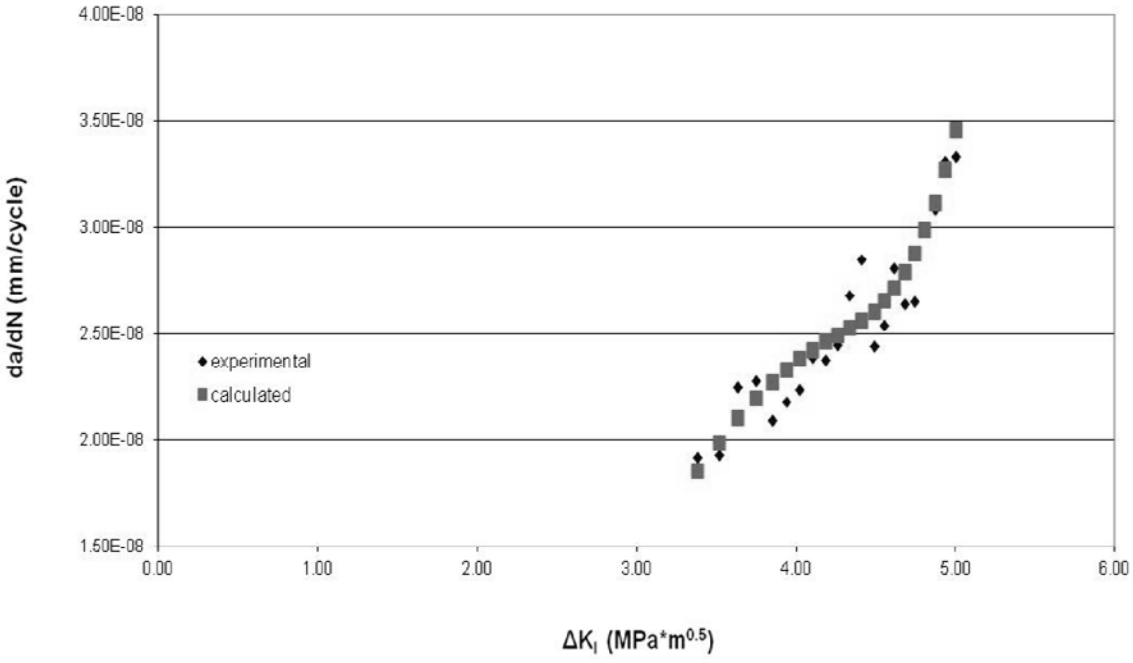

Figure C.18: Plot of the crack growth rate vs. the stress intensity factor for SSl-04.

Appendix D: SEM Images after Experimentation

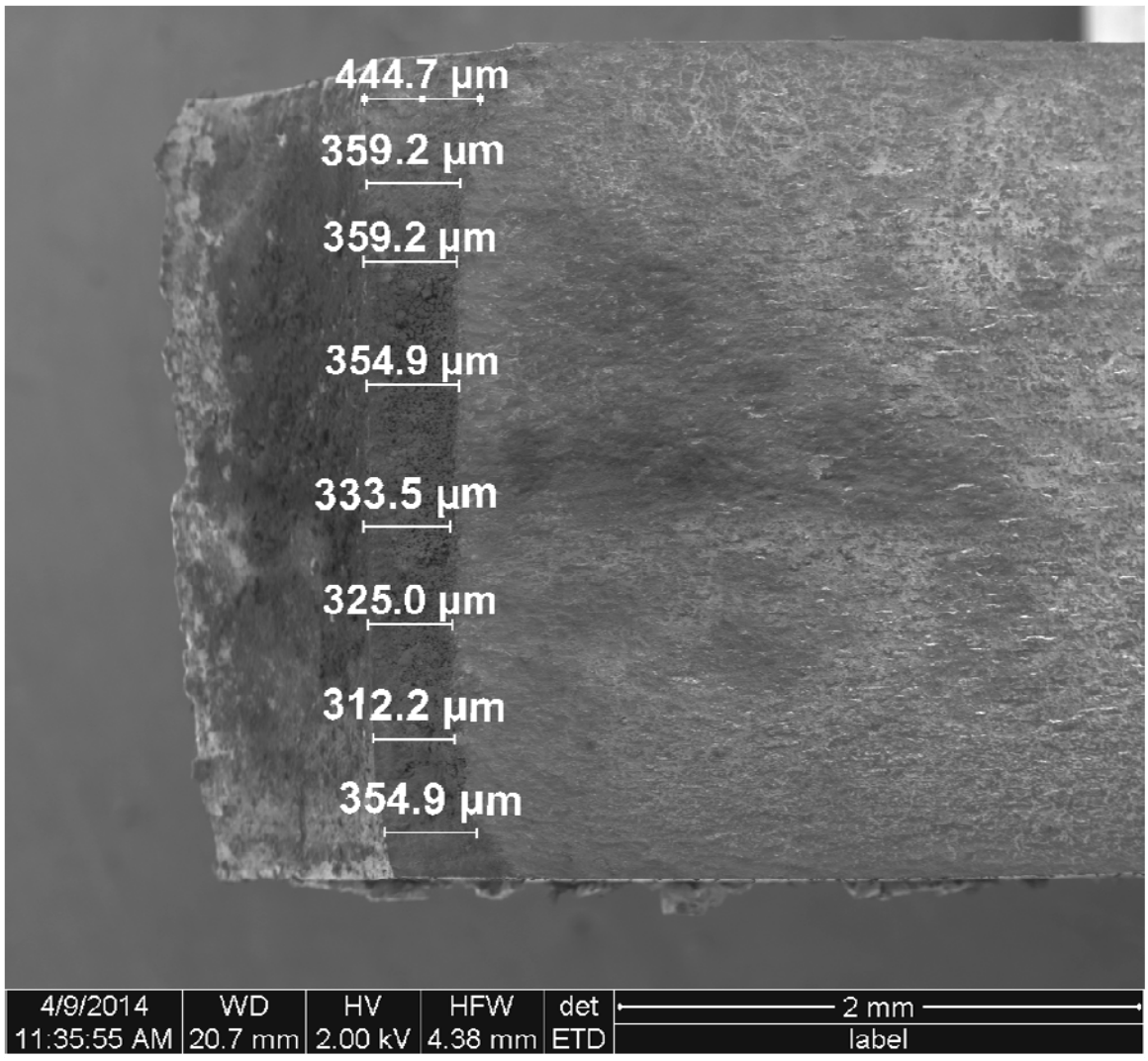

Figure D.1: Top view of the through pit specimen SSI-03 with measurement using the SEM.

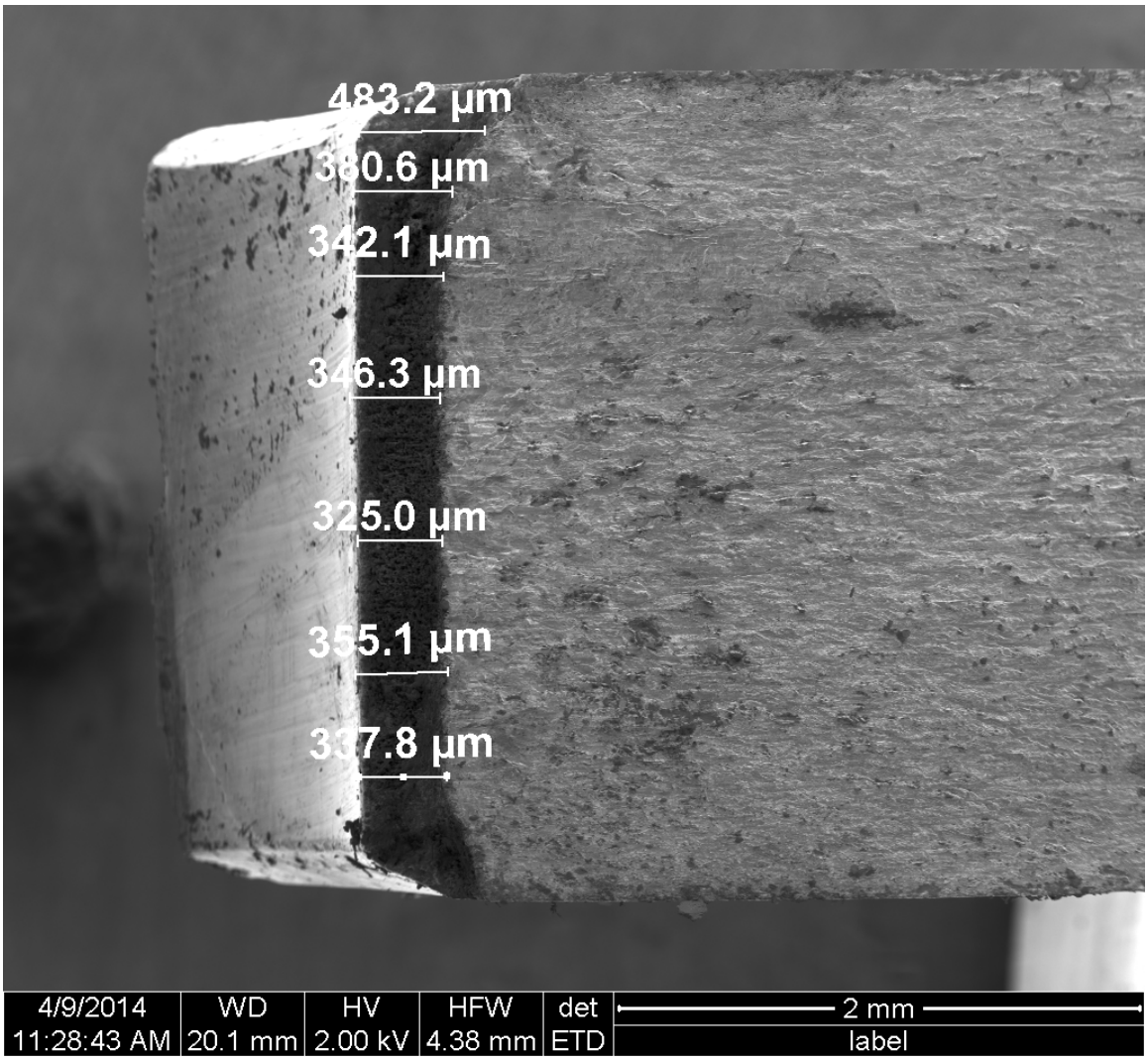

Figure D.2: Top view of the through pit specimen XAI-03 with measurement using the SEM.

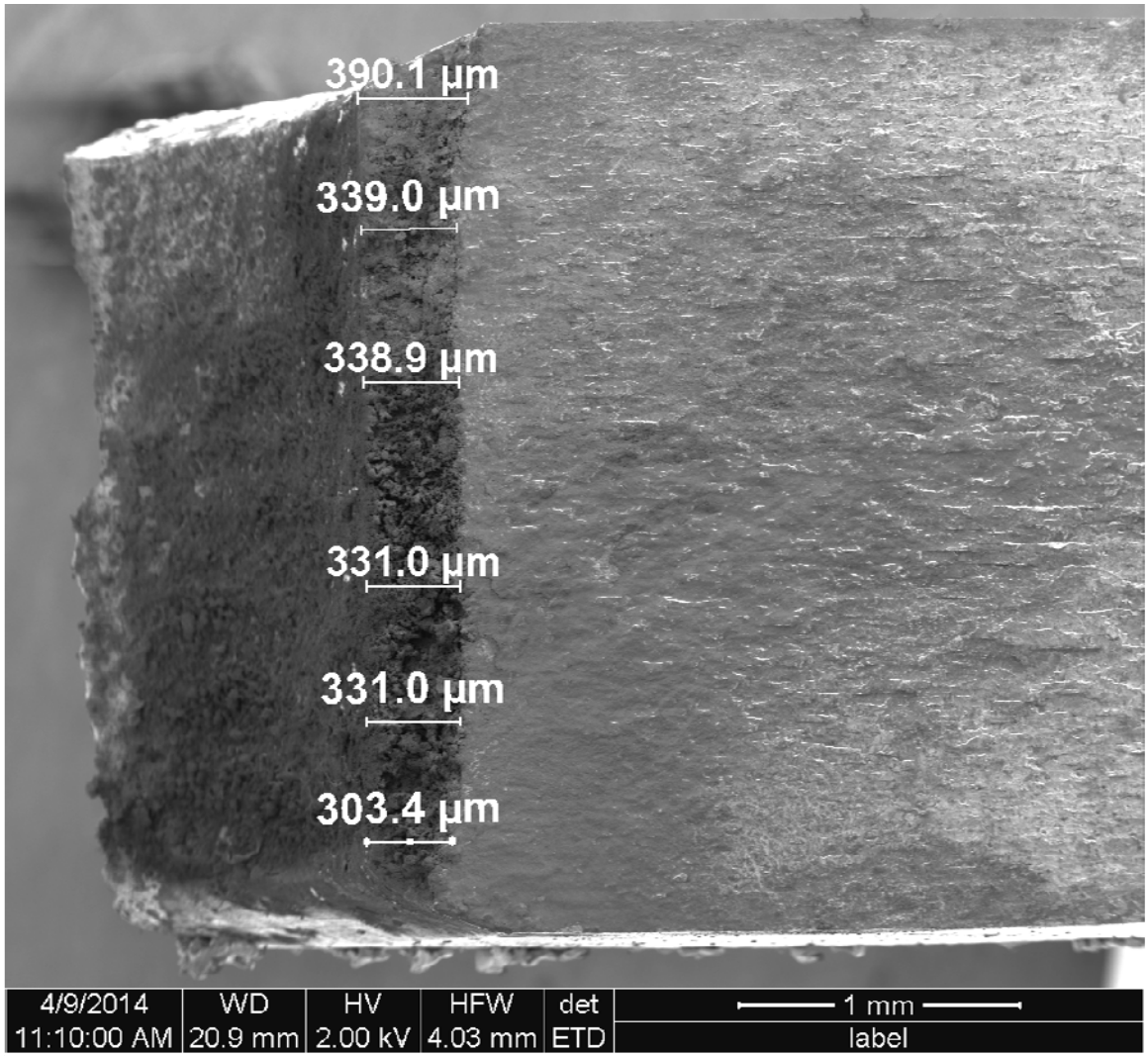

Figure D.3: Top view of the through pit specimen XSI-03 with measurement using the SEM.

Bibliography

[1] Anderson, P.R.G. and G. G. Garrett. "Fatigue crack growth rate variations in biaxial stress fields". *International Journal of Fracture*, 16:R111–116,1980.

[2] Anderson, T.L. Fracture Mechanics: Fundamentals and Applications. Taylor and Francis, 2005.

[3] ASM International Handbook Committee, "Metals Handbook, Vol.2 - Properties and Selection: Nonferrous Alloys and Special-Purpose Materials". ASM International, 1990.

[4] Bathias, C. and P.C. Paris. Gigacycle Fatigue in Mechanical Practice. Marcel Dekker, 2005.

[5] Bolotin, V. V. Mechanics of Fatigue. CRC Press, 1999.

[6] Burns, J.B. "The effect of initiation feature and environment on fatigue crack formation and early propagation in Al-Zn-Mg-Cu". PhD Dissertation, University of Virginia, 2010.

[7] Burns, J.T., S.Kim, and R.P. Gangloff. "Effect of corrosion severity on fatigue evolution in Al-Zn-Mg-Cu". *Corrosion Science*, 52:498–508, 2010.

[8] Castro, P.M.S.T., P.F.P. Matos, G.P. Moreira, and L.F.M. Silva. "An overview on fatigue analysis of aeronautical structural details: Open hole, single rivet lap-joint, and lap-joint panel". *Materials Science and Engineering: A*, 468-470:144–157, 2007. ISSN 0921-5093.

[9] Chen, G.S., K.C. Wan, M. Gao, R.P. Wei, and T.H. Flournoy. "Transition from pitting to fatigue crack growth modeling of corrosion fatigue crack nucleation in a 2024-T3 aluminum alloy". *Materials Science and Engineering*, 219:126–132, 2002.

[10] Chlistovsky, R.M., P.J. Heffernan, and D.L. DuQuesnay. "Corrosion-fatigue behaviour of 7075-T651 aluminum alloy subjected to periodic overloads". *International Journal of Fatigue*, 29:1941–1949, 2007.

[11] Davis, J.R. Corrosion of aluminum and aluminum alloys. Materials Park, OH: ASM International, 1999.

[12] Dolley, E. J., B. Lee, and R.P. Wei. "The effect of pitting corrosion on fatigue life". *Fatigue Fract Engng Mater Struct*, 23:555–560, 2000.

[13] Dowling, N.E. Mechanical Behavior of Materials. 3rd Ed. Pearson, 2007.

[14] DuQuesnay, D.L., P.R. Underhill, and H.J. Britt. "Fatigue crack growth from corrosion damage in 7075-T6511 aluminum alloy under aircraft loading". *International Journal of Fatigue*, 25:371–377, 2003.

[15] Ellyin, F. Fatigue Damage, Crack Growth and Life Prediction. Chapman&Hall, 1997.

[16] Frankel, G.S. and N. Sridhar. "Understanding localized corrosion". *Materialstoday*, October 2008, vol11, ISSN: 1369 7021

[17] Gangloff, R.P. "Environmental cracking- corrosion fatigue". *Corrosion Tests and Standards Manual ASM International*, 1–20, 2004.

[18] Hopper, C.D. and K.J. Miller. "Fatigue crack propagation in biaxial stress fields". *The Journal of Strain Analysis for Engineering Design*, 12:23–28, 1977.

[19] Hosford, W.F. Mechanical Behavior of Materials. Cambridge University Press, 2005.

[20] Hunt, E.M. "Crack initiation and growth behavior at corrosion pit in 7075-T6 high strength aluminum alloy". MS Thesis, Air Force Institute of Technology, OH, 2013.

[21] Jones, K. and D.W. Hoeppner. "Prior corrosion and fatigue of 2024-T3 aluminum alloy". *Corrosion Science*, 48:3109–3122, 2006.

[22] Kaminskii, A.A. and N.S. Sailov, "Spreading of cracks from the contours of elliptical openings in brittle plates under biaxial tensile stresses". *Soviet Applied Mechanics*, 11:167-173, 1975.

[23] Khalifa, M., F. Khan, and M. Haddara. "Inspection sampling of pitting corrosion". *Insight: Non-Destructive Testing & Condition Monitoring*, 55:290-296, 2013.

[24] Kim, S., J.T. Burns, and R.P. Gangloff. "Fatigue crack formation and growth from localized corrosion in AlZnMgCu". *Engineering Fracture Mechanics*, 76(0):651–667, 2009.

[25] Koch, G.H., M.P.H. Brongers, N.G. Thompson, Y.P. Virmani, J.H. Payer. "Corrosion cost and preventive strategies in the United States". *National Technical Information Service*, 2002.

[26] Koch, G.H. and E.L. Hagerdorn. "Effect of pre-existing corrosion of fatigue cracking of aluminum alloys 2024-T3 and 7075-T6". Air Force Research Laboratory, WPAFB, OH, 1995.

[27] Lados, D.A. and P.C. Paris. "Parameters and key trends affecting fatigue crack growth: A tribute to Professor Arthur J. McEvily's contributions". *Materials Science and Engineering: A*, 468-470:70-73, 2007.

[28] Lee, E.U. and R.E. Taylor. "Fatigue behavior of aluminum alloys under biaxial loading". *Engineering Fracture Mechanics*, 78:1555–1564, 2011.

[29] Liu, A.F. and D.F. Dittmer. "Effect of multiaxial loading on crack growth. Volume 2 compilation of experimental data". Northrop Corp Hawthorne, 1978.

[30] Lukas, P. and L. Kunz. "Small cracks nucleation, growth and implication to fatigue life". *International Journal of Fatigue*, 25(0):855–862, 2003.

[31] Marcus, P. Corrosion Mechanisms in Theory and Practice. CRC Press, 2011.

[32] Marshall, R. "Cutting corrosion costs". *Chemical Engineering*, 2008.

[33] McEvily, A.J. and W. Illg. "The rate of fatigue crack propagation in two aluminum alloys". NASA TN 4394, 1958.

[34] Misak, H.E., V.Y. Perel, V. Sabelkin, and S. Mall. "Biaxial tension-tension fatigue crack growth behavior of 2024-T3 under ambient air and salt water environments". Air Force Institute of Technology,OH, 2014.

[35] Misak, H.E., V.Y. Perel, V. Sabelkin, and S. Mall. "Corrosion fatigue crack growth behavior of 7075-T6 under biaxial tension-tension cyclic loading condition". *Engineering Fracture Mechanics*, 106:38–48, 2013. ISSN 0013-7944.

[36] Misak, H.E., V.Y. Perel, V. Sabelkin, and S. Mall. "Crack growth behavior of 7075-T6 under biaxial tension–tension fatigue". *International Journal of Fatigue*, 55:158–165, 2013.

[37] MTS Systems Corporation, "MTS Planar Biaxial Test System", 100-179-028, 2007.

[38] Nan, Z.Y., S. Ishihara, and T. Goshima. "Corrosion fatigue behavior of extruded magnesium alloy AZ31 in sodium chloride solution". *International Journal of Fatigue*, 38:1181–1188, 2008.

[39] Pao, P.S., P.S. Gill, and C.R. Feng. "On fatigue crack initiation from corrosion pits in 7075-T7351 aluminum alloy". *Scripta Materialia*, 43:391–396, 2000.

[03] Ro, Y., S.R. Agnew, G.H. Bray, and R.P. Gangloff. "Environment-exposure-dependent fatigue crack growth kinetics for Al–Cu–Mg/Li". *Materials Science and Engineering: A*, 468-470:88–97, 2007.

[41] Roberge, P.R. Corrosion Engineering: Principles and Practice. McGraw-Hill, 2008.

[42] Rong, W. "A fracture model of corrosion fatigue crack propagation of aluminum alloys based on the material elements fracture ahead of a crack tip". *International Journal of Fatigue*, 30:1376–1386, 2008.

[43] Sangid, M.D. "The physics of fatigue crack initiation". *International Journal of Fatigue*, 57:58-72, 2013.

[44] Sarinova, S., A. Hassan, P.J. Martyn, and D.J. Smith. "Fatigue crack closure of a corner crack: A comparison of experimental results with finite element predictions". *International Journal of Fatigue*, 27(8):914 – 919, 2005.

[45] Sankaran, K., K. R. Perez, and K.V. Jata. "Effects of pitting corrosion on the fatigue behavior of aluminum alloy 7075-T6: modeling and experimental studies". Air Force Research Laboratory, WPAFB, OH, 2000.

[46] Shanyavskiy, A. "Fatigue cracking simulation based on crack closure effects in Al-based sheet materials subjected to biaxial cyclic loads". *Engineering Fracture Mechanics*, 78:1516- 1528, 2011.

[47] Sunder, R. "Development of the Marker-TWIST load sequence for quantitative fractographic studies". *International Journal of Fatigue*, 2010.

[48] Sunder, R. and B.V. Ilchenko. "Fatigue crack growth under flight spectrum loading with superposed biaxial loading due to fuselage cabin pressure". *International Journal of Fatigue*, 33:1101–1110, 2011.

[49] Wang, Q.Y., N. Kawagoishi, Q. Chen. "Effect of pitting corrosion on very high cycle fatigue behavior". *Scripta Materialia*, 49:711-716, 2003.

[50] Wei, R.P. "Corrosion and fatigue of aluminum alloys chemistry, micro-mechanics and reliability". Final Technical Report-Grant F49620-93-1-0426, 1997.

[51] Xu-Dong, L., W. Xi-Shu, R. Huai-Hui, C. Yin-Long, and M. Zhi-Tao. "Effect of prior corrosion state on the fatigue small cracking behaviour of 6151-T6 aluminum alloy". *Corrosion Science*, 55:26–33, 2012.

[52] Yuuki, R., K. Akita, and N. Kishi. "The effect of biaxial stress and changes of state on fatigue crack growth behaviour". *Fatigue & Fracture of Engineering Materials & Structures*, 12:93-103, 1989.

REPORT DOCUMENTATION PAGE

Form Approved
OMB No. 074-0188

PLEASE DO NOT RETURN YOUR FORM TO THE ABOVE ADDRESS.

1. REPORT DATE *(DD-MM-YYYY)*	**2. REPORT TYPE**	**3. DATES COVERED** *(From – To)*
19-06-2014	Master's Thesis	August 2012 – June 2014

TITLE AND SUBTITLE

Crack initiation and growth behavior at corrosion pit in 7075-T6 under biaxial and uniaxial fatigue

5a. CONTRACT NUMBER

5b. GRANT NUMBER

5c. PROGRAM ELEMENT NUMBER

6. AUTHOR(S)

Dolu, Zafer, Capt, Turkish Army

5d. PROJECT NUMBER

5e. TASK NUMBER

5f. WORK UNIT NUMBER

7. PERFORMING ORGANIZATION NAMES(S) AND ADDRESS(S)
Air Force Institute of Technology
Graduate School of Engineering and Management (AFIT/EN)
2950 Hobson Way
Wright-Patterson AFB OH 45433-7765

8. PERFORMING ORGANIZATION REPORT NUMBER

AFIT-ENY-T-14-J-33

9. SPONSORING/MONITORING AGENCY NAME(S) AND ADDRESS(ES)
Rich Hays
Technical Corrosion Collaboration
Office of Secretary of Defense
Washington D.C.

Turkish Army
Turkish Army, 06100 Bakanliklar/Ankara ,TURKEY

10. SPONSOR/MONITOR'S ACRONYM(S)
TCC
OSD
Turkish Army

11. SPONSOR/MONITOR'S REPORT NUMBER(S)

12. DISTRIBUTION/AVAILABILITY STATEMENT
DISTRUBTION STATEMENT A. Approved for Public Release; Distribution Unlimited.

13. SUPPLEMENTARY NOTES

14. ABSTRACT

This thesis was investigated the effects of pre-existing corrosion on the fatigue crack initiation and fatigue crack growth behavior of the typical aircraft aluminum alloy 7075-T6, by using a fracture mechanics approach. Initiation and crack growth behavior was investigated under in-plane biaxial tension–tension fatigue with stress ratio of 0.1 and biaxiality stress ratio, λ =1. Cruciform specimens with a center hole, having a corrosion pit at 45° to the specimen's arms, were tested in a biaxial fatigue test machine in laboratory air and saltwater (3.5% NaCl) environments. Crack initiated and propagated coplanar with the pit in L–T orientation. For the sake of comparison, uniaxial fatigue tests with stress ratio of 0.1 in laboratory air and saltwater (3.5% NaCl) environments were also conducted. The number of cycles until initiation of the fatigue crack and the crack growth rate were observed and measured by optical and scanning electron microscopy. This research shows that corrosive environment of saltwater reduces the required number of cycles for crack initiation under uniaxial and biaxial loading conditions when compared to those in ambient laboratory air. In all tests corrosive environment shortens the fatigue life of the specimens under uniaxial and biaxial loading conditions. In ambient air, numbers of cycles for crack initiation under biaxial and uniaxial loading conditions are almost the same, on the other hand in saltwater environment crack occurs in lesser number of cycles in biaxial loading condition relative to uniaxial loading condition. The crack growth rate is faster in the saltwater environment than the corresponding value in ambient air environment at a given ΔK in both loading conditions. In ambient air environment biaxial and uniaxial crack growth rates were almost similar. But in saltwater environment biaxial fatigue have faster crack growth rate than uniaxial fatigue. For uniaxial fatigue with the stress ratio of 0.1 crack initiates later than the one with R=0.5 for a given ΔK value because of the crack closure effect. Also the crack growth rate for R=0.5 is higher than the one with R=0.1.

15. SUBJECT TERMS
Corrosion, Fatigue, Fracture Mechanics, Crack Initiation, Crack Growth Rate, Aluminum Alloys

16. SECURITY CLASSIFICATION OF:			**17. LIMITATION OF ABSTRACT**	**18. NUMBER OF PAGES**	**19a. NAME OF RESPONSIBLE PERSON**
a. REPORT	**b. ABSTRACT**	**c. THIS PAGE**			Shankar Mall, Ph. D. (ENY)
U	**U**	**U**	**UU**	123	**19b. TELEPHONE NUMBER** *(Include area code)* (937) 255-6565, ext 4587; Shankar.Mall@afit.edu

Standard Form 298 (Rev. 8–98)
Prescribed by ANSI Std. Z39.18